DESIGNING SWITCHABLE SOLVENTS FOR SUSTAINABLE PROCESS DEVELOPMENT

A Dissertation
Presented to
The Academic Faculty

By

Ryan J. Hart

In Partial Fulfillment
Of the Requirements for the Degree
Doctor of Philosophy in the
School of Chemical & Biomolecular Engineering

Georgia Institute of Technology

May 2011

DESIGNING SWITCHABLE SOLVENTS FOR SUSTAINABLE PROCESS DEVELOPMENT

Approved by:

Dr. Charles Eckert, Advisor
School of Chemical & Biomolecular
Engineering
Georgia Institute of Technology

Dr. Charles Liotta, Co-Advisor
School of Chemistry & Biochemistry
Georgia Institute of Technology

Dr. William Koros
School of Chemical & Biomolecular
Engineering
Georgia Institute of Technology

Dr. Christopher Jones
School of Chemical & Biomolecular
Engineering
Georgia Institute of Technology

Dr. Dennis Hess
School of Chemical & Biomolecular
Engineering
Georgia Institute of Technology

Date Approved: November 17, 2010

To my loving Family -

None of this would be possible without you.

ACKNOWLEDGEMENTS

me your advice, letting me make my own decisions, and being there next to me when I made mistakes. To Dad – my best friend, biggest fan, and role model – and Mom – the most caring and beautiful person on the planet – thank you for making me the man I am today. I only hope that I can make you as proud as you've made me. Granny and Gramps, you're the cornerstones of the family. Your faith in me has given me the strength to pursue any dream. I will never forget watching the 3 Stooges with a bowl full of milk and popcorn, the hugs after my high school football games, or your smiles on Christmas morning. And Uncle Dave and Aunt Laura, thank you for always opening your home to me and being there for me when I needed you most.

Lastly, I want to acknowledge all the people I've worked with, taken classes with, coached me, and taught me. I've learned from you all, and without those experiences this milestone wouldn't have been possible.

TABLE OF CONTENTS

LIST OF TABLES

LIST OF FIGURES

LIST OF ABBREVIATIONS

[bmim][BF$_4$]	1-butyl-3-methylimidazolium tetrafluoroborate
[bmim][BTA]	1-butyl-3-methylimidazolium bis(trifluoromethanesulfonyl)amide
[bmim][PF$_6$]	1-butyl-3-methylimidazolium hexaflurophosphate
Ac	Acetate
ATR	Attenuated total reflectance
Boc	*tert*-Butyloxycarbonyl
CA	Cellulose acetate
CaH$_2$	Calcium hydride
CDCl$_3$	Deuterated chloroform
CO$_2$	Carbon dioxide
DBU	1,8-diazabicyclo[5.4.0]undec-7-ene
DLaTGS	Deuterated L-alanine doped triglycene sulphate
DMSO	Dimethylsulfoxide
DPU	1,3-diphenylurea
DSC	Differential scanning calorimetry
EMSA	(3-aminopropyl)ethyldimethylsilane
EOR	Enhanced oil recover
EPA	U.S. Environmental Protection Agency
FT-IR	Fourier transform infrared
GC-MS	Gas chromatography mass-spectrometry
HPLC	High performance liquid chromatography
IL	Ionic liquid
IR	Infrared

MEA	Monoethanolamine
MgSO$_4$	Magnesium sulfate
ML	Molecular liquid
NaCl	Sodium chloride
NaOH	Sodium hydroxide
NBA	N-Boc-aniline
NMP	N-methylpyrrolidone
NMR	Nuclear magnetic resonance
OATS	Organic-aqueous tunable solvents
Pd(OAc)$_2$	Palladium acetate
PdCl$_2$	Palladium chloride
Pt-DVDs	Platinum(0)-1,3-divinyl-1,1,3,3-tetramethyldisiloxane
R-OH	Alcohol (general)
RST	Regular Solution Theory
S/N	Signal-to-noise ratio
scCO$_2$	Supercritical carbon dioxide
SFC	Supercritical fluid chromatography
TESA	(3-aminopropyl)triethoxysilane
TEtSA	(3-aminopropyl)triethylsilane
THSA	(3-aminopropyl)trihexylsilane
TMBG	N,N,N',N'-tetramethyl-N"-butylguanidine
TMSA	(3-aminopropyl)trimethoxysilane
TMSCN	Trimethylsilyl cyanice
TON	Turn-over number
TPP	Triphenylphosphine
TPSA	(3-aminopropyl)tripropylsilane

| vdW | van der Waals |
| ZnSe | Zinc selenide |

LIST OF SYMBOLS

A_i	Absorbance of species "i"
b	Pathlength
C_i	Concentration of species "i"
d_e	Effective pathlength
D_i	Diffusion coefficient of species "i"
d_p	Penetration depth
E_a	Activation energy
f_i	Fugacity of species "i"
H_i	Henry's Law constant of species "i"
ℓ	Sample thickness
MW_i	Molecular weight of species "i"
n_{12}	Refractive index of mixture
n_i	Refractive index of species "i"
P_i	Partial pressure of species "i"
S	Swelling
T_{evap}	Evaporation temperature
T_{rev}	Reversal temperature
V_i	Molar volume of species "i"
x_i	Mole fraction of species "i"
α_i	Absorption coefficient of species "i"
ΔH_{abs}	Enthalpy of absorption
ΔH_{rev}	Enthalpy of reversal
δ_i	Solubility parameter of species "i"

ΔRI	Refractive index change
ΔS_{abs}	Entropy of absorption
ε_i	Extinction coefficient of species "i"
η	Viscosity
θ_i	Incident angle
λ_{max}	Wavelength of maximum absorption
v	Vibrational frequency
ρ_i	Density of species "i"
φ	Association factor
Φ_i	Volume fraction of species "i"

SUMMARY

Reversible ionic liquids represent a novel class of switchable solvents, where the structure and properties of the solvent system can be easily switched back and forth from a molecular liquid to an ionic liquid. Harnessing the switchable properties, practical opportunities for sustainable technology development are envisioned. Broadening the scope and applicability of reversible ionic liquids is the ability to easily alter the molecular structure, resulting in a multitude of solvent structures and corresponding properties that can be strategically modified for specific applications. This concept of "designer solvents" is only possible by first understanding structure-property relationships, and using this information to develop new compounds with enhanced properties.

Explored in this thesis are two classes of reversible ionic liquids: (1) one component and (2) two component. Each solvent class exhibits differing properties, and the full characterization of each class is given to aid readers in understanding the potential of their use in sustainable processing. Additionally, limitations in behavior are addressed, with recommendations on specific molecular modifications to overcome these challenges. Reactions and separations are typically thought of as two separate unit processes; it will be shown that with the advent of the two component liquids, the two can be coupled yielding an efficient solvent for reactions with the added benefit of facile catalyst and product recovery.

A new technique is described to probe the CO_2 induced solvent switch, and further applied to understanding the relationship between one component structure and CO_2 separation potential. This allowed for the design of materials with enhanced physical absorption properties. Lastly, the highly viscous nature of the ionic liquid is problematic with regards to industrial processing, and is addressed with a useful mitigation strategy offered.

CHAPTER 1   INTRODUCTION

The 21st century has ushered in a new cultural paradigm that is quickly gaining momentum as consumer driven research and development must appeal to a global scale – sustainability. More and more, the concept of environmentally sustainable (commonly referred to as "green") technologies are emerging in public policy, governmental investments, marketing campaigns, consumer products, and just about anything that can be eaten, bought, or sold. This concept of sustainability is steadily becoming firmly ingrained in every facet of the global economy, having widespread affects on nearly every commercial and private sector. Though not necessarily an equal distribution; sectors such as the chemical industry are burdened by a disproportionate amount of focus due to the innate environmental impact that is suffered as a result of by-product formations and waste generation. Combined with the recent governmental subsidies aimed at promoting sustainable technology development appealing to consumer support within smaller start-up companies, the well-established chemical industry faces numerous technological and economic challenges for the successful development of viable sustainable technologies.

The foundation of the chemical industry rests heavily on solvents. Solvents are easily identifiable by everyone from mechanics who need to clean mechanical parts, medical professionals who need to clean and sterilize medical instruments, teachers who need to clean white boards, to the average consumer who needs to clean up after a child's birthday party. Pertinent to the chemical industry, solvents are a way of bringing molecules together in the same phase, facilitating reaction. More solvents are commonly used to separate the products from the reaction mixture. And then more solvents are

used to clean the process for reuse. The prolific use of solvents in the chemical industry leads to significant amounts of waste production, where the treatment (recycle or disposal) of the waste is always a function of cost.[1]

Historically, several solvent systems with limited environmental impact have made the way from research and development to commercial processing. Most notable is carbon dioxide (CO_2), which has been heavily studied as a solvent for extractions.[2-6] CO_2 processing technologies have been commercialized decades ago for the decaffeination of coffee and dry-cleaning applications, but haven't seen heavy marketing as a sustainable technology until recently. Another example of CO_2 having a beneficial environmental impact is enhanced oil recovery (EOR). CO_2 is an unwanted byproduct from natural gas refining, and has been compressed, transported, and injected into spent oil reserves, drastically increasing the productivity of the oil wells.[7] The alternative to CO_2, here, is using water for enhanced recovery. The water is heavily contaminated after the EOR process, and must be purified following strict EPA regulations. The use of CO_2 for EOR capitalizes on the byproduct of one process to increase oil production in another, eliminating large amounts of contaminated water and limiting the amount of CO_2 that is simply vented to the atmosphere during natural gas refining.

The Eckert-Liotta Research Group has a history of exploring innovative solvent systems for sustainable technology development. The types of solvent systems studied can be conveniently separated into two classes: (1) tunable and (2) switchable. Tunable solvent systems exhibit continuous changes in solvent properties by application of a stimulus, such as temperature and pressure. Supercritical fluids comprise a large portion of tunable solvents. Other examples include gas expanded liquids,[8-12] organic-aqueous tunable solvents (OATS),[13-15] and near-critical fluids.[16-18]

In contrast to tunable solvents are switchable solvents, which undergo a step-

2

wise change in properties upon application of a stimulus. The appeal of switchable solvents is that within one set of conditions the solvent displays a favorable set of properties for facilitating reactions or bringing solutes together, and within another set of conditions the solvent properties are altered drastically. This switch presents opportunities for sustainable technology development. Consider a given chemical process that normally requires the use of multiple solvents over the course of numerous processing steps. One switchable solvent could ideally replace the multitude of solvents normally required, simplifying the overall processing scheme and eliminating the wastes incurred with conventional solvents.

An example of a switchable solvent is piperylene sulfone, which exhibits properties similar to dimethylsulfoxide (DMSO).[19-21] DMSO is a fantastic solvent, capable of dissolving a broad range of compounds. DMSO is also a terrible solvent, being extremely difficult to remove and particularly toxic. Piperylene sulfone overcomes the separation difficulties associated with DMSO by decomposing into volatile species when slightly heated. Thus, heat is the switch.

Another class of switchable solvents, the focus of this thesis, is reversible ionic liquids. Reversible ionic liquids undergo a transformation from a relatively nonpolar solvent to a polar solvent when exposed to CO_2.[22-25] Two subsets of reversible ionic liquids have been described: (1) two component systems comprised of a mixture of an amidine or guanidine and alcohol and (2) one component systems containing a silyl-amine moiety. Both subsets offer advantages and disadvantages for specific applications, as neither is a panacea.

Presented here is the design and development of reversible ionic liquids for sustainable processing applications. It will be shown that the solvent structures can be easily altered, offering a virtually limitless combination of prospective sustainable

solvents. Discussed in Chapter 2 are the synthesis and characterization, divided into the two solvent subsets, with reflection on the differences and similarities between the two and effect of solvent structure on the observed solvent properties for both the molecular and ionic forms.

The work in Chapter 3 describes a reflectance infrared spectroscopic technique that probes both the chemical reaction of the molecular form with CO_2, and the physically absorbed (unreacted) CO_2 in the solvent. CO_2 serves as the switch for reversible ionic liquids, and understanding the relationship between CO_2 partial pressures and system temperatures on this switch is critical for the development of sustainable processes utilizing reversible ionic liquids.

Chapter 4 discusses the use of the two component reversible ionic liquids for application to reaction/separation systems. The polarity switch observed from the conversion of the molecular liquid to ionic liquid is exploited to combine a solvent system capable of bringing reactants together, facilitating reaction, and offering a facile separation of the products and catalysts from the solvent. The limitations of using these innovative solvents are also discussed.

The application of the one component reversible ionic liquids to CO_2 capture is presented in Chapter 5. Here, the switch yields the separation. In addition to the chemical reaction, the resulting ionic form is shown to afford considerable physical absorption of CO_2 for enhanced capture capacities. Taking advantage of this dual-capture mechanism, the structures of the one component reversible ionic liquids are strategically altered to increase the lower energy physical absorption mechanism. Also discussed are the viscosities and chemical absorption uptake rates, important for the industrial viability of these sustainable solvents.

Finally, the reader is presented with the "Conclusions and Recommendations,"

summarizing the work to date and offering insight into the future direction of the development of reversible ionic liquids for sustainable processing. Knowledge of the reversible ionic liquid structure on solvent properties and application to the selected processes can be a useful guide for the design of next generation switchable solvents.

References

(1)   Alberini, A.; Bartholomew, J. *Contemp. Econ. Policy* **1999**, *17*, 309.

(2)   Bartle, K. D.; Clifford, A. A.; Jafar, S. A.; Shilstone, G. F. *Journal of Physical and Chemical Reference Data* **1991**, *20*, 713.

(3)   Reverchon, E. *Journal of Supercritical Fluids* **1997**, *10*, 1.

(4)   Eckert, C. A.; Pouillot, F. L. L.; Knutson, B. L.; Gurdial, G. S.; Scott, L. S. *Journal of Supercritical Fluids* **1995**, *8*, 1.

(5)   Kazarian, S. G.; Brantley, N. H.; Eckert, C. A. *Chemtech* **1999**, *29*, 36.

(6)   Tomasko, D. L.; Macnaughton, S. J.; Foster, N. R.; Eckert, C. A. *Separation Science and Technology* **1995**, *30*, 1901.

(7)   Blunt, M.; Fayers, F. J.; Orr, F. M. *Energy Conversion and Management* **1993**, *34*, 1197.

(8)   Jessop, P. G.; Stanley, R. R.; Brown, R. A.; Eckert, C. A.; Liotta, C. L.; Ngo, T. T.; Pollet, P.; Royal Soc Chemistry: 2003, p 123.

(9)   Eckert, C. A.; Liotta, C. L.; Bush, D.; Brown, J. S.; Hallett, J. P. *Journal of Physical Chemistry B* **2004**, *108*, 18108.

(10)   Chamblee, T. S.; Weikel, R. R.; Nolen, S. A.; Liotta, C. L.; Eckert, C. A. *Green Chemistry* **2004**, *6*, 382.

(11)   Xie, X. F.; Liotta, C. L.; Eckert, C. A. *Industrial & Engineering Chemistry Research* **2004**, *43*, 7907.

(12)   Weikel, R. R.; Hallett, J. P.; Liotta, C. L.; Eckert, C. A. *Industrial & Engineering Chemistry Research* **2007**, *46*, 5252.

(13)   Lu, J.; Lazzaroni, J.; Hallett, J. P.; Bommarius, A. S.; Liotta, C. L.; Eckert, C. A. *Industrial & Engineering Chemistry Research* **2004**, *43*, 1586.

(14)   Broering, J. M.; Hill, E. M.; Hallett, J. P.; Liotta, C. L.; Eckert, C. A.; Bommarius, A. S. *Angewandte Chemie-International Edition* **2006**, *45*, 4670.

(15)   Hill, E. M.; Broering, J. M.; Hallett, J. P.; Bommarius, A. S.; Liotta, C. L.; Eckert, C. A. *Green Chemistry* **2007**, *9*, 888.

(16)   Chandler, K.; Liotta, C. L.; Eckert, C. A.; Schiraldi, D. *Aiche Journal* **1998**, *44*, 2080.

(17)   Chandler, K.; Deng, F. H.; Dillow, A. K.; Liotta, C. L.; Eckert, C. A. *Industrial & Engineering Chemistry Research* **1997**, *36*, 5175.

(18)   Lesutis, H. P.; Glaser, R.; Liotta, C. L.; Eckert, C. A. *Chemical Communications* **1999**, 2063.

(19)   Vinci, D.; Donaldson, M.; Hallett, J. P.; John, E. A.; Pollet, P.; Thomas, C. A.; Grilly, J. D.; Jessop, P. G.; Liotta, C. L.; Eckert, C. A. *Chemical Communications* **2007**, 1427.

(20)   Jiang, N.; Vinci, D.; Liotta, C. L.; Eckert, C. A.; Ragauskas, A. J. *Industrial & Engineering Chemistry Research* **2008**, *47*, 627.

(21)   Donaldson, M. E.; Mestre, V. L.; Vinci, D.; Liotta, C. L.; Eckert, C. A. *Industrial & Engineering Chemistry Research* **2009**, *48*, 2542.

(22)   Heldebrant, D. J.; Jessop, P. G.; Thomas, C. A.; Eckert, C. A.; Liotta, C. L. *Journal of Organic Chemistry* **2005**, *70*, 5335.

(23)   Jessop, P. G.; Heldebrant, D. J.; Li, X. W.; Eckert, C. A.; Liotta, C. L. *Nature* **2005**, *436*, 1102.

(24)   Phan, L.; Chiu, D.; Heldebrant, D. J.; Huttenhower, H.; John, E.; Li, X. W.; Pollet, P.; Wang, R. Y.; Eckert, C. A.; Liotta, C. L.; Jessop, P. G. *Industrial & Engineering Chemistry Research* **2008**, *47*, 539.

(25)   Blasucci, V.; Dilek, C.; Huttenhower, H.; John, E.; Llopis-Mestre, V.; Pollet, P.; Eckert, C. A.; Liotta, C. L. *Chemical Communications* **2009**, 116.

CHAPTER 2   SYNTHESIS AND CHARACTERIZATION OF REVERSIBLE IONIC LIQUIDS

Introduction and Background on Reversible Ionic Liquids

A large number of chemical processes involving reactions and separations are performed in solution. The solvent provides a means of bringing reactants together to facilitate reaction. It also provides a means of temperature control for both endothermic and exothermic reactions. The difference in solute solubilities in various solvents is the basis for crystallization and extraction as unit operations in separation processes. The chemical industry has a continuous demand for better solvent alternatives for chemical processes -- solvents in which reactions can occur in high yields at reasonable rates under relatively mild reaction conditions, where product isolation is facile, and where recycle of the solvent system is possible.

Tunable solvents are defined as solvents that change their physico-chemical properties continuously upon variation of external stimuli such as pressure, temperature, or composition. An illustrative example is provided by the biphasic system containing room temperature ionic liquids (ILs) and supercritical carbon dioxide (scCO$_2$), where the physico-chemical properties such as gas solubility, viscosity, and melting points depend strongly on the amount of dissolved carbon dioxide (CO$_2$) present in the IL phase.[1] Such changes can drastically influence the chemical reactivity in these systems, as demonstrated by catalytic hydrogenation reactions in IL/scCO$_2$.[2] In contrast, switchable solvents change properties as a step-wise function via changes in their molecular structure upon application of external stimuli. In other words, they can be switched "on" and "off" by reversible chemical transformations. The Liotta-Eckert-Jessop groups

reported the first example of switchable solvent, which can be switched back and forth from a molecular liquid to an ionic liquid upon reaction with CO_2.[3,4] A schematic representation is shown for the 1,8-diazabicyclo[5.4.0]undec-7-ene (DBU) and alcohol system (Figure 2.1).
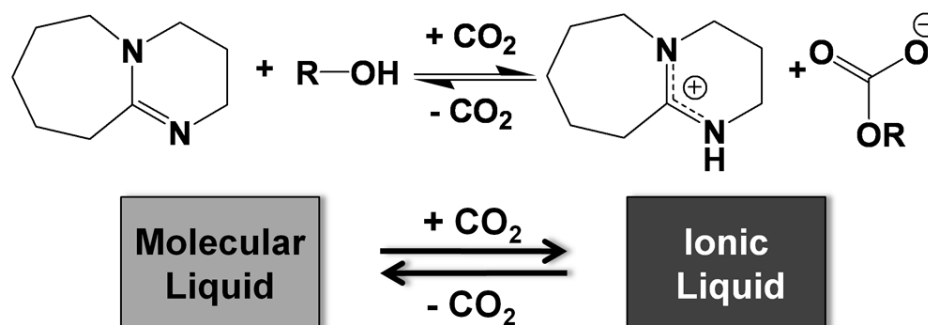
Figure 2.1. Reversible switch from a molecular liquid mixture of DBU and alcohol (R-OH) to the ionic liquid [DBUH]$^+$[RCO$_3$]$^-$ upon addition of CO_2.

The two-component systems presented here are composed of an equimolar mixture of N,N,N',N'-tetramethyl-N"-butylguanidine (TMBG) or DBU and an alcohol such as methanol. It should be noted that Weiss and coworkers have investigated other two-component systems involving guanidines or amidines with amines.[5-7] Just like the DBU/alcohol system, the TMBG/alcohol system reacts with CO_2 (under atmospheric conditions) to form the corresponding ionic liquid, N,N,N',N'-tetramethyl-N"-butyl-guanidinium alkylcarbonate (Figure 2.2). The reaction of alcohols with CO_2 in the presence of amidines or guanidines to form ionic liquids is an equilibrium reaction governed by many factors such as structure, temperature, and pressure. The reaction of the base and alcohol mixture with CO_2 undergoes several steps, the first of which is the reaction of the alcohol with CO_2 to form the alkyl-carbonic acid, followed by the

protonation of the base to form the ionic pair. A spectroscopic technique to examine the pKa of CO_2 and alcohols has been investigated, and concludes that the acid strength of the alkyl-carbonic acids is higher for shorter chain length alcohols.[8] Thus, the relative reaction rates would be faster for the shorter chain length alcohols.
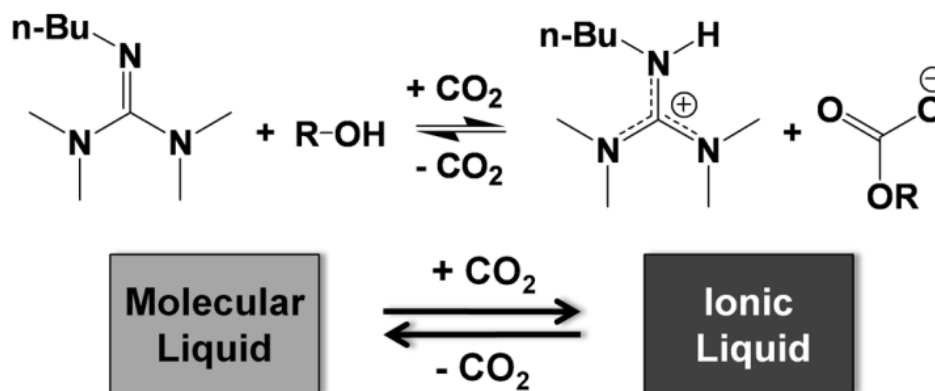
Figure 2.2. Reversible switch from a molecular liquid mixture of TMBG and alcohol (R-OH) to the ionic liquid [TMBGH]$^+$[RCO$_3$]$^-$ upon addition of CO$_2$.

The major distinction between the one-component and the two-component systems is that the one-component system does not require the presence of an equimolar amount of alcohol, simplifying the reaction system and subsequent processing schemes. The reaction of CO_2 with the one-component amine precursors, trialkoxy- or trialkyl- silylpropylamines, forms the corresponding ionic liquids (Figure 2.3). It should be emphasized that the reaction of amines with CO_2 to form carbamic acids and/or carbamates has long been known and used for CO_2 separation.[9-11] In addition, the formation of carbamates decreases the nucleophilicity of the nitrogen, making the reversible carbamate formation a successful protecting strategy for the amine group.[12-14]

10
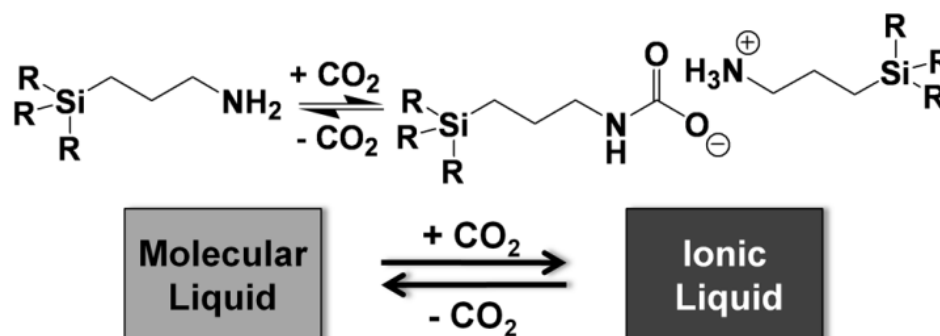
Figure 2.3. One-component system: reversible switch from a molecular liquid (trialkoxy- or trialkyl- silylpropylamine) to its corresponding ionic liquid upon addition of CO_2.

The synthesis and characterization of both classes of reversible ionic liquids is reported herein, with an emphasis on the stepwise property change upon switching from the neutral to the ionic state and back. Note that the characterization techniques employed for each class of materials reflects the intended applications of the solvent systems, i.e. coupling reactions and separations in two-component reversible ionic liquids (Chapter 4) and carbon capture using one-component reversible ionic liquids (Chapter 5).

One-component Reversible Ionic Liquids

Materials

The alkoxy- substituted aminosilanes are commercially available and used as received; (3-aminopropyl)trimethoxysilane (Fluka, 97%), (3-aminopropyl)triethoxysilane (Sigma-Aldrich, 98%). The alkyl- substituted aminosilanes are synthesized by the procedure described below, using the following materials: allylamine (Sigma-Aldrich, 99+%), triethylsilane (Sigma-Aldrich, 99%), tripropylsilane (Sigma-Aldrich, 99%),

trihexylsilane (Sigma-Aldrich, 98%), ethyldimethylsilane (Sigma-Aldrich, 98%), diisopropyl(1H,1H,2H,2H-perfluoropentyl)silane (Fluorous Technologies, 98%), platinum(0)-1,3-divinyl-1,1,3,3-tetramethyldisiloxane (Sigma-Aldrich, ~2% solution in xylene), and anhydrous toluene (Sigma-Aldrich, 99.8%). Carbon dioxide was supercritical fluid chromatography (SFC) grade (Air Gas, 99.999%) and further purified via a Matheson gas purifier and filter cartridge (Model 450B, Type 451 filter). All materials except the toluene and CO_2 were stored in a nitrogen-filled glovebox until used.

Synthesis of (3-aminopropyl)trialkylsilanes

The general reaction scheme for the synthesis of silyl-amine based (one component) reversible ionic liquids is shown (Figure 2.4).[15]
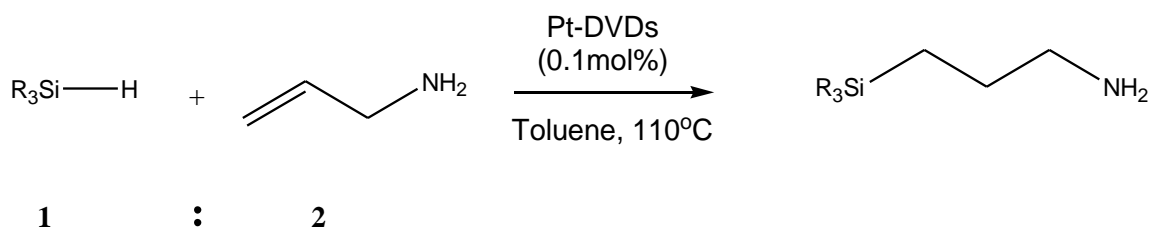
Figure 2.4. One-step synthetic scheme for silyl-amine based reversible ionic liquids.

Two equivalents of allyl amine (relative to the silane) are added in toluene, and heated over reflux using a condenser with tap water as the heat transfer fluid. The progression of the reaction is monitored by examining the ^{1}H NMR of the reaction mixture, and the reaction is stopped when the reaction is considered complete as evidenced by the disappearance of the silane proton ($\delta \sim 3.6$ppm). In scenarios where the reaction was incomplete and appears to show no change over a 24 hour period,

another equivalent of the Pt-DVDs (Platinum(0)-1,3-divinyl-1,1,3,3-tetramethyldisiloxane in xylene) is added. This is likely due to the age of the catalyst. Once the reaction has been cooled to room temperature, the unreacted allyl amine and toluene are removed with a rotary evaporator. The remaining mixture is distilled to remove the catalyst. The product has been characterized using ^{1}H and ^{13}C NMR, elemental analysis, FT-IR, Nile Red polarity measurements, refractive index, stability, and density measurements.

The reaction time correlates with the bulkiness of the silane substrate; larger silanes require longer reaction times to complete. The hydrosilation reaction utilizing platinum catalysts is well known, with the first step of the cycle involving the insertion of the Si-H bond on the metal center.[16] It then follows that the kinetics of this step are slowed by the bulkier R- groups on the silane, resulting in a kinetic decrease for the entire cycle.

The synthetic scheme being employed affords two main benefits for the design of reversible ionic liquids for the sustainable development of chemical processes: (1) the synthesis is simple and efficient and (2) the molecular architecture of the solvent can be easily tuned by using silanes with different substitution. This allows for the development of a plethora of compounds to be tested for various applications, as well as ensuring that the optimally designed solvent will be capable of scaling to synthesis on an industrial level. Additionally, as information is gained on existing compounds, it is possible to identify molecular structures for improved processing properties and alter the current synthetic techniques by simple substitution of silanes.

The cost of the material is an important factor in determining the economic viability of any solvent system designed for industrial implementation. However, this information is difficult for academics to evaluate, and will be properly quantified with support from industrial collaborators. Nevertheless, some observations can be made

regarding the synthesis and relative cost of these one-component reversible ionic liquids:

1. The cost of silanes is significant. But with the increasing industrial developments of photovoltaics and the growing demand for cost effective syntheses of silanes, the cost has been dropping. Because of the anticipated growth of solar panels in the commercial sector, these costs are expected to decrease.

2. The allyl amine and toluene are relatively cheap. Although recycle attempts have not yet been initiated in our laboratory, their separation from the final product is facile and could lead to reuse in an industrial scheme.

3. The Pt-DVDs is relatively expensive. Studies examining the turn-over number (TON) should be conducted for application to industrial scale synthesis.

Formation of Ionic Liquid

The one-component reversible ionic liquids are prepared by bubbling CO_2 through the solution at 1 atmosphere of pressure until the molecular liquid is completely reacted to ionic liquid. The reaction is highly exothermic and the resulting ionic liquid exhibits a viscosity much higher than the molecular liquid.

Approximately 1-2 mL of the molecular liquid is placed in a 2 dram vial that has been capped with a rubber septum and purged with argon for 10 minutes, to ensure no moisture is present. Water present can react with the CO_2 to form the bicarbonate, which is more stable than the alkylcarbonate and can drastically alter the observed properties of the ionic liquid. The CO_2 is fed through the liquid by using a 10 gauge needle that reaches to the bottom of the vial, making sure to vent the vial in order to prevent

pressure build up and loss of the septa seal.

The resulting ionic liquids are highly viscous, which limits the transport of CO_2 into and out of the sample. Because of the transport limitation, the ionic liquids are relatively stable when removed from the 1 atmosphere of CO_2 in the vial, enabling researchers to transfer the sample from the vial to various experimental apparatuses for testing. Reversal of the ionic liquid back to the molecular liquid can be rapidly achieved by bubbling N_2 (or other inert gases) through the ionic liquid or by heating at temperatures above $60^{\circ}C$. The sparging results in reversion by (1) lowering the concentration of CO_2 in the head space of the vial, (2) stripping the CO_2 from the solution and (3) vigorously mixing the solution to enhance the mass transport rate of CO_2 out of the solution. Heating the sample results in reversion by (1) lowering the equilibrium constant of the reaction, (2) decreasing the solubility of CO_2 in the solution and (3) increasing the mass transport rate of CO_2 out of the solution. Relatively, heating the ionic liquids is a faster method of reversing the reaction than sparging.

The reversible ionic liquid formation has been characterized using ^1H and ^{13}C NMR, elemental analysis, FT-IR, differential scanning calorimetry, Nile Red polarity measurements, refractive index, and density measurements.

Structures of One-Component Reversible Ionic Liquids

The molecular liquid structures of the one-component reversible ionic liquids studied here are given (Figure 2.5). The detailed characterization of both molecular and ionic forms of the materials follows.
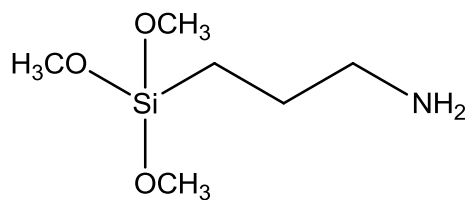
(3-aminopropyl)trimethoxysilane **(TMSA)**
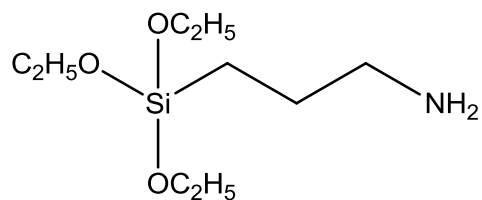
(3-aminopropyl)triethoxysilane **(TESA)**
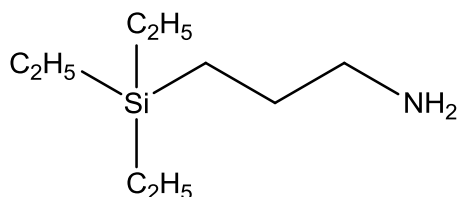
(3-aminopropyl)triethylsilane **(TEtSA)**
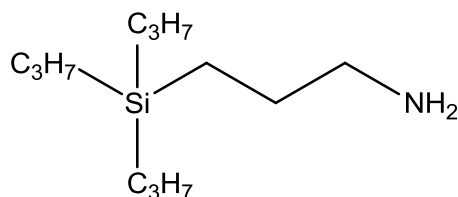
(3-aminopropyl)tripropylsilane **(TPSA)**
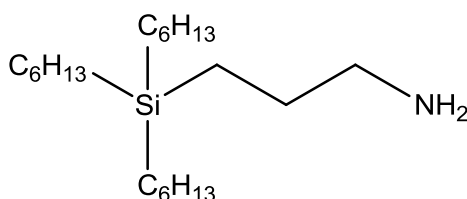
(3-aminopropyl)trihexylsilane **(THSA)**
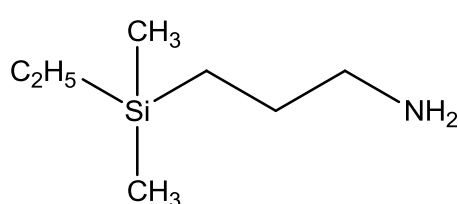
(3-aminopropyl)ethyldimethylsilane **(EMSA)**
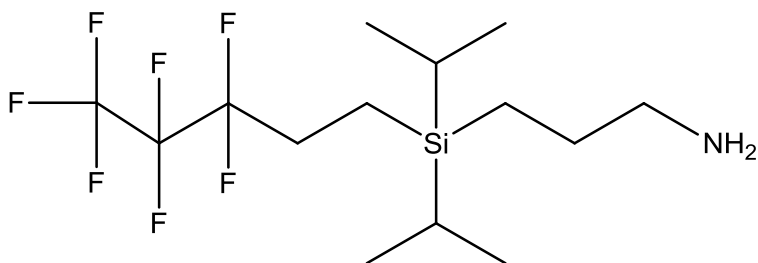
(3-aminopropyl)diisopropyl(1H,1H,2H,2H-perfluoropentyl)silane **(FSA)**

Figure 2.5. The structures of the molecular liquid form (and abbreviations) for the one-component reversible ionic liquids studied.

The NMR experiments were run at room temperature using either (1) a Varian-Mercury VX 400MHz spectrometer located in the Georgia Tech Institute of Bioengineering and Bioscience or (2) a Bruker AMX 400MHz spectrometer located in the Georgia Tech NMR Center. The NMRs for the molecular liquids were performed by diluting the sample in deuterated chloroform ($CDCl_3$). In order to prevent reversion and overcome the difficulty arising from the high viscosity of the ionic liquid samples, neat NMRs were run for the ionic liquids. The standard NMR tube was loaded with the molecular liquid, and CO_2 was bubbled until complete conversion to the ionic liquid was observed. A capillary tube containing the lock solvent $CDCl_3$ was placed inside the sample.

The conversion of the molecular liquid to the ionic liquid is observed in the ^{1}H NMR spectra for all compounds by the shift of all peaks that corresponds to the formation of the ammonium/carbamate of the ionic liquid. Cases of incomplete conversion are evidenced by the presence of both molecular proton peaks and ionic liquid peaks. The ^{1}H NMR spectra are quantitative with an error of 1-2%. Using the ionic liquid preparation technique described above, we observed no peaks present for the molecular liquid in the ^{1}H NMRs of the ionic liquids; the conversion was assumed to be complete (>98%). The ^{13}C NMR revealed shifts of all ionic liquid peaks relative the molecular liquid peaks, and the appearance of a quaternary carbon at *ca.* 160 ppm that is consistent with the formation of the carbamate. The observed ^{1}H and ^{13}C NMR shifts (δ, ppm) and the corresponding splitting pattern (singlet = s, doublet = d, triplet = t, quartet = q, pentet = p, and multiplet = m; broad peaks are denoted with 'br') and integration values for the seven molecular liquids and seven ionic liquids are given:

TMSA Molecular Liquid:

^{1}H: 3.9(s,9);2.9(t,2); 1.8(m,2); 0.9(t,2)

^{13}C: 49.7, 45.0, 27.1, 6.1

TMSA Ionic Liquid:

^{1}H: 6.0(br,3); 4.5(br,1); 3.5(br,18); 3.0(br,2); 1.6(br,2); 0.2(br,4)

^{13}C: 162.6, 50.0, 43.9, 42.8, 23.8, 23.2, 5.8

TESA Molecular Liquid:

^{1}H: 4.1(m,6); 2.9(t,2); 1.8(m,2); 1.5(t,9); 0.9(t,2)

^{13}C: 51.2, 45.5, 18.9, 17.9, 8.8

TESA Ionic Liquid:

^{1}H: 9.6(br,3); 6.0(br,1); 4.0(br,12); 3.2(br,2); 3.0(br,2); 1.9(br,2); 1.7(br,2); 1.4(br,18); 0.8(br,4)

^{13}C: 162.5, 57.7, 44.1, 41.5, 23.7, 21.3, 17.9, 7.6, 7.4

TEtSA Molecular Liquid:

^{1}H: 2.59(t,2); 1.38(p,2); 1.02(s,2); 0.86(t,9); 0.45(q,8)

^{13}C: 45.68, 28.08, 8.10, 7.15, 3.07

TEtSA Ionic Liquid:

^{1}H: 9.22(br,3); 5.84(br,1); 3.09(br,4); 1.58, 1.05, 0.64(3br,38)

^{13}C: 163.01, 45.52, 43.06, 25.23, 22.56, 9.07, 7.65, 7.61, 3.71

TPSA Molecular Liquid:

^{1}H: 2.59(t,2); 1.38(p,2); 1.27(m,6); 1.17(s,2); 0.89(t,9); 0.43(q,8)

^{13}C: 45.78, 28.27, 18.48, 17.35, 15.20, 9.47

TPSA Ionic Liquid:

^{1}H: 9.54(br,3); 5.76(br,1); 3.14(br,4); 1.46, 1.07, 0.65(3br,74)

^{13}C: 162.45, 44.9, 25.0, 21.5, 18.63, 17.59, 15.41, 15.26, 10.0

THSA Molecular Liquid:

^{1}H: 2.63(t,2); 1.39(p,2); 1.25(s,br),26); 0.87(t,9); 0.47(m,8)

^{13}C: 45.73, 33.45, 31.40, 28.22, 23.71, 22.50, 13.95, 12.26, 9.30

THSA Ionic Liquid:

^{1}H: 9.77(br,3); 5.59(br,1); 3.20(br,3); 1.46, 1.04, 0.70(3br,94)

^{13}C: 162.34, 45.28, 33.76, 31.72, 25.03, 24.00, 22.80, 14.11, 12.52, 10.05

EMSA Molecular Liquid:

^{1}H: 2.63(t,2); 1.35(p,2); 1.22(s,2); 0.86(t,9); 0.51(q,2)

^{13}C: 47.43, 27.65, 8.21, 7.15, 4.21, 3.07

EMSA Ionic Liquid:

Was not run due to solid formation.

FSA Molecular Liquid:

^{1}H: 2.68(t,2); 2.03(m,2); 1.44(p,2); 1.013(s,16); 0.79(m,2); 0.58(m,2)

^{13}C: 45.9, 28.0, 25.9(trip), 18.1, 11.0, 6.4, -1.0

FSA Ionic Liquid:

Unable to obtain due to high viscosity of ionic liquid

Elemental Analysis

The elemental analyses were conducted by Atlantic Microlab, Inc. located in Norcross, GA. The molecular liquid samples were stored under argon and mailed to the lab. The ionic liquids were delivered in person and run immediately in order to prevent reversion and maintain the integrity of the samples. The ionic liquid samples were prepared and stored under a CO_2 atmosphere in a dry ice cooler during the transportation from Georgia Tech to Atlantic Microlab, Inc. Once delivered, they were stored in the refrigerator at Atlantic Microlab, Inc. and run within 12 hours. The atoms

tested for include carbon (C), hydrogen (H), and nitrogen (N). The elemental analysis of oxygen was expressed to be inaccurate (by employees at Atlantic Microlab, Inc.) relative to the other 3 compounds, and was therefore not requested. The theoretical values for the ionic liquid samples were determined assuming a 1:2 CO_2:amine ratio. The actual values were consistent for both molecular liquid and ionic liquid samples, confirming purity of the starting material and the stoichiometric reaction of the molecular liquids with CO_2 to form the ionic liquid.

The elemental analysis of the EMSA compound was not performed as the ionic species was found to be a thermally unstable solid. This issue is discussed in more detail in the DSC section of this chapter. The expected and measured percentages of elements for the six one-component molecular liquids and six corresponding ionic liquids are given:

TMSA Molecular Liquid:	Expected: C(40.19), H(9.56), N(7.81)
	Actual: C(39.09), H(9.84), N(7.36)
TMSA Ionic Liquid:	Expected: C(38.78), H(8.51), N(6.96)
	Actual: C(38.34), H(8.57), N(6.95)
TESA Molecular Liquid:	Expected: C(48.83), H(10.47), N(6.33)
	Actual: C(48.29), H(10.56), N(6.05)
TESA Ionic Liquid:	Expected: C(46.88), H(9.53), N(5.76)
	Actual: C(46.66), H(9.49), N(5.77)
TEtSA Molecular Liquid:	Expected: C(62.35), H(13.37), N(8.08)
	Actual: C(62.41), H(13.42), N(7.94)
TEtSA Ionic Liquid:	Expected: C(58.40), H(11.87), N(7.17)
	Actual: C(57.93), H(11.79), N(6.91)

TPSA Molecular Liquid: Expected: C(66.90), H(13.57), N(6.50)

Actual: C(66.74), H(13.64), N(6.35)

TPSA Ionic Liquid: Expected: C(63.23), H(12.31), N(5.90)

Actual: C(62.78), H(12.31), N(5.72)

THSA Molecular Liquid: Expected: C(73.82), H(13.86), N(4.10)

Actual: C(72.87), H(13.59), N(4.07)

THSA Ionic Liquid: Expected: C(71.00), H(13.03), N(3.85)

Actual: C(70.92), H(13.12), N(3.74)

FSA Molecular Liquid: Expected: C(45.52), H(7.09), N(3.79)

Actual: C(45.29), H(7.12), N(3.84)

FSA Ionic Liquid: Expected: C(44.49), H(6.69), N(3.58)

Actual: C(44.42), H(6.69), N(3.58)

FT-IR

The Fourier transform infrared (FT-IR) absorbance measurements were collected with a Shimadzu IRPrestige21 using a DLaTGS detector, with 32 scans and a resolution of 1 cm^{-1}. A Specac, Ltd. heated "Golden Gate" attenuated total reflectance (ATR) accessory with diamond crystal and zinc selenide (ZnSe) focusing lenses was used for the room temperature collection of the molecular and ionic liquid spectra. The spectra for the one-component molecular liquids is given in Figure 2.6. Although the structures of the molecular precursor molecules are all very similar, the FT-IR are visibly unique to each material. The detailed peak assignments for the one-component molecular liquids is given in much detail in Appendix A.
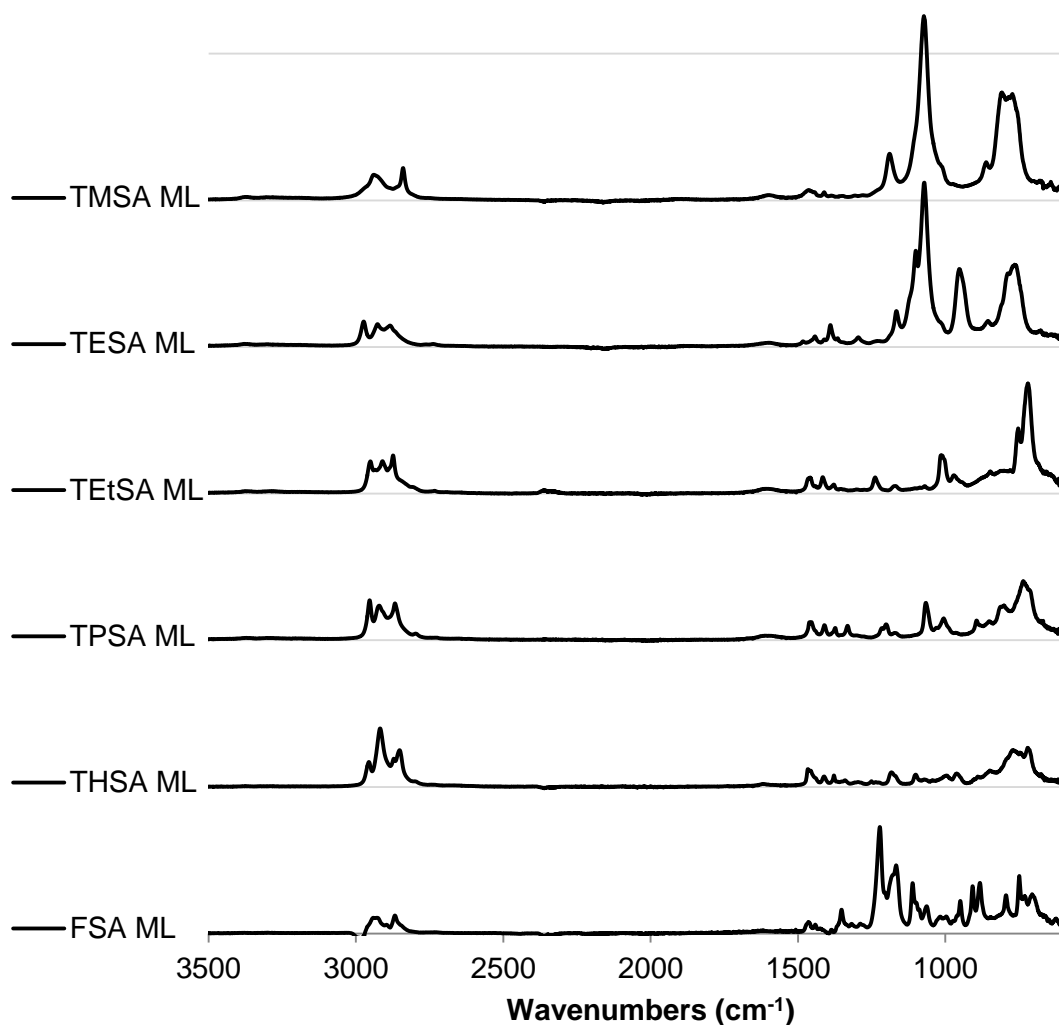
Figure 2.6. The FT-IR spectra of the one-component molecular liquids.

Upon addition of CO_2, the molecular liquid forms the corresponding ionic liquid, where the FT-IRs for the six one-component ionic liquids is given in Figure 2.7. The change of molecular liquid structure to ionic liquid is observed by the appearance of (1) a broad ammonium (-NH_3^+) peak that covers the range of 2300-3300 cm^{-1} and (2) a carbamate (-CO_2^-) peak at *ca.* 1700 cm^{-1}. Typically carbonyl stretch vibrations are very sharp and intense, but for the carbamates they appear moderately intense and slightly

broad due to the resonance stabilization with the amine functionality. There is also a small peak observed at 2400 cm^{-1} in the TMSA and THSA samples corresponding to the asymmetric stretch vibration of physically observed (or "free") CO_2 that is entrained in the ionic liquids.
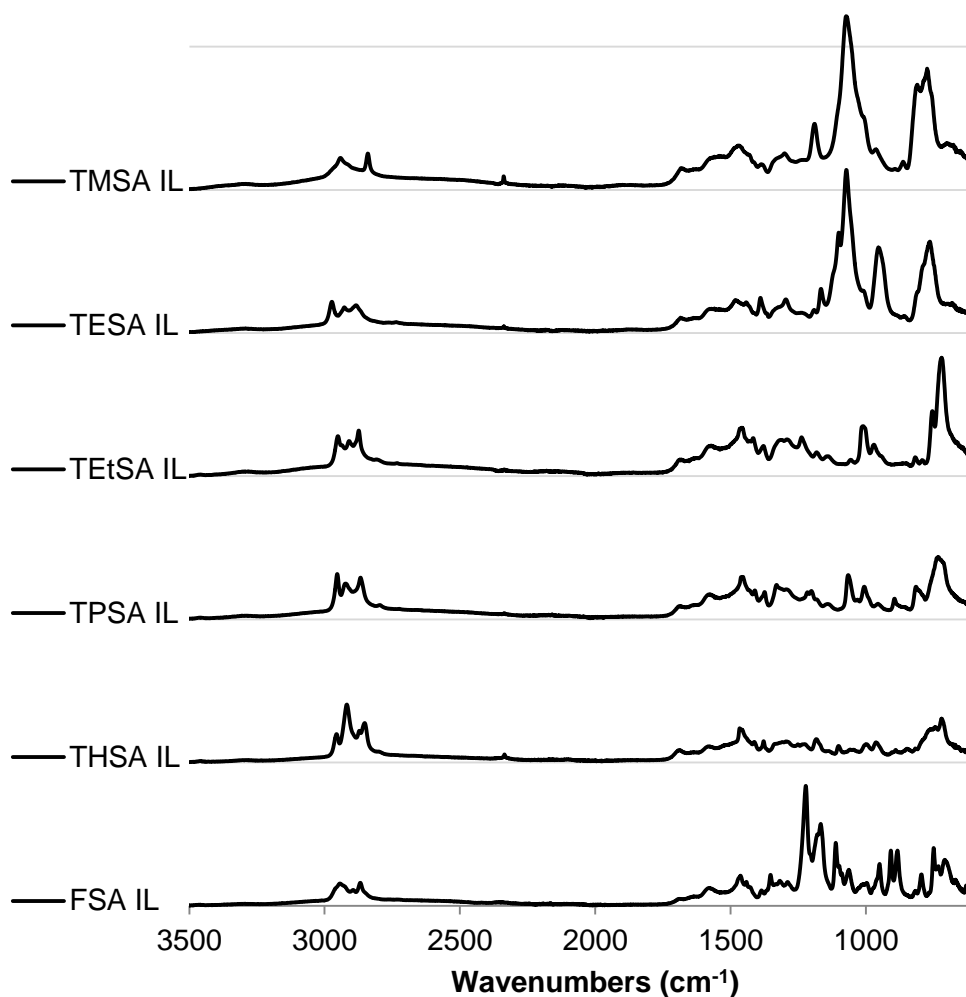
Figure 2.7. The FT-IR spectra of the one-component ionic liquids, showing the formation of the carbamate and ammonium.

Much detail is given to the FT-IR of the molecular and ionic liquid conversion in Chapter 3, with an emphasis on the quantification of conversion and physical absorption capacity of the free CO_2 in the ionic liquids.

Differential Scanning Calorimetry (DSC)

The DSC was performed using a Q20 TA Instruments DSC with an external cooling unit, using platinum hermetic pans. The sample size was < 5mg, and the temperature profile was operated from -30ºC to 400ºC at a temperature ramp rate of 5ºC/minute with a convective nitrogen flow of 50 mL/min. The DSC was examined for the ionic liquid form of all seven one-component ionic materials, a summary of results is provided in Table 2.1. A sample DSC is shown in Figure 2.8 with a discussion of the significant events following.

The DSC plot highlights three values relevant to the reversibility of the ionic liquids: enthalpy of reversal (ΔH_{rev}), reversal temperature (T_{rev}), and degradation/evaporation temperature (T_{evap}). The peaks revealed by DSC are indicative of phase transformations or other enthalpic processes, and are called endotherms (indicating energy is required) when pointing down and exotherms (indicating energy is generated) when pointing up. The first endotherm shown in Figure 2.8 at a maximum temperature of 97°C corresponds to the reversal of the ionic liquid. The integration of the peak with respect to the mass of the sample gives rise to the enthalpy of reversal, shown to be 199.5 J/g for TPSA.
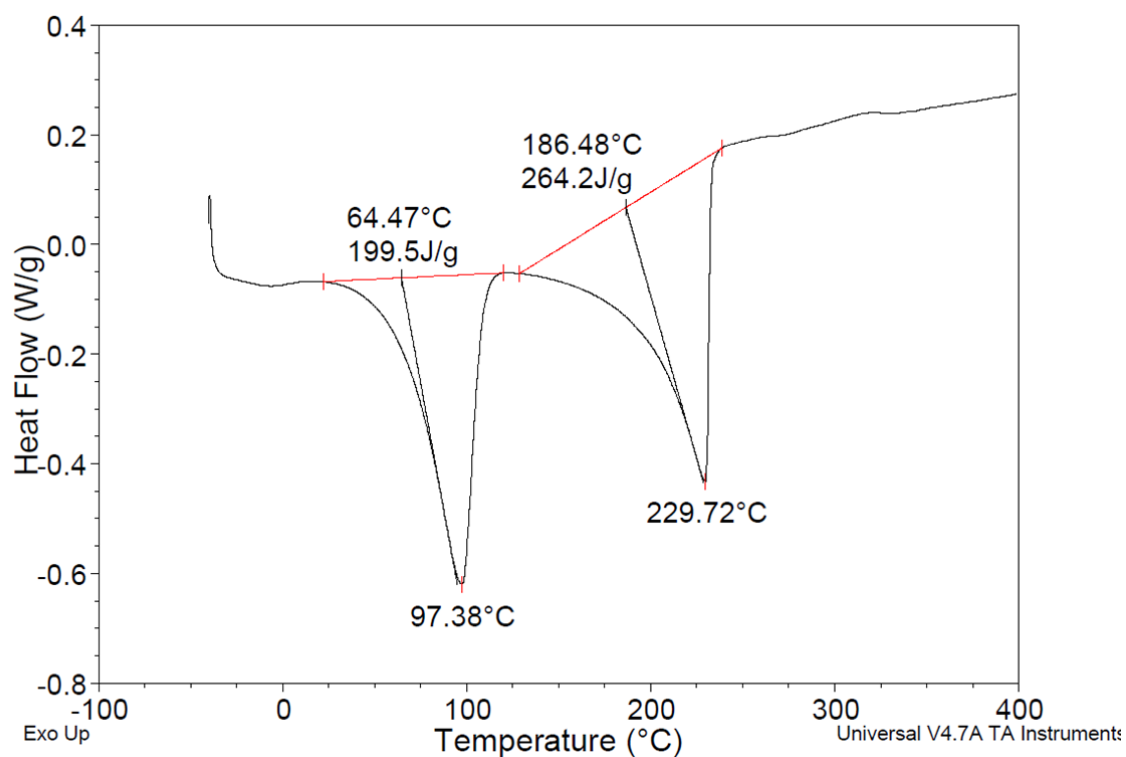
Figure 2.8. The DSC of TPSA, highlighting the enthalpy of reversal, reversal temperature, and degradation/evaporation temperature.

Table 2.1. Summary of the DSC results for the one-component ionic liquids.

Ionic Liquid	T_{rev} (°C)	ΔH_{rev} (J/g)	T_{evap} (°C)
TMSA	65	690	210
TESA	60	500	220
TEtSA	70	270	160
TPSA	65	200	190
THSA	50	150	250
FSA	50	150	160
EMSA	40	--	--

The interpretation of DSC results for liquid samples is much more convoluted than the interpretation of DSC for solid samples. The enthalpy of reversal describes the enthalpy of the reaction (energy required to reverse the reaction creating CO_2) combined with the enthalpy of desorption (energy required for CO_2 to desorb out of the liquid) and some enthalpy of vaporization (energy required to evaporate the molecular liquid after reversal). Additionally, as some of the ionic liquid is reversed back to the molecular liquid, another process could be occurring where the unreacted amine solvates the ionic liquid and dissociates the ions resulting in an enthalpy of dissociation. Although the enthalpy of reaction is likely to be the largest contributor to the overall enthalpy of reversal, it is difficult to extract much practical information from the DSC.

An important consideration in the interpretation of DSC data is the temperature profile, as it has a strong effect on the broadness of the peaks and temperatures at which transitions occur. The 5°C/minute ramp was chosen because it gives highly reproducible results in terms of temperatures and peak shapes for all materials tested. For example, the reversal temperature, which is found from the intercept of the tangent of the peak to the baseline of the peak, was found to be 64°C for TPSA using the method described here. The reversal temperatures for the materials TMSA, TESA, TEtSA, and TPSA were reported using a temperature profile of 20°C/minute or 30°C/minute, and found to be 60-100°C higher than the values reported here.[17,18] Nevertheless, the DSC can be very useful for determining trends among compounds when the method applied is consistent.

The last value of importance is the temperature of evaporation/degradation which corresponds to the second endotherm in the DSC. It is again, found from the intercept of the tangent with the baseline and found to be 186°C for TPSA. For all the

ionic liquids, the evaporation/degradation temperature is more than 150°C than the reversal temperature. This observation suggests that a "clean" reversal is observed, where the solvent reversal occurs at a drastically different temperature than the loss of the solvent.

Nile Red Polarity Measurements

Solvatochromism is the study of a response of a molecular probe when exposed to radiation, where the wavelength of light absorbed is related to some physical or chemical property of the solvent environment surrounding the probe. The probes are always very dilute in a solvent, such that no probe molecules can interact with one another and the presence of the probe doesn't alter the properties of the solvent. The probe molecule is "excited" by the exposure to radiation, and the wavelength of maximum absorbance is related to the energy of this "excited" state. The energy of the excited state is altered by the surrounding solvent environment. Therefore, the molecular probes used in solvatochromic studies enable researchers to probe specific solvent properties on a molecular level. Solvatochromic probes have successfully been applied to determining solvent polarity, acidity, and basicity.[19] However, many probes can react with solvents that contain dissociable protons, prohibiting their use in reactive solvents such as reversible ionic liquids.

The Nile Red probe (Figure 2.9) has been successfully applied to determine the relative polarity of ionic liquids containing dissociable protons, and was therefore chosen to examine reversible ionic liquids.[20]
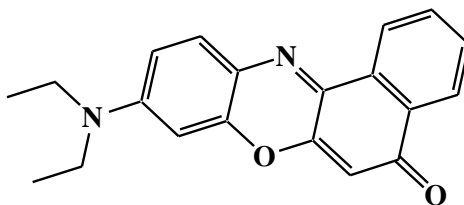
Figure 2.9. The structure of the molecular probe Nile Red; where the wavelength of maximum absorption is used to determine the relative polarity of the molecular and ionic liquids.

The Nile Red experiments show for the one-component systems that the conversion from the molecular solvent form to the ionic form results in a drastic change in polarity (Figure 2.10).
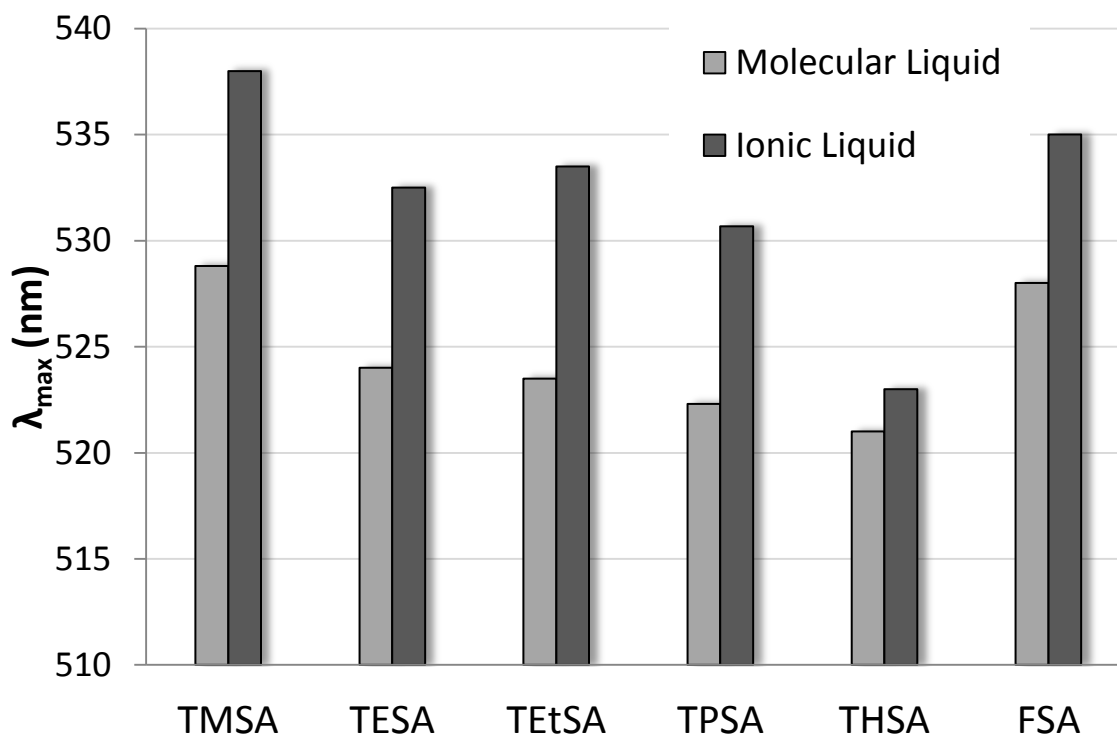
Figure 2.10. The relative polarity of the molecular and ionic liquid forms of the one-component reversible ionic liquids, expressed as the wavelength of maximum absorption (λ_{max}, nm) of the Nile Red probe in the solvent.

The change in polarity is due to the formation of the ionic species, and it is observed that the magnitude in change of polarity as the molecular liquid is converted to the ionic liquid decreases as the carbon density on the silicon is increased. Additionally, the relative magnitude of the polarity of either the molecular or the ionic liquid form decreases as the carbon density on silicon increases. The molar volume of the ionic charge is unchanged for all the species, but the molecules become more lipophilic (less polar) as more carbons are placed on the silicon. In the case of THSA, the ionic charge is so isolated by the long hydrocarbon chains that there is a very small change in polarity between the molecular and ionic liquids.

Refractive Index

The refractive indices of both the molecular and ionic liquid forms were measured using a Reichert Arias 500 Abbe-style refractometer, connected to a circulated cooling bath with glycol as the heat transfer fluid, enabling measurements from 0°C to 75°C. The refractometer is a semi-automatic design which eliminates the need for users to interpret the shadowline intercept, resulting in an accuracy of ±0.0001 regardless of user. This is important because the refractive index can be used to describe the composition of the prepared samples, i.e. the extent of conversion from molecular liquid to ionic liquid, in order to perform experiments as a function of conversion or to ensure consistent product formation among separate researchers. In addition to being a simple and effective assay of composition, the refractive index information plays a pivotal role in understanding the reflectance spectroscopy of materials, as discussed in great detail in Chapter 3.

The refractive indices for the molecular liquids are given in Figure 2.11 and the refractive indices of the ionic liquids are given in Figure 2.12. All measurements were run in triplicate, and the error bars are within the size of the data point symbols.
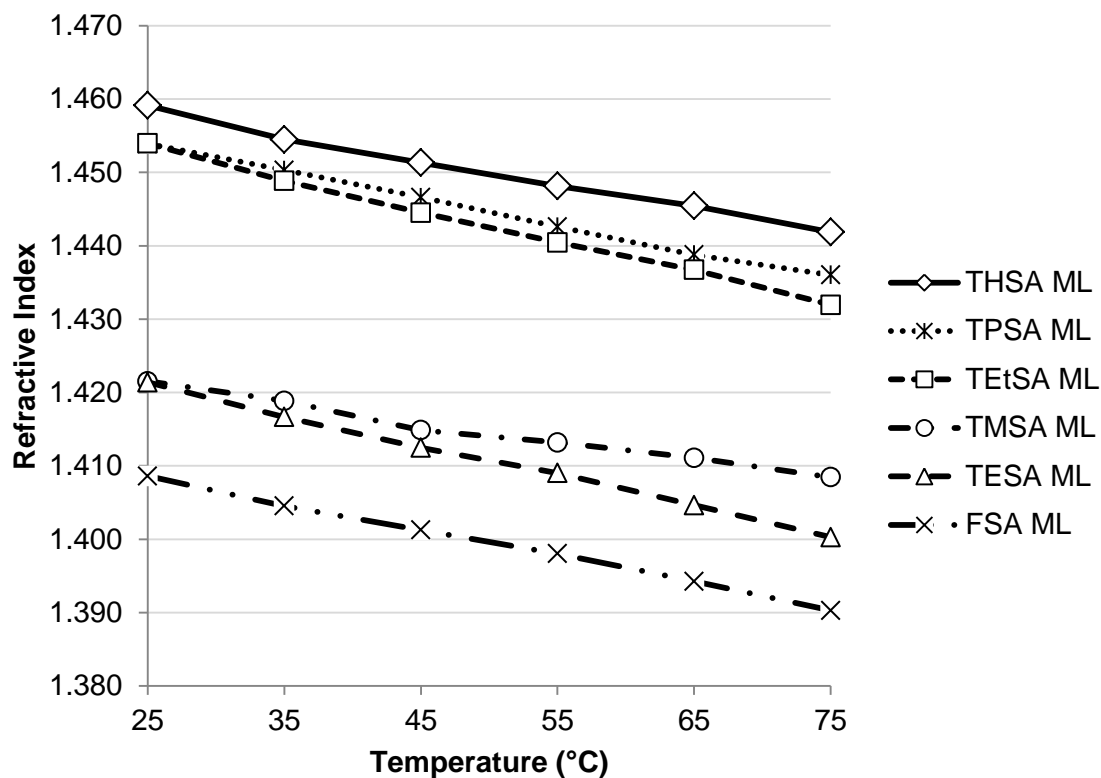
Figure 2.11. The refractive indices of the molecular liquid forms of the one-component reversible ionic liquids as a function of temperature.

The refractive indices for both molecular and ionic liquid forms decrease linearly with respect to temperature, consistent with published results regarding the thermal effect on refractive indices of conventional (non-reversible) ionic liquids.[21] Although the samples become much less stable at higher temperatures, the error bars are within the size of the data point symbols. This is likely attributed to the high accuracy of the equipment and reproducible sample formation and experimental procedure.

The refractive index change (ΔRI) that arises from the conversion of the molecular liquid to ionic liquid samples is approximately 0.02 for a specific structure at a fixed temperature. Because the refractometer has an accuracy of ±0.0001, the refractive

index of a mixture of molecular and ionic liquid can be used to determine the conversion to a precision of ±0.5%. Due to the small sample size requirement, rapid acquisition, and availability of the refractometer, it serves as a viable option to ^{1}H NMR for the determination of molecular liquid to ionic liquid conversion.
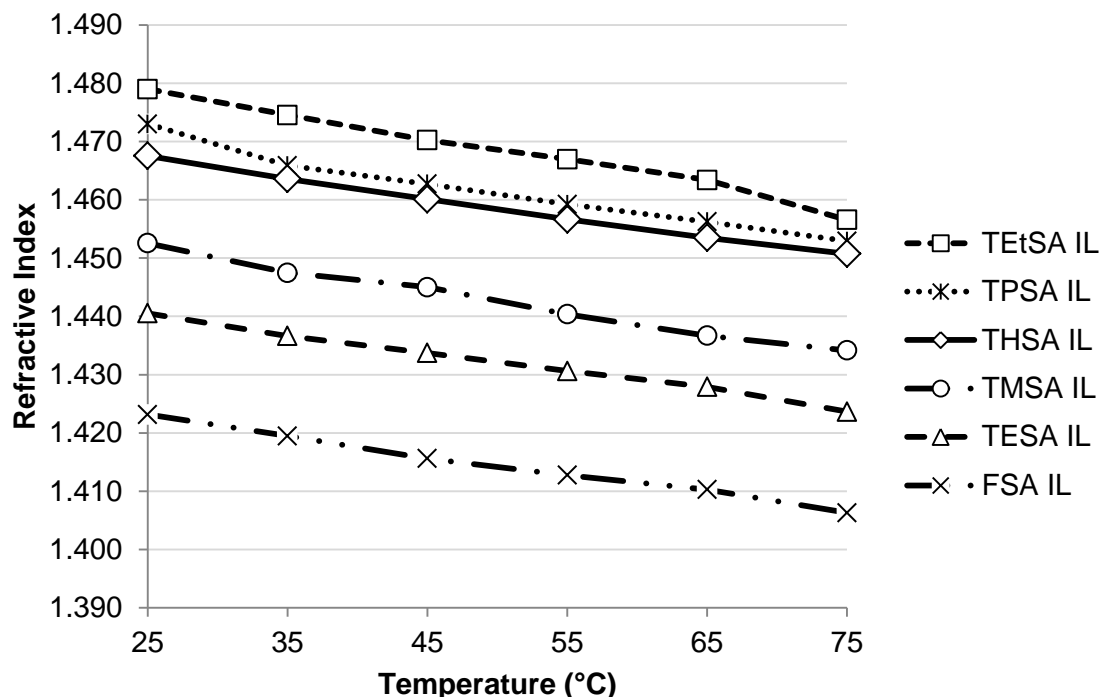
Figure 2.12. The refractive indices of the ionic liquid forms of the one-component reversible ionic liquids as a function of temperature.

The use of refractive index to determine composition relies on either knowledge of the refractive index change as a function of composition determined via another technique or the application of mixing rules to the pure component (molecular liquid or ionic liquid) refractive index information. Of all the mixing rules applied to predicting the refractive index of a binary mixture, the Lorentz-Lorenz volumetric mixing rule has shown to be the most accurate for a broad range of liquids and temperatures.[22] The Lorentz-

Lorenz mixing rule applied to a binary mixture is given,

$$\frac{n_{12}^2 - 1}{n_{12}^2 + 2} = \phi_1 \frac{n_1^2 - 1}{n_1^2 + 2} + \phi_2 \frac{n_2^2 - 1}{n_2^2 + 2} \qquad (2.1)$$

where n_{12} is the refractive index of the mixture, n_i is the refractive index of the pure species, and Φ_i corresponds to the volume fraction of that species given,

$$\phi_1 = \frac{x_1 v_1}{\sum_i x_i v_i} \qquad (2.2)$$

where x is the mole fraction and v is the molar volume of component i.

Carballo and coworkers released an extensive study that examined the refractive index of binary mixtures of ionic liquids and organic solvents, and used the information to determine the validity of the Lorentz-Lorenz mixing rule for determining composition from the refractive index of the mixture.[23] They studied two ionic liquids and five organic solvents having a broad range of refractive indices, molar volumes, and dielectric constants. The conclusion from the paper was that the Lorentz-Lorenz mixing worked extremely well for predicting the composition; in most cases the error from the mixing rule prediction was within the experimental error of their composition assays. In the worst case, the error of the mixing rule approximation was less than ±5% of the experimentally determined value.

A graph showing the calculated mixture refractive index versus mole fraction of ionic liquid is shown for the TPSA molecular to ionic liquid conversion at 25°C, given in Figure 2.13. Two approximation techniques are shown, (1) the Lorentz-Lorenz mixing rule and (2) linear with respect to mole fraction. It can be seen from Figure 2.13 that using a linear approximation for determining composition from the experimentally measured refractive index of the mixture could result in serious deviation from the Lorentz-Lorenz mixing rule, as much as 50%. Thus, the refractive index for the binary

mixture of molecular and ionic liquid can be an effective tool for determining the composition when applying the Lorentz-Lorenz mixing rule.
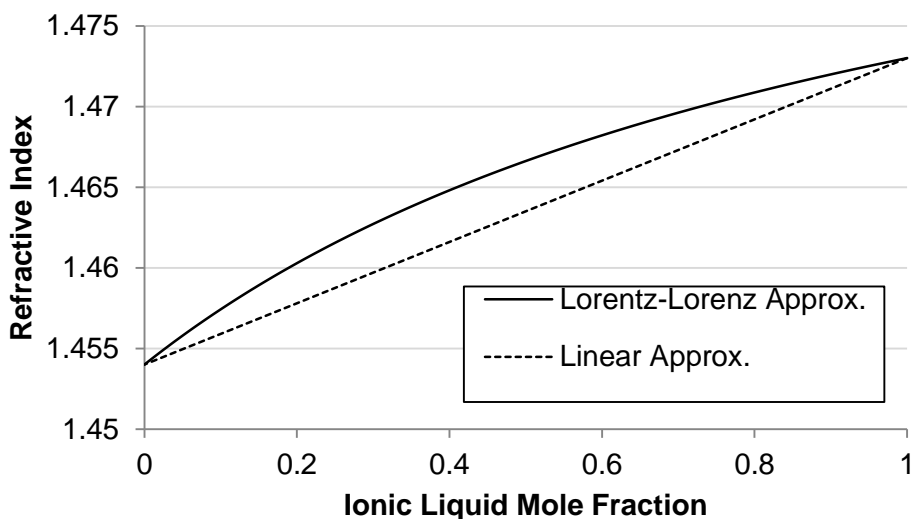
Figure 2.13. Plot of refractive index versus ionic liquid mole fraction for TPSA at 25°C.

<u>Density</u>

Density measurements were performed using an Anton Paar DMA 38 density meter capable of measurements from 15°C to 40°C with an accuracy of ±0.001 g/mL. This style of densitometer is a vibrating tube densitometer; containing a "U-shaped" tube that is vibrated at its natural frequency. When a sample is placed inside the tube, the frequency of vibration is dampened proportional to the density of the sample. This is important because the reversible ionic liquids are unstable, and the vibrations have resulted in reversal and the formation of CO_2 "pockets" in the sample. The densitometer records measurements when a stable density is observed over a 15 second period. The design of the densitometer limited the measurement of the ionic liquids at higher

temperatures, except for TEtSA which was successfully analyzed up to 40°C.

The densities of the molecular liquids were measured from 25°C to 40°C, and are shown in Figure 2.14. The densities of TEtSA, TPSA, and THSA are all very close in value, with substantially higher densities observed for the TMSA, TESA, and FSA molecular liquids. The molecular liquid densities as a function of temperature appear to follow a linear trend, although the temperature range examined is very limited and gross errors could be observed if extrapolations deviate far from this range.
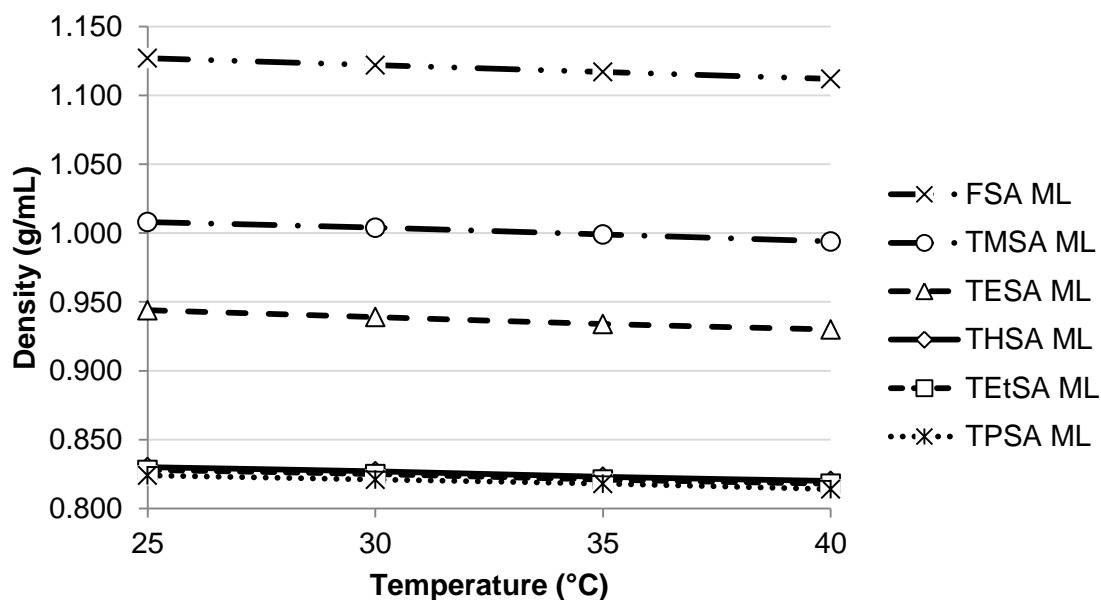
Figure 2.14. The one-component molecular liquid densities as a function of temperature.

The densities of the ionic liquids are given in Figure 2.15. The TEtSA ionic liquid sample was the only material that was successfully measured over the entire temperature range, and the two alkoxy- materials were successfully measured only at 25°C. Due to the operation of the densitometer, the vibrations caused pockets of CO_2 to

be formed and rise to the interface of the liquid and vibrating tube, causing the density to fluctuate and the densitometer was not able to converge on a density reading within the specifications of density stability.
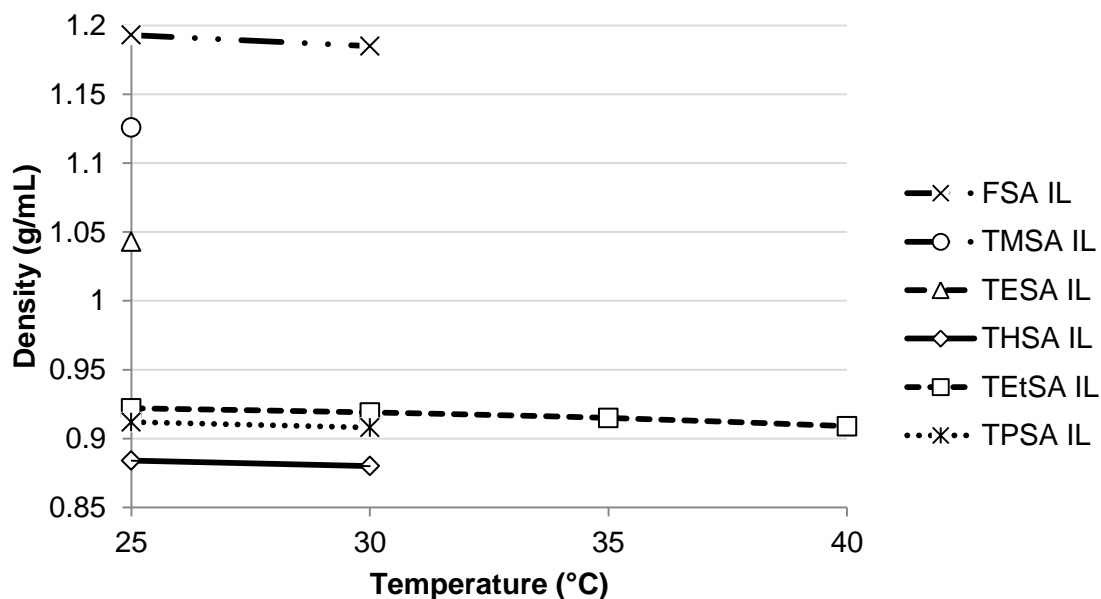
Figure 2.15. The one-component ionic liquid densities as a function of temperature.

The density of the TEtSA ionic liquid appears to decrease linearly with respect to temperature. This trend has been observed to be true for conventional room temperature ionic liquids (non-reversible) over broad temperature ranges.[21,23] All materials exhibit a change in density of approximately 0.075 g/mL as they are converted from the molecular liquid to ionic liquid, consistent the addition of carbon dioxide that results in the increase in molecular weight.

<u>Stability of Molecular Liquid</u>

The presence of water can result in the cleavage of the Si-O-C bond in the trialkoxysilylpropylamines (TESA, TMSA). The trialkylsilylpropylamines (TEtSA, TPSA, THSA, FSA) were developed to overcome this shortcoming, as water is present in a broad range of chemical processes and feedstocks. Stability tests were performed on TESA and TEtSA to compare the relative water and oxygen resistance in an attempt to estimate the shelf-life of the materials. Three samples of each material were prepared: (1) a reference stored under argon, (2) 10% water under air, and (3) 0% water under air. Aliquots were taken weekly and examined with ^{1}H NMR to determine the extent of degradation, if any.

The trialkoxy- material TESA showed no degradation over the course of two months in either sample that was free of water, (1) and (3). The sample containing 10% water exhibited significant degradation after the first week (approximately 5%). The integration results for the degradation products were only semi-quantitative, as the structure(s) of the degradation product(s) wasn't confirmed. After two weeks, the TESA sample containing 10% water exhibited twice the degradation of that for week 1. The weeks following showed no further degradation. This is due to all of the water in the sample being consumed by the degradation reaction pathway. It is likely that if water were continuously provided to the trialkoxy- materials, degradation would result in the loss of all of the molecular liquid.

The trialkyl- material TEtSA showed no loss of structural integrity over the period of several months in all three samples. This is an important observation for the application of the one-component reversible ionic liquid solvents to applications where water is present, required, or produced. Additionally, stability in aqueous and oxygen containing environments is promising for the industrial viability of the materials.

Two-component Reversible Ionic Liquids

Materials

      All materials in this section were reagent grade purchased from Sigma-Aldrich, unless otherwise stated. The tetramethylurea, oxalyl chloride, and butylamine were stored in a nitrogen filled glove box prior to use. The 1,8-Diazabicyclo[5-4-0]undec-7-ene (DBU) (Sigma-Aldrich, 98%) was received as a yellow-ish liquid, and vacuum distilled to produce a clear liquid that was determined to be pure by ^{1}H NMR. Carbon dioxide was supercritical fluid chromatography (SFC) grade (Air Gas, 99.999%) and further purified via a Matheson gas purifier and filter cartridge (Model 450B, Type 451 filter).

Synthesis of N,N,N',N'-tetramethyl-N"-butylguanidine (TMBG)

      The general reaction scheme for the synthesis of N,N,N',N'-tetramethyl-N"-butylguanidine (TMBG) is shown (Figure 2.16).
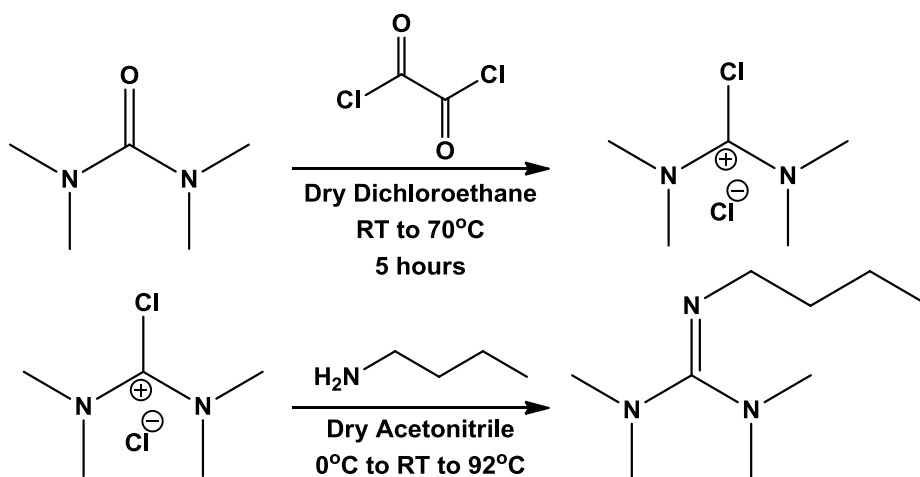
Figure 2.16. The multi-step synthetic procedure for N,N,N',N'-tetramethyl-N"-butylguanidine (TMBG).

Tetramethylurea (0.08 mol) was stirred in dry dichloroethane (80 mL) for approximately 5 minutes. More than 2 equivalents of oxalyl chloride (0.18 mol) were slowly added to the reaction mixture as the reaction is highly exothermic. The mixture was then refluxed at 60°C for 5 hours. The dichloroethane solvent was then removed via vacuum after the mixture cooled to room temperature. The dry acetonitrile (75 mL) was used to dissolve the dichloride intermediate. The reaction vessel was then cooled to 0°C. Two equivalents of butylamine (0.16 mol) were dissolved in 15mL of dry acetonitrile and the mixture was added dropwise to the dissolved dichloride intermediate, again to limit the heat generated by the reaction. After the reaction warmed to room temperature, it was refluxed at 92°C for 1 hour. The solvent was then removed with a rotary evaporator, and the residue was treated with 30 mL of 30% aqueous sodium hydroxide (NaOH). The product was then extracted with diethyl ether three successive times using 20 mL of ether each time, dried with magnesium sulfate ($MgSO_4$), and concentrated to give a yellow-ish oil. The final TMBG product was obtained by vacuum distillation to obtain a clear liquid. The overall yield was found to be 80%. The NMR and elemental analyses of TMBG are given:

N,N,N',N'-tetramethyl-N''-butylguanidine: ^{1}H NMR ($CDCl_3$): 0.784 (t, 3), 1.22 (m, 2), 1.39 (m, 2), 2.53 (s, 6), 2.62 (s, 6), 2.99 (t, 2). ^{13}C NMR ($CDCl_3$):13.69, 20.32, 34.26, 38.39, 39.36, 48.69, 161.45. DEPT-135 (neat): up-13, 40, 42, 49; down-23, 36, 50. Elemental analysis: Expected; C(59.37), H(11.96), N(20.77) Actual; C(59.21), H(12.3), N(21.5)

Relative to the synthetic procedure for the one-component silyl-amine based reversible ionic liquids, the synthesis of TMBG is much more complicated, generates significantly more amounts of waste, and is extremely sensitive to moisture. In fact, if the reaction mixture is exposed to the atmosphere for even small amounts of time (up to the

step where the aqueous NaOH is added) the reaction will be ruined, as evidenced by the reaction mixture turning a dark brown color. The optimized procedure described here is a result of the tenacious work of a former co-worker, Hillary Huttenhower. For a more detailed description of the synthetic development, as well as examples of modifications made to the structure of TMBG, please see Hillary Huttenhower's PhD Thesis (Prof. Liotta, Georgia Tech, 2010).

Formation of Ionic Liquid

Just as with the one-component system, the two-component reversible ionic liquids are prepared by bubbling CO_2 through equimolar solutions of TMBG or DBU and various alcohols (from methanol to dodecanol) (Figure 2.1 and Figure 2.2).

The neutral solvent mixtures of either TMBG/alcohol or DBU/alcohol are prepared with approximately 5% excess alcohol when using C_1-C_4 alcohols (methanol, ethanol, n-propyl alcohol, and butanol) because small chain-length alcohols have higher vapor pressures and would be the majority of solvent lost due the high exotherm of the reaction. Approximately 1-2 mL of the mixed neutral solvent mixture is placed in a 2 dram vial that has been capped with a rubber septum and purged with argon for 10 minutes, to ensure no moisture is present. Water present can react with the CO_2 to form the bicarbonate, which is more stable than the alkylcarbonate and can drastically alter the observed properties of the ionic liquid. For example, even small amounts of water (<1%) in the DBU/alcohol systems results in solid salt formation. The CO_2 is fed through the liquid by using a 10 gauge needle that reaches to the bottom of the vial, making sure to vent the vial in order to prevent pressure build up and loss of the septa seal. As with the one-component reversible ionic liquids, the resulting two-component ionic liquids are highly viscous.

The reversible formation of the ionic products was characterized by ^{1}H and ^{13}C NMR, FT-IR, melting points, differential scanning calorimetry (DSC), conductivity measurements, and Nile Red polarity measurements.

<u>^{1}H/^{13}C NMR</u>

The NMR experiments for the two-component reversible ionic liquids were run at room temperature using a Varian-Mercury VX 400MHz spectrometer located in the Georgia Tech Institute of Bioengineering and Bioscience. The NMRs for both the molecular and ionic liquids were performed by diluting the sample in deuterated chloroform ($CDCl_3$). The ionic liquid samples were prepared as described above, and due to the high viscosity were first diluted in $CDCl_3$ before being transferred to the NMR tube.

The ^{1}H NMR for an equimolar mixture of TMBG and methanol molecular liquid is given in Figure 2.17. Note the two intense peaks at *ca*. 3.0 ppm, corresponding to the inequivalent protons located on the four methyl groups of the guanidine. Asymmetry is introduced by the presence of the butyl group on guanidine, resulting in separation of the methyl protons.

The ^{1}H NMR of an equimolar mixture of TMBG and methanol is shown in Figure 2.18, where the molecular liquid is only partially converted to the ionic liquid. Note the convergence of the two separate peaks at *ca*. 3.0 ppm to one peak. This is due to the resonance stabilization of the double bond in guanidine, resulting in rotation of the molecule across the bond and symmetry of the methyl protons on the nitrogens. The appearance of another peak is also evident at *ca*. 4.0 ppm, corresponding to the methyl protons of the carbonate formed upon the reaction of the alcohol with CO_2. The ^{1}H NMR can be successfully used to determine the conversion of the molecular liquid to ionic

liquid by taking the ratio of the numbers of protons for the alkyl-carbonate (4.0 ppm) to

the protons for the unreacted alcohol at *ca*. 3.6 ppm.
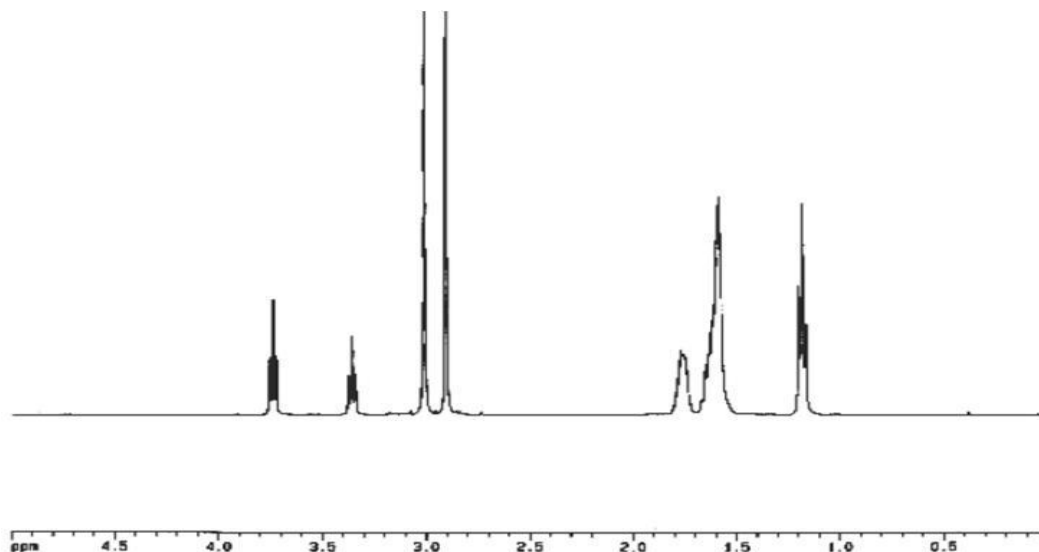
Figure 2.17. The ^{1}H NMR of an equimolar mixture of TMBG and methanol molecular liquid.
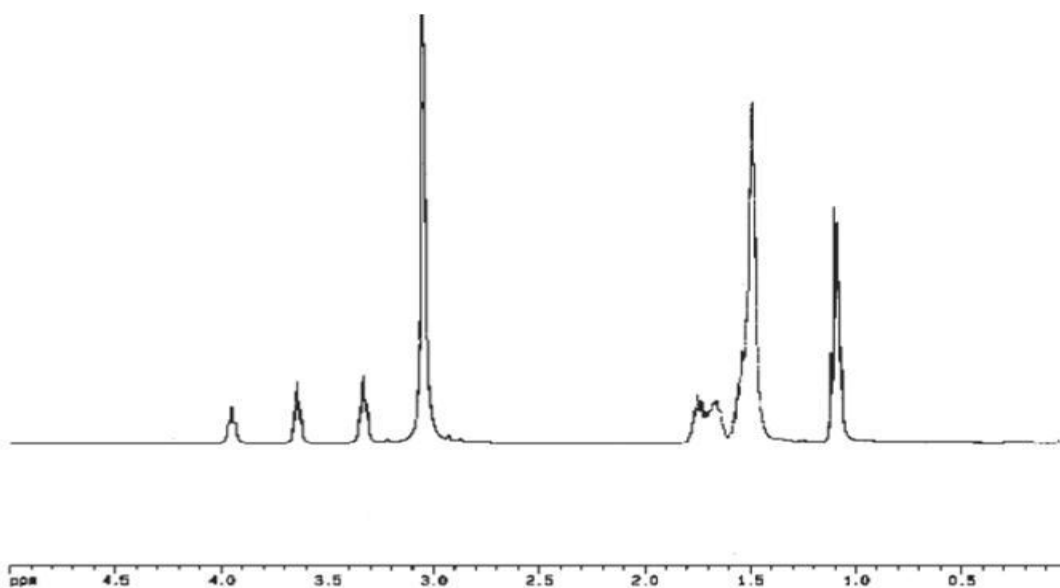
Figure 2.18. The ^{1}H NMR of an equimolar mixture of TMBG and methanol, partially converted to ionic liquid.

The FT-IR spectra for the two-component reversible ionic liquids were obtained using a Bruker Vector-22 with a Spectra-Tech Tunnel ATR cell, with a scan range of 400-4000 cm^{-1} and a resolution of 2 cm^{-1}. The Tunnel ATR cell is a type of cylindrical internal reflectance cell that utilizes a zinc selenide (ZnSe) optical crystal running parallel to the infrared radiation resulting in multiple reflections of the infrared signal along the length of the cylinder (approximately 10 reflections). The result of multiple reflections is enhanced sensitivity. However, the design of the cell limits the application to high pressure systems utilizing ionic liquids because the seal at the crystal-reactor interface is achieved by a circular Teflon spring seal. The seal is prone to leaking at high pressures, and can contribute to errors in the background scan by trapping some previous sample material between the seal and crystal. Additionally, due the high viscosity of the ionic liquids, the sample cell had to be completely disassembled to allow for thorough cleaning adequate to achieving sufficient background scans. Regardless of experimentation difficulties, a spectrum for the reaction of TMBG and methanol with CO_2 to form the ionic liquid is shown in Figure 2.19.

The experiment that was conducted to obtain the spectrum in Figure 2.19 involved starting with an equimolar mixture of TMBG and methanol under a headspace of nitrogen at room temperature and a pressure of 0 gauge, giving the "No CO_2" line. The "No CO_2" spectra shows a broad peak from 3000-3300 cm^{-1}, corresponding to the O-H stretch vibration of the alcohol. The cell was then charged with 20 bar of CO_2, and a spectrum was collected immediately, yielding the "20 bar (initial)" spectrum. It can be seen in the "initial spectrum" the immediate appearance of a sharp peak at 2400 cm^{-1} for the asymmetric stretch vibration of CO_2, the appearance of two sharp shoulders at 1700 cm^{-1} for the hydrogen bonded and non-hydrogen bonded carbonyl stretch vibration (from

the carbonate), and the disappearance of the alcohol stretch vibration; all consistent with the reaction of the molecular liquid and CO_2 to form the ionic liquid. The "10 minute" scan shows a slight decrease in the asymmetric stretch of CO_2, corresponding to further reaction of CO_2 with the molecular liquid. And at equilibrium, the concentration of unreacted CO_2 in the solvent is below the detection limit. Equilibrium was determined when the spectra was unchanged for 30 minutes.
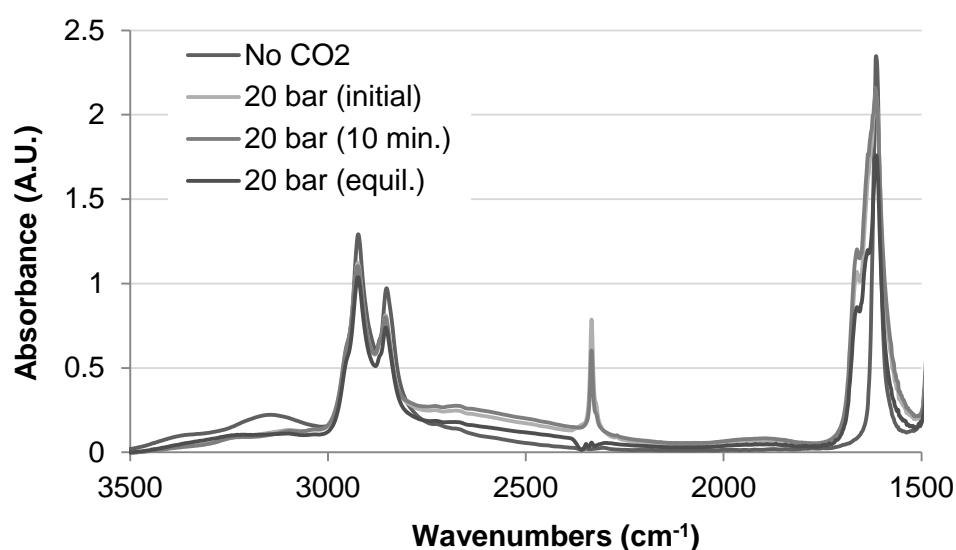
Figure 2.19. The ATR FT-IR spectra showing the conversion of molecular TMBG/methanol to the ionic form.

Differential Scanning Calorimetry (DSC)

The DSC was performed using a Q20 TA Instruments DSC using platinum hermetic pans. The sample size was < 5 mg, and the temperature profile was operated from 25°C to 300°C at a temperature ramp rate of 20°C/minute with a convective nitrogen flow of 50 mL/min. The DSC for the ionic liquid of TMBG and methanol is shown

in Figure 2.20.

The DSC of the TMBG/methanol ionic liquid shows two distinct peaks that overlap; one peak with a maximum at 75°C and the other peak with a maximum of 125°C. The two peaks correspond to the reversal of the ionic liquid and the evaporation of the methanol. The loss of the solvent clearly accompanies the loss of CO_2, which is problematic for processing as another processing step would need to be utilized in order to separate the solvent from the CO_2.
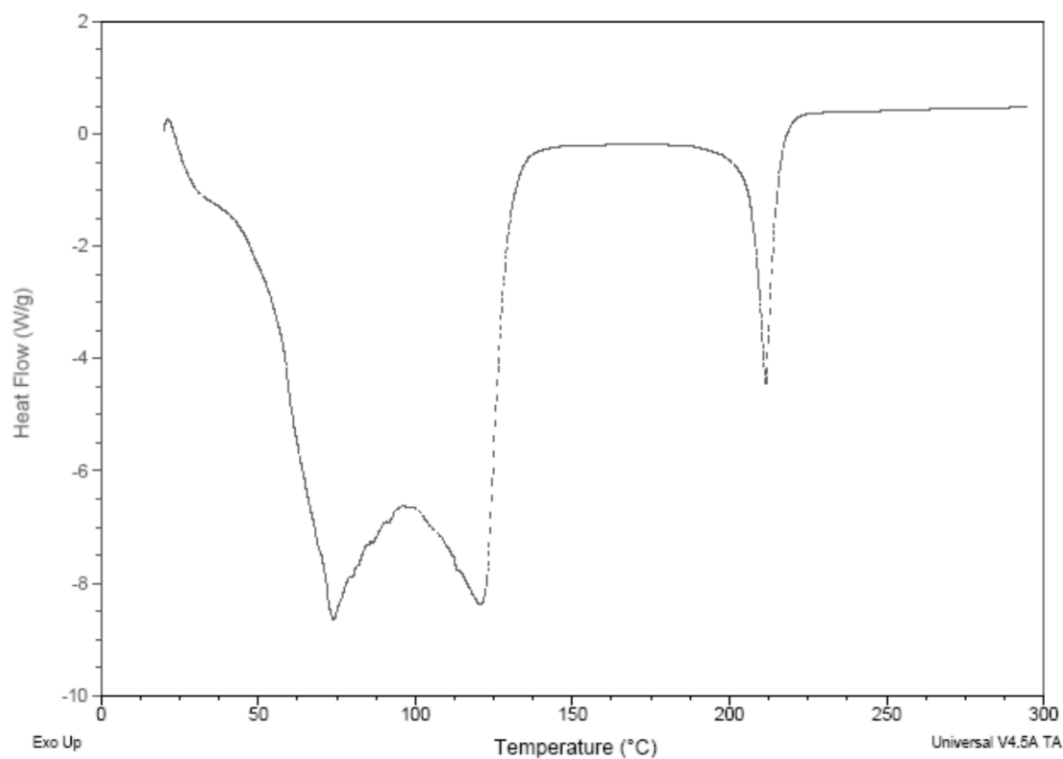
Figure 2.20. The DSC thermogram for the TMBG/methanol ionic liquid.

<u>Nile Red Polarity Measurements</u>

Equimolar mixtures of DBU/alcohol or TMBG/alcohol become significantly more polar when exposed to CO_2, as shown by the shift of the λ_{max} to longer wavelengths (Figure 2.21). For example, the TMBG/methanol mixture exhibits a λ_{max} of 538 nm while the λ_{max} of the corresponding ionic liquid (N,N,N',N'-tetramethyl-N"-butylguanidinium methylcarbonate) is 554 nm, corresponding to a shift of 16 nm. Such a shift in λ_{max} represents a polarity switch akin to going from chloroform to acetic acid. The Nile Red experiments suggest that the polarity of both molecular and ionic forms depend on the length of the alkyl chain on the alcohol. However, the reported λ_{max} values fall well within the range found for non-switchable ionic liquids.[24,25]
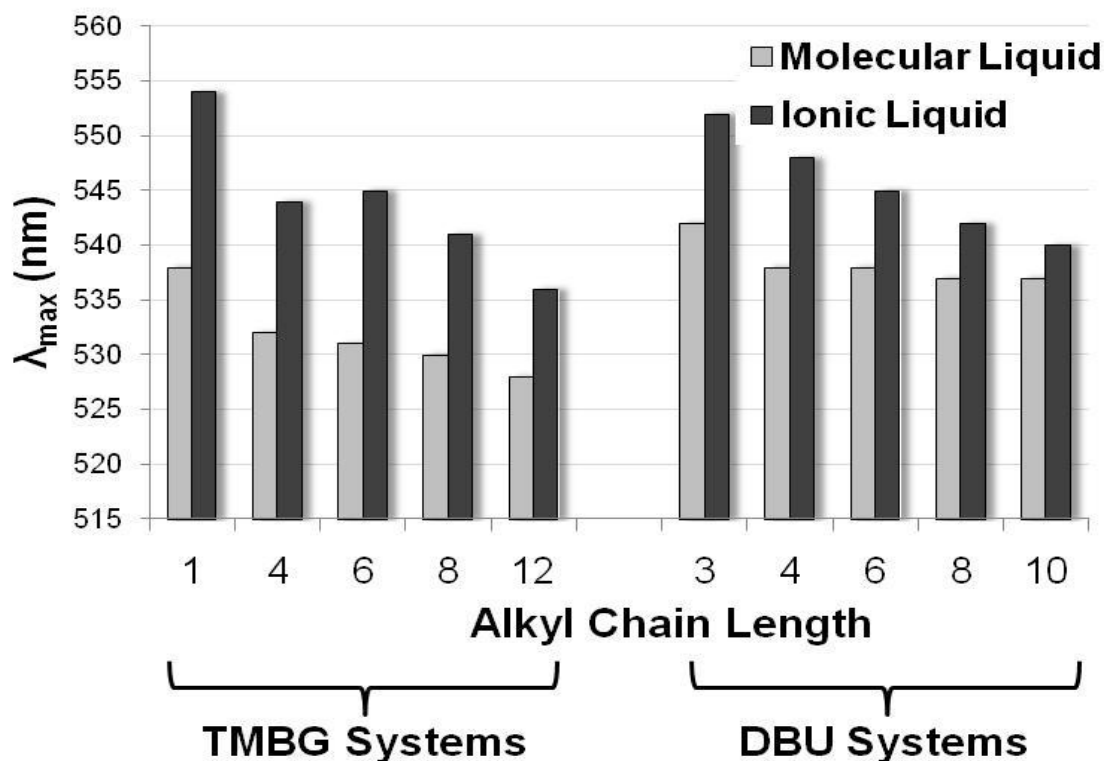
Figure 2.21. The polarity of the neutral and ionic forms of the DBU/alcohol and TMBG/alcohol solvents as a function of the alcohol chain length.

45

The many possible combinations of base and alcohol give a wide selection of solvent switches. Using shorter alcohols gives a greater difference between the polarities of the ionic and neutral forms of the solvent. Furthermore, switchable solvents based on TMBG have a larger switch in polarity compared to those based upon DBU; the ionic forms of the two systems are nearly comparable while the neutral form of TMBG is significantly less polar than that of DBU.

Melting Points
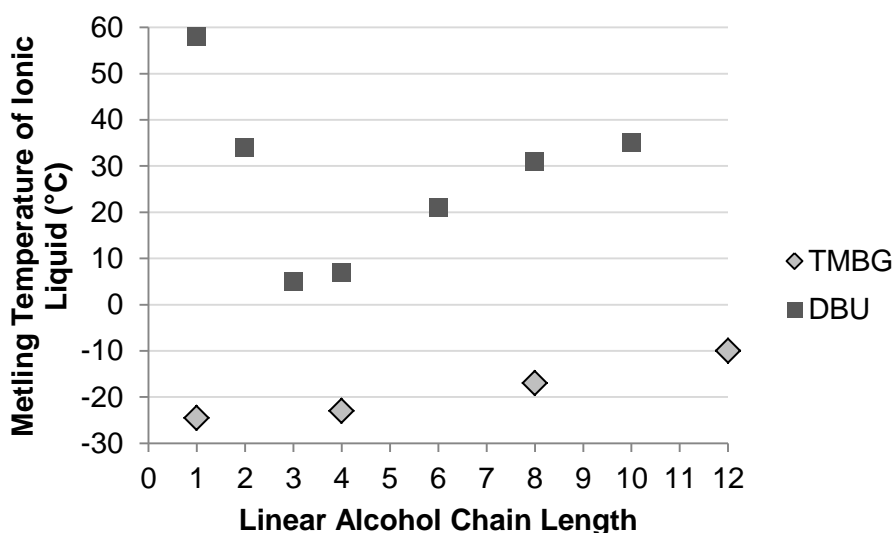
Figure 2.22. The melting points of TMBG or DBU ionic liquids formed with the reaction of CO_2 and linear alcohols ranging from methanol (C_1) to dodecanol (C_{12}).

The melting points of the ionic liquids were determined by first combining an equimolar amount of either TMBG or DBU and the specified alcohol in an NMR tube, forming the ionic liquid by vigorously bubbling CO_2 through the solution, and then

capping the NMR tube with a septa and sealing with parafilm. This tube was placed into a round bottom flask filled with isopropanol containing a thermometer, and placed into a dry ice/acetone bath to induce freezing of the ionic liquid. The isopropanol flask containing the ionic liquid in an NMR tube was then allowed to heat slowly until the melting was observed. This procedure was performed three times for each sample.

Conductivity

Conductivities were measured using a ThermoOrion Model 115 Meter. An equimolar solution of TMBG and methanol (5.56 mmol) was dissolved in approximately 4mL of $CDCl_3$. The CO_2 was then bubbled through the solution and conductivity measurements were taken (Figure 2.23).
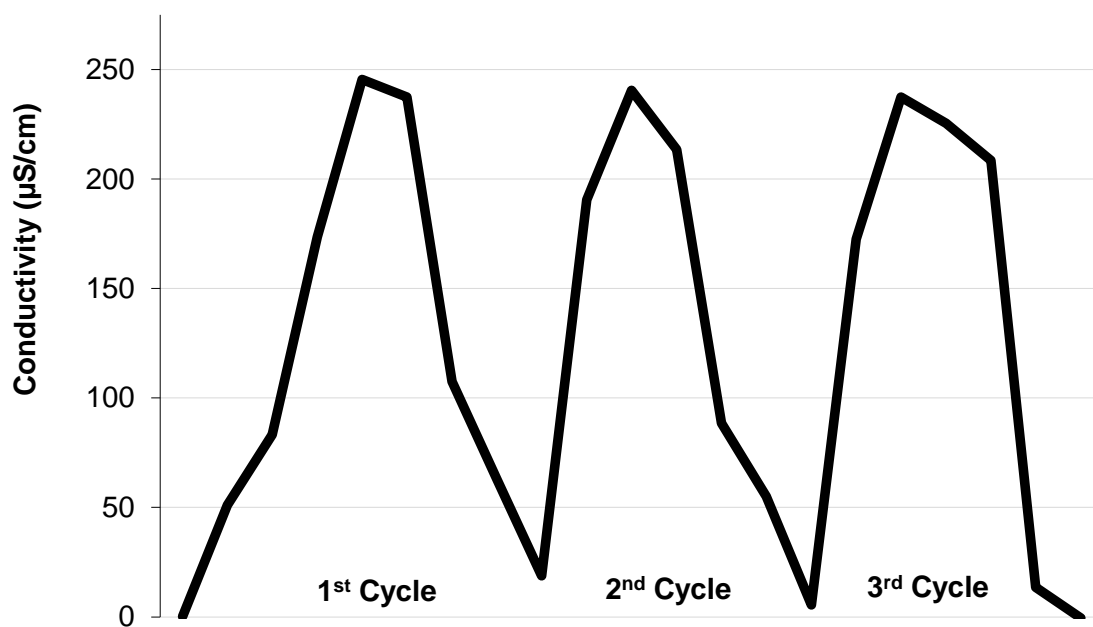
Figure 2.23. The conductivity (µS/cm) of TMBG/methanol in CDCl$_3$ solvent as a function of CO$_2$ addition and the thermally driven elimination.

At the beginning of the experiment, the equimolar mixture of TMBG/methanol in chloroform is a poor conductor (0 μS/cm). As CO_2 is bubbled into the solution, conductivity increases sharply to 250 μS/cm. This is consistent with the formation of the ionic species. Upon heating, the solution conductivity decreases to approximately 0 μS/cm, confirming the complete reversal of the ionic liquid to the molecular liquid. The conductivity measurements clearly demonstrate the reversibility and repeatability of the formation of the ionic versus molecular species for three consecutive cycles.

Conclusions

Presented here are the complete synthesis and characterization of two classes of switchable solvent systems: one-component reversible ionic liquids and two-component reversible ionic liquids. From a processing standpoint, the one-component system is superior to the two-component system due to the elimination of the need for stoichiometric alcohol. With the two-component system, the DSC results indicated that some of the alcohol is lost with the release of CO_2 (especially the lower MW alcohols). However, for the one-component system the loss of CO_2 occurs at a temperature substantially different (>100°C) from the evaporation of the molecular liquid. The one-component system also affords ease of processing and ionic liquid preparation, as the consideration of reactant stoichiometry can be ignored (when compared to the two-component systems).

In both solvent systems a significant change in solvent properties is achieved by conversion of the molecular liquid solvent to the ionic liquid solvent. With regards to solvent polarity, the switch observed in the two-component systems is more considerable than in the one-component systems. However, both systems exhibit

tunable properties with respect to structure, indicating the potential to optimize the solvent structure given a specific application.

The target application for the two-component system is the coupling of reactions and separations, discussed in great detail in Chapter 4. As for the one-component reversible ionic liquid system, the target application is carbon capture from combustion effluent, discussed in Chapter 5. Although significant advantages can be exploited by the use of these switchable solvent systems, due to the reactive nature of the solvents challenges will inevitably arise and are discussed throughout this thesis.

References

(1)   Langanke, J.; Leitner, W. In *Topics in Organometallic Chemistry (Volume 23)*; Springer Berlin/Heidelberg: 2008; Vol. 23, p 91.

(2)   Solinas, M.; Pfaltz, A.; Cozzi, P. G.; Leitner, W. *Journal of the American Chemical Society* **2004**, *126*, 16142.

(3)   Jessop, P. G.; Heldebrant, D. J.; Li, X. W.; Eckert, C. A.; Liotta, C. L. *Nature* **2005**, *436*, 1102.

(4)   Phan, L.; Chiu, D.; Heldebrant, D. J.; Huttenhower, H.; John, E.; Li, X. W.; Pollet, P.; Wang, R. Y.; Eckert, C. A.; Liotta, C. L.; Jessop, P. G. *Industrial & Engineering Chemistry Research* **2008**, *47*, 539.

(5)   Yamada, T.; Lukac, P. J.; George, M.; Weiss, R. G. *Chemistry of Materials* **2007**, *19*, 967.

(6)   Yamada, T.; Lukac, P. J.; Yu, T.; Weiss, R. G. *Chemistry of Materials* **2007**, *19*, 4761.

(7)   Yu, T.; Yamada, T.; Gaviola, G. C.; Weiss, R. G. *Chemistry of Materials* **2008**, *20*, 5337.

(8)   Gohres, J. L.; Marin, A. T.; Lu, J.; Liotta, C. L.; Eckert, C. A. *Industrial & Engineering Chemistry Research* **2009**, *48*, 1302.

(9)   Dibenedetto, A.; Aresta, M.; Fragale, C.; Narracci, M. *Green Chemistry* **2002**, *4*, 439.

(10)   Aresta, M.; Ballivet-Tkatchenko, D.; Dell'Amico, D. B.; Bonnet, M. C.; Boschi, D.; Calderazzo, F.; Faure, R. E.; Labella, L.; Marchetti, F. *Chemical Communications* **2000**, 1099.

(11)   Hirst, L. L.; Pinkel, II *Industrial and Engineering Chemistry* **1936**, *28*, 1313.

(12)   Furstner, A.; Ackermann, L.; Beck, K.; Hori, H.; Koch, D.; Langemann, K.; Liebl, M.; Six, C.; Leitner, W. *Journal of the American Chemical Society* **2001**, *123*, 9000.

(13)   Xie, X. F.; Liotta, C. L.; Eckert, C. A. *Industrial & Engineering Chemistry Research* **2004**, *43*, 7907.

(14)   Wittmann, K.; Wisniewski, W.; Mynott, R.; Leitner, W.; Kranemann, C. L.; Rische, T.; Eilbracht, P.; Kluwer, S.; Ernsting, J. M.; Elsevier, C. L. *Chemistry-a European Journal* **2001**, *7*, 4584.

(15)   Marzinke, M.; Mac, J.; August, T.; Telepchak, M.   United States, 2001; Vol. 6,177,583.

(16)   Chalk, A. J.; Harrod, J. F. *Journal of the American Chemical Society* **1965**, *87*, 16.

(17)   Blasucci, V.; Dilek, C.; Huttenhower, H.; John, E.; Llopis-Mestre, V.; Pollet, P.; Eckert, C. A.; Liotta, C. L. *Chemical Communications* **2009**, 116.

(18)   Blasucci, V.; Hart, R.; Mestre, V. L.; Hahne, D. J.; Burlager, M.; Huttenhower, H.; Thio, B. J. R.; Pollet, P.; Liotta, C. L.; Eckert, C. A. *Fuel* **2010**, *89*, 1315.

(19)   Reichardt, C. *Solvents and solvent effects in organic chemistry*; 3rd, updated and enl. ed. ed.; Wiley-VCH: Weinheim :, 2003.

(20)   Ogihara, W.; Aoyama, T.; Ohno, H. *Chemistry Letters* **2004**, *33*, 1414.

(21)   Tariq, M.; Forte, P. A. S.; Gomes, M. F. C.; Lopes, J. N. C.; Rebelo, L. P. N. *Journal of Chemical Thermodynamics* **2009**, *41*, 790.

(22)   Mehra, R. *Proceedings of the Indian Academy of Sciences-Chemical Sciences* **2003**, *115*, 147.

(23)   Iglesias-Otero, M. A.; Troncoso, J.; Carballo, E.; Romani, L. *Journal of Chemical Thermodynamics* **2008**, *40*, 949.

(24)   Carmichael, A. J.; Earle, M. J.; Holbrey, J. D.; McCormac, P. B.; Seddon, K. R. *Organic Letters* **1999**, *1*, 997.

(25)   Carmichael, A. J.; Seddon, K. R. *J. Phys. Org. Chem.* **2000**, *13*, 591.

CHAPTER 3 A SPECTROSCOPIC TECHNIQUE FOR THE
DECOUPLED MEASUREMENT OF CHEMICAL AND
PHYSICAL ABSORPTION IN REACTIVE SOLVENT
SYSTEMS

Introduction

Reactive solvent systems offer highly selective separations, useful for processes were the species being separated is dilute in concentration. For the application to CO_2 capture, amine based solvents have received much attention. The molecular design of such solvents for the application to CO_2 capture will be discussed in Chapter 5. Presented here is the development of a reflectance spectroscopic technique for determining the physical and chemical absorption of CO_2 in the reactive solvent systems. Common techniques for examining CO_2 absorption capacities in a broad range of materials are the use of gravimetric[1-4] or volumetric[5,6] experimental apparatuses. Because only the mass/molar uptake is determined from such techniques, it is difficult to differentiate between chemical and physical absorption.

In the presence of CO_2, (3-aminopropyl)triethylsilane (TEtSA) reacts to form the carbamate (-) and ammonium (+) ionic liquid (Figure 3.1).
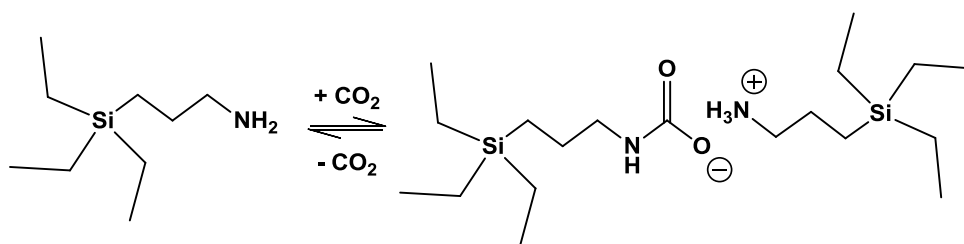
Figure 3.1. The reversible reaction of (3-aminopropyl)triethylsilane (TEtSA) with carbon dioxide (CO_2) to form the corresponding carbamate (-) and ammonium (+) ionic liquid.

52

The reaction is reversible, with the forward reaction (resulting in the formation of the ionic pair) is exothermic and the reverse reaction is endothermic. The conversion of the neutral amine to the ionic liquid is dependent on the concentration of CO_2 in the liquid phase and the temperature of the system. Once the ionic liquid is formed, considerable physical absorption of CO_2 can be achieved.

As with all analytical techniques, assumptions are made to compensate for unknown variables or to alleviate solution rigor in the quantitative ATR IR method described herein. The background on both IR and ATR spectroscopy is presented in Appendix A to provide the reader with sufficient information to evaluate the validity of the assumptions made and resulting accuracy of the technique applied to the determination of physical and chemical absorption of CO_2 in TEtSA, and the information necessary to correct for these assumptions in scenarios where the technique is applied to systems where the constraints associated with the assumptions are violated.

In order to properly apply the ATR IR technique to determine the concentration of unreacted (free) and reacted CO_2 in TEtSA as a function of CO_2 pressure (directly related to the solubility of CO_2 in solution) and system temperatures, one must first identify the key spectral changes that are observed during CO_2 dissolution and TEtSA conversion (Figure 3.2).

Three regions of interest are identified:

1. Region I (3100-2600 cm^{-1}) contains the C-H stretch vibrations in the molecular liquid sample and reveals the broad –NH_3^+ stretch vibration from the ammonium cation of the ionic liquid.

2. Region II (2400-2260 cm^{-1}) contains no vibrational bands in the molecular liquid, but clearly shows the asymmetric stretch for CO_2 (v_3 mode) with some slight overlap of the –NH_3^+ stretch that extends to about 2000 cm^{-1}.

3. Region III (1740-1520 cm^{-1}) contains the weakly absorbing N-H

deformation band in the molecular liquid and the carbonyl C=O stretch vibration from the carbamate anion of the ionic liquid. This band appears broad due to resonance with the nitrogen atom.
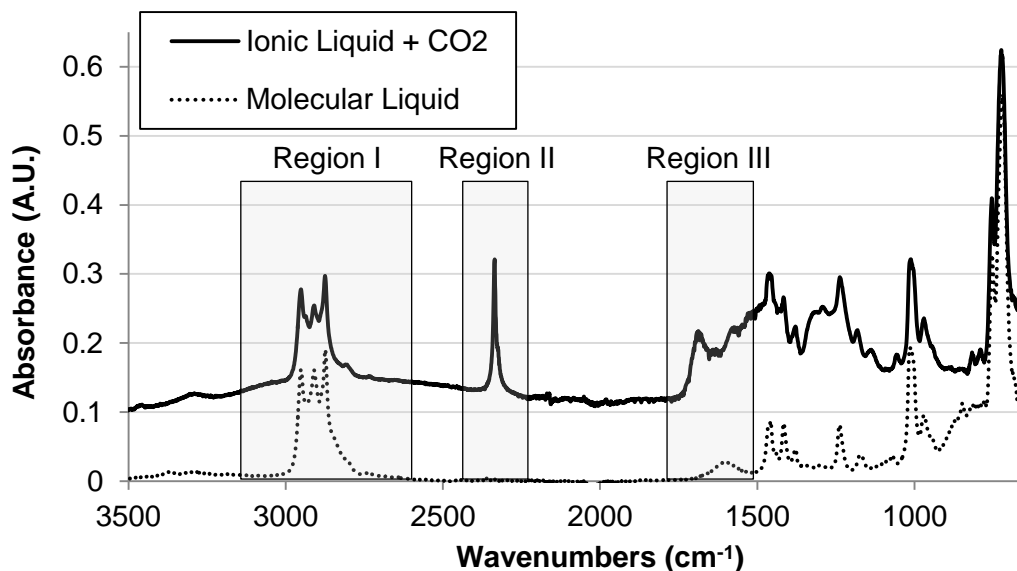
Figure 3.2. The spectrum of TEtSA neutral amine (dashed) and TEtSA ionic liquid with dissolved CO_2 (solid).

The solution procedure to determine the extent of ionic liquid formation and unreacted CO_2 dissolved in the solution requires the application of the Beer-Lambert Law. Ideally, one isolated band is used for the quantitative analysis of IR spectra. This is not feasible in this application. Thus, one must consider the additive property of absorbance; the absorbance of each species contributes the overall absorbance,[7]

$$A_T = \sum_i \varepsilon_i b c_i \qquad (3.1)$$

where ε is extinction coefficient (cm/mol or cm^2/mol), b is pathlength (cm), and c is concentration (mol/cm^3).

For the TEtSA and CO_2 system, only three species are present at any given time.

However, each of the three regions contains the overlap from only two species. Commonly, software is used to deconvolute the overlapping peaks into the individual peaks for analysis. This is attainable because the peaks produced in IR are Gaussian, meaning they are symmetric and can be deconvoluted using Gaussian fits of the contributing curves. The approach used here involves integrating the area and representing the absorbance of the entire region as the sum of the individual contributing species.

The absorbance areas over the range given for each "region of interest" were used for the analysis due to account for any peak deformations that could result from inter-molecular interactions introduced as the reaction progress. The regions were selected to cover all peaks appropriately; except for the case of Region I. The ammonium stretch vibration band was truncated to a range that captured >90% of the overall peak area.

Throughout this chapter, we will examine how the conversion and sorption affect the three variables of the Beer-Lambert Law for the system of TEtSA and CO_2. When the TEtSA molecular liquid comes in contact with CO_2, the reaction proceeds to the ionic liquid form. Upon further addition of CO_2, the resulting ionic liquid is capable of the physical absorption of CO_2. The solution procedure could be developed to account for the simultaneous affects of chemical reaction and physical absorption, yielding three equations and three unknowns. For the ease of analysis, and to establish the analytical techniques to appeal to a broader range of systems, the solution will be examined as two separate scenarios: (1) the physical absorption of CO_2 into the ionic liquid, and (2) the chemical reaction of CO_2 with the TEtSA molecular liquid to give the ionic liquid.

Experimental Methods

<u>Materials</u>

High performance liquid chromatographic (HPLC) grade methanol and isopropanol were used as received (Sigma-Aldrich, HPLC 99+%). The water was obtained in-house using a Barnstead B-Pure dual filter water filtration system, with the product water having a resistivity >18 MΩ. Carbon dioxide (CO_2) was supercritical fluid chromatography (SFC) grade (Air Gas, 99.999%) and further purified via a Matheson gas purifier and filter cartridge (Model 450B, Type 451 filter) to remove water. The (3-aminopropyl)triethylsilane (TEtSA) was prepared by previously published techniques,[8,9] $^1H/^{13}C$ NMR and IR spectroscopy were used to ensure purities of >98%. The ionic form of TEtSA was prepared by bubbling CO_2 (regulated at 40 psi) through approximately 2mL of TEtSA in a 2 dram borosilicate vial, using a 10 gauge needle completely submerged in the fluid for one hour (60 min.); completion of the reaction was confirmed with $^1H/^{13}C$ NMR and elemental analysis.

<u>High Pressure ATR IR Experimental Apparatus</u>

A Shimadzu IRPrestige-21 FT-IR spectrophotometer (with a DLaTGS detector) was used for collection of the IR spectroscopic data. For all measurements, a total of 32 scans with a resolution of 1.0 cm^{-1} were used. The ATR IR accessory used in this study was the Heated Golden ATR offered by Specac, Ltd. The Heated Golden Gate has a Type IIa diamond optical crystal, ZnSe focusing lenses, and is capable of measurements at temperatures up to 200°C(±0.5°C) using the supplied external temperature controller. The Heated Golden Gate apparatus was not modified to accommodate the high pressure measurements. Rather, a custom built stainless steel reactor was designed to replace the supplied sapphire anvil (Figure 3.3).
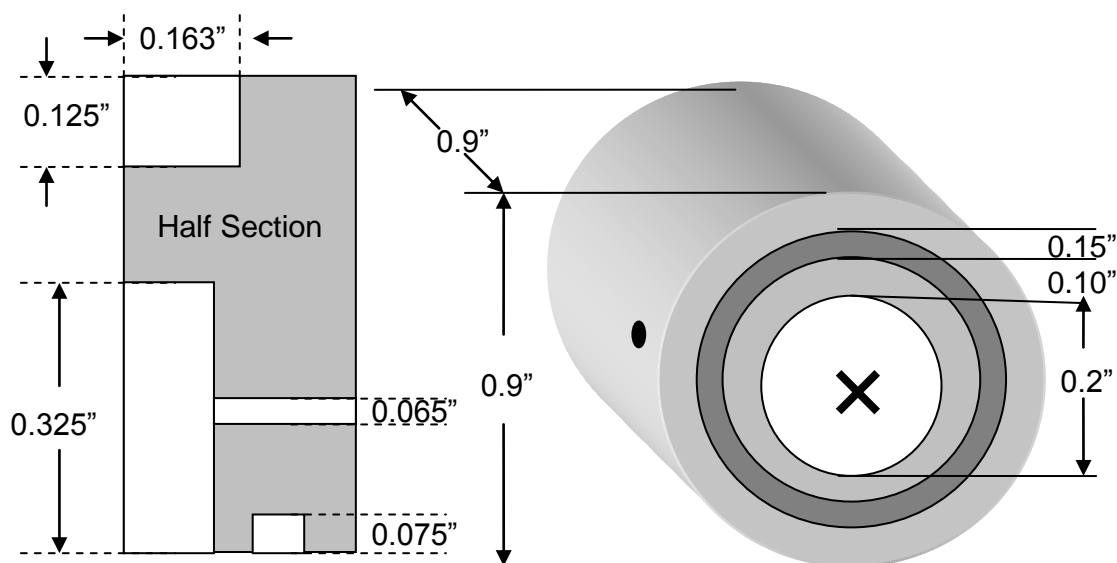
Figure 3.3. Schematic of the custom built high pressure ATR IR reactor for use with the Specac, Ltd. Heated Golden Gate ATR accessory.

The reactor was designed in collaboration with Prof. Sergei Kazarian of Imperial College London, and it was machined from 316 stainless steel with tight tolerances (±0.001"). Approximately 12" of HiP 1/16" 316 stainless steel tubing was fixed in the 0.065" inlet port with the use of silver solder, to withstand high temperatures. As there is only one inlet in the reactor, the design was not intended for analyzing constant flow processes. However, the design allows for modification to accommodate such experiments. The 0.075" recess was used to maintain alignment of the Kalrez O-ring that sealed the base of the reactor to the diamond-embedded tungsten carbide puck on the Heated Golden Gate. The bridge on the Heated Golden Gate was secured and the retaining nut (normally used to press the anvil against the sample) was tightened according to the manufacturer's specification to seal completely the reactor against the puck. The apparatus was successfully tested at a temperature of 150°C and pressure of

1500 psi.

The low viscosity samples (molecular liquid precursor) were loaded into the reactor by first securing the reactor into the Heated Golden Gate accessory, as described above, then attaching a vacuum pump to the HiP needle valve on the inlet of the reactor. Vacuum was maintained and the apparatus was heated to the desired temperature, allowing a minimum of 15 minutes after achieving desired temperature to ensure thermal equilibrium of the apparatus. The needle valve was closed and the vacuum pump was removed from the system, then the background spectrum was collected. Approximately 50 µL of sample was introduced to the reactor using a syringe with an HiP machined fitting adapter, utilizing the vacuum inside the reactor to pull in the sample. The sample was allowed to migrate to the surface of the puck and reach thermal equilibrium (approximately 15 min.).

The high viscosity ionic form of TEtSA was loaded into the reactor by first bringing the apparatus to temperature, then placing ~ 10 µL of the sample onto the surface of the diamond. The reactor was then secured. This is because the ionic form of TEtSA can reverse quickly under vacuum and high shear stress, both of which are present under the typical sample loading procedure. The pressures recorded were then corrected for the atmospheric pressure of air also loaded in the reactor. The experiment proceeded after first allowing the sample to come to thermal equilibrium for 15 minutes (at longer times the reversion is considerable).

Experiments were performed by monitoring the change in absorbance spectrum versus pressure of carbon dioxide at constant temperature. The CO_2 was introduced to the reactor using an ISCO syringe pump (Model 500D) in the pressures range from 0-1000 psia; an Omega 1000 psia transducer was used to monitor the pressure during experimentation. Equilibrium measurements were determined by monitoring the resulting

spectra. At each pressure, the system was considered at equilibrium when there was no observable change between spectra over a 15 minute period. The time to reach equilibrium was found to be around one hour. The diamond surface and reactor were cleaned vigorously with water and HPLC isopropanol in between experiments. Insufficient cleaning would lead to contamination of the system, which is readily apparent by observing large negative peaks in the sample spectrum. Although the system is highly susceptible to contamination, this method ensures the utmost integrity of sample quality and measurements taken.

Results and Discussion

<u>Determination of Physical Absorption Capacity in Ionic Liquid Form</u>

An understanding of the physical absorption of CO_2 in the ionic liquid form of the reactive solvent is critical for the development of a solvent with enhanced CO_2 capture capacities. The physical absorption mechanism is an attractive alternative to chemical absorption due to the low thermal requirement for regeneration of the solvent (discussed in great detail in Chapter 5). The use of reflectance infrared spectroscopy for the purpose of quantifying the concentration of physically absorbed CO_2 in the ionic liquid offers several benefits over traditional techniques:

1. Small sample volumes are required ($\sim$ 50 μL), minimizing the amount of material required and affording rapid uptake time scales.
2. Measurements are collected *in situ*; elimination of sampling improves accuracy and avoids disrupting the phase behavior of the system.
3. Infrared spectrum confirms the identity of the solvent, allowing users to verify sample stability under various experimental conditions.
4. Gives insight into the displacement of solvent upon absorption of CO_2.

The affect of physical absorption of CO_2 in the ionic liquid form on the reflectance infrared spectrum results in the appearance of the asymmetric stretch vibration of CO_2 (Region II) and a density change in the sample due to displacement of the ionic liquid by the absorbed CO_2 (swelling, observed as a change in peak intensities for Region I). If the density of the sample is unchanged by the absorption of CO_2, one would expect no changes to be observed in Region I. However, density changes upon the addition of CO_2 are likely. To compensate for the density changes, the swelling parameter (S, %) is introduced as

$$S = 1 - \frac{\rho_s}{\rho_{IL}}$$ (3.2)

where ρ_s (g/cm^3) is the density of the sample with a given amount of CO_2 physically absorbed and ρ_{IL} (g/cm^3) is the density of the ionic liquid with no CO_2 present.

The density of the ionic liquid does not necessarily need to be known, as the value is best determined from application of the Beer-Lambert Law to Region I for the initial reflectance infrared spectrum when no CO_2 is present,

$$\rho_{IL} = \frac{A_I^0 MW_{IL}}{\varepsilon_I^0 b_I^0}$$ (3.3)

where A_I^0 (cm^{-1}) is the integrated absorbance area for Region I, MW_{IL} (g/mol) is the molecular weight of the ionic liquid, ε_I^0 (cm/mol) is the effective extinction coefficient for the species in Region I, and b_I^0 (cm) is the effective pathlength for Region I, all when no CO_2 is present.

The magnitude of swelling can then be determined by the solution of the Beer-Lambert Law applied to Region I for subsequent experiments when CO_2 has been introduced to the reactor and physically absorbed into the ionic liquid,

$$A_I^s = \varepsilon_I^s b_I^s \left(\frac{\rho_s}{MW_{IL}}\right)$$ (3.4)

where A_I^s (cm^{-1}) is the integrated absorbance area for Region I, ε_I^s (cm/mol) is the extinction coefficient for the species in Region I, and b_I^s (cm) is the effective pathlength for Region I, all for the case when physically absorbed CO_2 is present in the liquid phase. Substitution of Equation 3.2 and Equation 3.3 into Equation 3.4 yields

$$A_I^s = \varepsilon_I^s b_I^s \left(\frac{\rho_{IL}(1-S)}{MW_{IL}}\right) = A_I^0 \left(\frac{\varepsilon_I^s}{\varepsilon_I^0}\right)\left(\frac{b_I^s}{b_I^0}\right)\left(\frac{MW_{IL}}{MW_{IL}}\right)(1-S). \qquad (3.5)$$

As there is no reaction or appearance of CO_2 peaks in Region I, it can be assumed that the extinction coefficient does not change, resulting in the disappearance of that term from Equation 3.5. Additionally, if the refractive index of the sample does not change considerably upon the absorption of CO_2, the pathlength term can also be eliminated. The affect of CO_2 dissolution on refractive index of the TEtSA ionic liquid is not known. However, Kazarian and coworkers found that in the system of poly (dimethylsiloxane) and high pressure CO_2, the refractive index change was $\Delta n_2 < 0.025$ over the pressure range of 0 - 100 bar and solubility of CO_2 up to 40% by weight[10]. The systems studied here are at much lower pressures and CO_2 solubilities. The estimated error in making this assumption is therefore assumed to be < 5% for the case of high CO_2 absorption (maximum pressure of apparatus) and would ultimately be lower for lower concentrations of CO_2 in the ionic liquid phase.

Thus, the swelling of the ionic liquid can be reduced to a simple equation where the only known parameters are the absorbance spectrum of the sample and the initial absorbance spectrum, given as

$$S = 1 - \frac{A_I^s}{A_I^0} \qquad (3.6)$$

which is valid when the initial spectrum is for the fully formed ionic liquid (i.e. no unreacted amine present).

The concentration of physically absorbed CO_2 can now be determined from the analysis of Region II considering the appearance of the asymmetric stretch vibration of CO_2 and the small amount of overlap from the ammonium stretch vibration,

$$A_{II}^s = \varepsilon_{CO2} b_{II} c_{CO2} + A_{II}^0 (1 - S) \qquad (3.7)$$

where A_{II}^s (cm^{-1}) is the integrated absorbance area of Region II, ε_{CO2} (cm/mol) is the extinction coefficient of the physically absorbed CO_2, b_{II} (cm) is the effective pathlength for Region II, c_{CO2} (mol/cm^3) is the desired value of physically absorbed CO_2, and the $A_{II}^0(1-S)$ (cm^{-1}) term is the swelling corrected integrated absorbance area for the ammonium overlap in Region II found from a similar treatment of Equation 3.5. The assumption made here is that the ammonium stretch vibration is affected only by displacement due to CO_2 absorption; valid for the case that the initial spectrum corresponds to the fully formed ionic liquid.

Thus, the quantitative assessment of the physically absorbed CO_2 in the ionic form of TEtSA is found by application of the Beer-Lambert Law, requiring knowledge of only the effective pathlength for Region II and extinction coefficient of the asymmetric stretch vibration of CO_2 (ε_{CO2}, cm/mol). The effective pathlength of Region II implies knowledge of the refractive index of the ionic liquid (n_2) at the temperature of the experiment.

The determination of ε_{CO2} is found experimentally in a system containing physically absorbed CO_2 for which the concentration is known at the experimentation temperatures and pressures (calibration sample). The system chosen here is the binary mixture of methanol and CO_2, for which the phase behavior data has been reported.[11] Methanol is an ideal solvent for this purpose as it has no overlapping peaks with the asymmetric stretch vibration of CO_2, and is known to absorb considerable amounts of

CO_2 at 35°C and pressures up to 50 bar. The effective pathlength for the calibration and ionic liquid samples is significantly different, due to the differing refractive indices of methanol (n_2 = 1.325 at 35°C) and TEtSA ionic liquid (n_2 = 1.475 at 35°C), and must be considered in both the determination of ε_{CO2} and subsequent solution for c_{CO2} in the ionic liquid.

The ε_{CO2} is found from the plot of A/b (cm^{-2}) versus c_{CO2} (mol/cm^3) in the methanol and CO_2 system at 35°C, given in Figure 3.4.
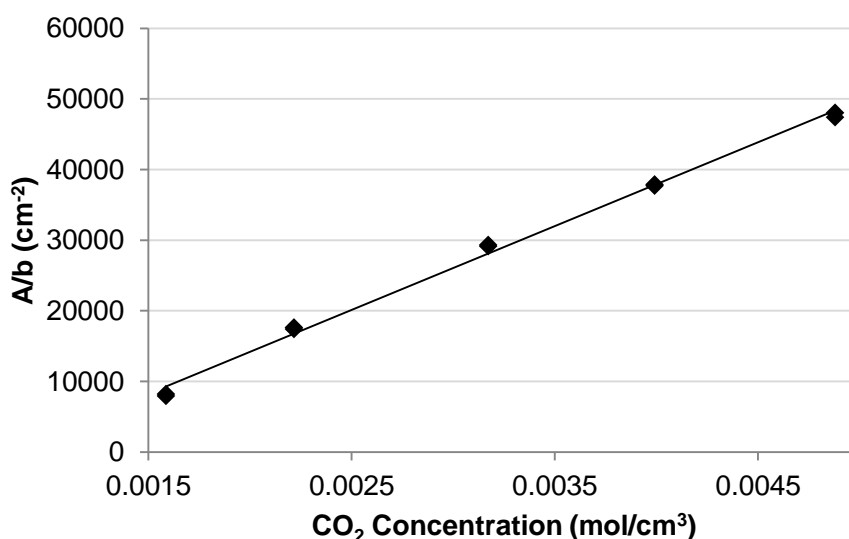
Figure 3.4. Determination of extinction coefficient (ε, cm/mol) by calibration of <u>absorbance area</u> (A, cm^{-1}) over pathlength (b, cm) versus known concentrations of carbon dioxide in methanol at 35°C.[11]

The ε_{CO2} value was found to be 1.187 x 10^7 cm/mol and the detection limit of carbon dioxide in solution using this technique was found to be 8.0 x 10^{-5} mol/mL. Excellent linearity between A/b (cm^{-2}) versus CO_2 concentration (mol/cm^3) is observed in Figure 3.4, confirming the validity of the Beer-Lambert Law and the assumption that the

refractive index change upon addition of CO_2 is negligible. The change in refractive index would not follow a linear trend with respect to CO_2 concentration, as described in Chapter 2, and was considered constant over the entire CO_2 concentration range in the analysis that yielded Figure 3.4.

It should be emphasized that the ε_{CO2} (cm/mol) value determined from Figure 3.4 is for the case where the absorbance values are taken as the integrated areas taken over the range of $2260 - 2400$ cm^{-1}. The effective pathlength term (b_{II}, cm) was determined as the average of values over the integrated range, using the average of Equations A.4 and A.5 (found in Appendix A), and is highly dependent on the refractive index of the calibration fluid.

Determining the area integrated absorbance values is arduous relative to using the peak maxima values. A plot of A/b (cm^{-1}) versus CO_2 concentration in the methanol and CO_2 system is given in Figure 3.5, again assuming a constant pathlength over the entire CO_2 concentration range, in order to compare the accuracy of using integrated areas versus peak maxima.

The ε_{CO2} value found by using the CO_2 asymmetric stretch vibration peak maxima values in Figure 3.5 was 3.65 x 10^5 cm^2/mol. It is obvious that the fit of A/b versus CO_2 concentration is much improved for the case where the integrated absorbance areas are used (yielding ε_{CO2} in units cm/mol) as opposed to using the peak maxima (yielding ε_{CO2} in units cm^2/mol). Thus, absorbance areas are used for the analysis. Additionally, the analysis technique used (area vs. maxima) in determining the extinction coefficient from a calibration sample must be consistent with the analysis of the unknown samples.

To validate the ε_{CO2} value reported here using the integrated absorbance areas, the system of CO_2 and water was examined at 35°C, given in Figure 3.6. A comparison of the extinction coefficient values previously reported is provided in Appendix B.
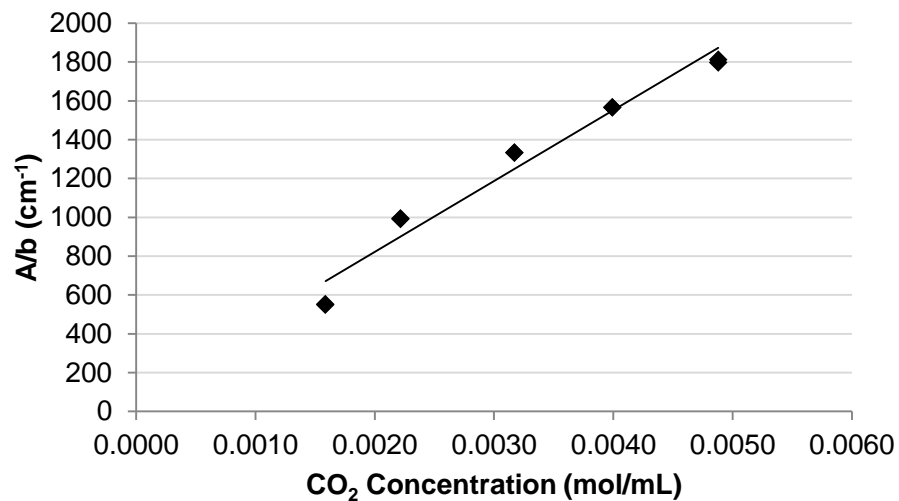
Figure 3.5. Determination of extinction coefficient (ε, cm²/mol) by calibration of <u>maximum absorbance</u> (A, A.U.) over pathlength (b, cm) versus known concentrations of carbon dioxide in methanol at 35°C.[11]
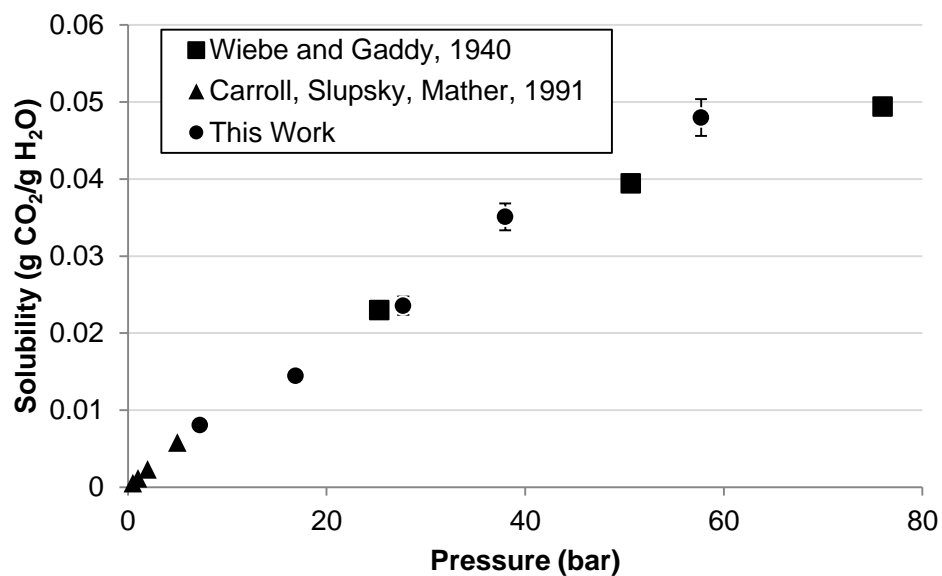
Figure 3.6. The solubility of CO_2 (g CO_2/g H_2O) versus total pressure (bar) comparing the technique described here to reported values, at 35°C.

The measured solubility of CO_2 in water (g CO_2/g H_2O) measured with the technique described here is in good agreement with the reported values given at low pressure by Carroll and coworkers[12] and at high pressures by Wiebe and Gaddy.[13] The solution procedure accounted for the refractive index of water, $n_2 = 1.335$. Thus, the ε_{CO2} reported here is valid for the determination of physically absorbed CO_2 utilizing the experimental apparatus presented.

With the calibration and validation of the physical absorption of CO_2 using the reflectance infrared spectroscopic satisfied, the CO_2 absorption in the TEtSA ionic liquid can now be examined with confidence.

As the pressure of CO_2 is increased in the system, the asymmetric stretch vibration of CO_2 in the reflectance infrared spectrum also increases, corresponding to an increase in CO_2 solubility shown in Figure 3.7.
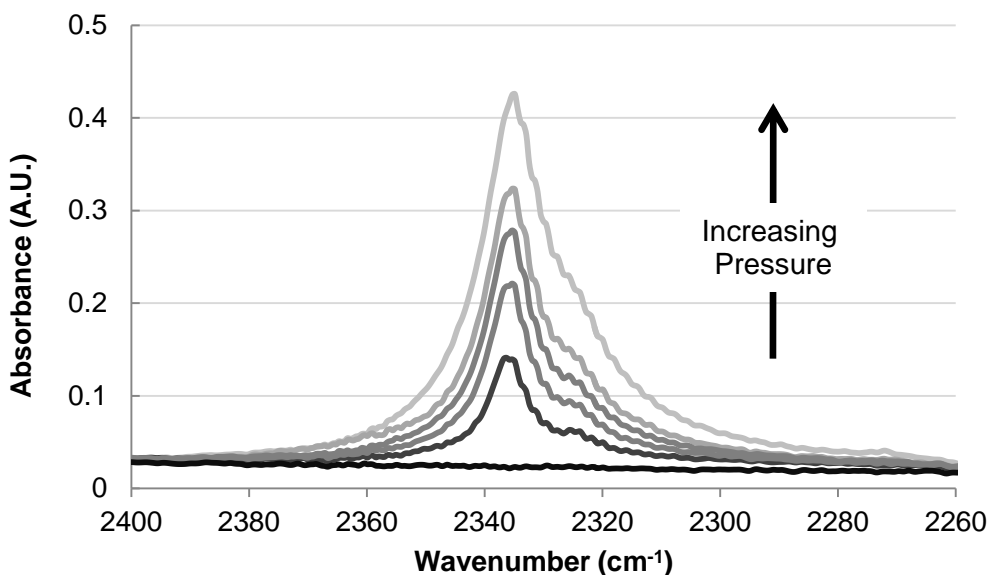
Figure 3.7. The increasing asymmetric stretch vibration of physically absorbed CO_2 as a function of CO_2 pressure.

The concentration of CO_2 (mol/cm^3) in the ionic liquid phase versus pressure (bar) is provided at 35°C and 50°C in Figure 3.8. It is seen that the concentration of CO_2 physically absorbed by the TEtSA ionic liquid increases almost linearly with respect to system pressure over the entire pressure range studied. This behavior is consistent with CO_2 absorption into traditional ionic liquids, and will be discussed in great detail in Chapter 5. Additionally, as the temperature of the system is increased, the absorption (or solubility) is decreased. This, too, is expected regarding gas solubility in ionic liquids.
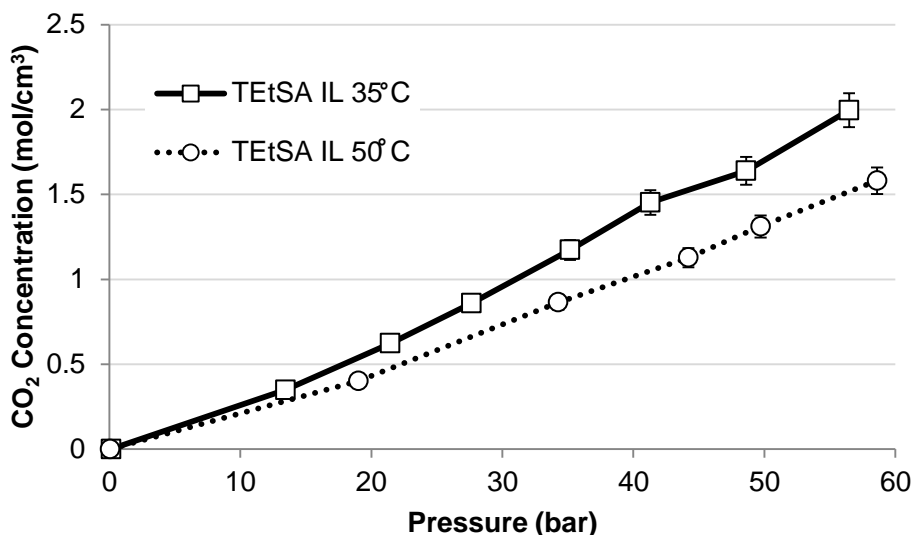
Figure 3.8. The experimentally determined concentration of CO_2 (mol/cm^3) physically absorbed in the TEtSA ionic liquid phase as a function of pressure (bar), measured at 35°C and 50°C.

The swelling information for the reversible ionic liquids is also obtained from the reflectance infrared spectroscopic technique, and is given in Figure 3.9. The swelling of the TEtSA ionic liquid phase is consistent with the displacement of the ionic liquid as CO_2 is physically absorbed in the solution. Considering the large amounts of CO_2 that

are absorbed over the pressure range studied, the swelling is quite small. The physically absorbed CO_2 likely occupies the void space of the fluid, as will be described in Chapter 5. Additionally, it appears as though the swelling values taper at higher pressures, indicative of the approach to the saturation point at the given temperature.
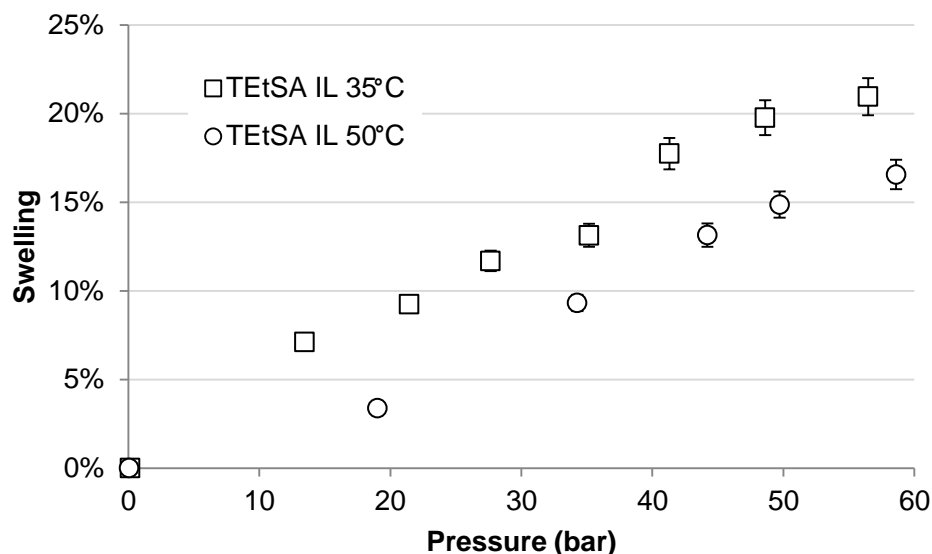
Figure 3.9. The swelling of the TEtSA ionic liquid phase due to displacement by physically absorbed CO_2, as a function of pressure (bar) at 35°C and 50°C.

Determination of Chemical Absorption Capacity in Molecular Liquid

The chemical absorption of CO_2 in the molecular liquid form of the reactive solvent is critical for the highly selective separation of CO_2 from streams with low concentrations and/or low partial pressures of CO_2. *Ex situ* experiments have been performed to examine the CO_2 absorption capacity in the TEtSA molecular liquid at 35°C and a CO_2 pressure of 1 bar, and the resulting ionic liquid was shown to capture the stoichiometric amount of CO_2 (i.e. one mole of CO_2 per two moles of amine) using $^1H/^{13}C$ NMR, refractive index, and elemental analysis (see Chapter 2 for more details). The

objective of using the reflectance infrared spectroscopic technique to examine the chemical absorption of CO_2 in the TEtSA molecular liquid is to probe the uptake rate of CO_2 into the stagnant solvent. Such information is crucial for extending the application of this material to an industrial scale CO_2 capture process.

The reaction of CO_2 with the molecular form of TEtSA results in the transformation of the amine to an ammonium/carbamate pair. The effect of this transformation of the infrared spectrum is the appearance of the broad ammonium peak in Region I and the carbamate peak in Region III. The C-H bonds in the molecular structure do not undergo any chemical transformations. Thus, the change in the C-H stretch vibration observed in Region I is attributed to the density change as the molecular liquid is converted to the ionic liquid, calculated using the Beer-Lambert Law (and temporarily ignoring the appearance of the ammonium peak, to be discussed further) and assuming the extinction coefficient for the C-H stretch vibrations (ε_{C-H}, cm/mol) and effective pathlength (b_I, cm) are unchanged, yielding

$$A_{C-H} = \varepsilon_{C-H} b_I \left(\frac{\rho_{ML}}{MW_{ML}} \right) (1 - x_{IL}) + \varepsilon_{C-H} b_I \left(\frac{\rho_{IL}}{MW_{IL}} \right) (2x_{IL}) \qquad (3.8)$$

where A_{C-H} (cm^{-1}) is the integrated absorbance area of the C-H stretch vibration, ρ_{ML} (g/cm^3) is the density and MW_{ML} (g/mol) is molecular weight of the molecular liquid, ρ_{IL} (g/cm^3) is the density and MW_{IL} (g/mol) is molecular weight of the ionic liquid, and x_{IL} is the mole fraction of ionic liquid in the mixture. The factor of "2" in the ionic liquid term corresponds to the stoichiometry of reaction, as there are twice as many C-H bonds in one mole of ionic liquid relative to the molecular liquid.

At the low partial pressures of CO_2 where the chemical absorption dominates the capture capacity, it is assumed that the physically absorbed CO_2 is negligible. This is a valid assumption as the asymmetric stretch vibration of CO_2 is not observed in the

spectrum for which $P_{CO2} < 10$ bar, implying the concentration of physically absorbed CO_2 is below the detection limit of the technique (0.08 mol/cm^3). Relative to the maximum chemical absorption capacity of the TEtSA molecular liquid (2.3 mol/cm^3), the physical absorption concentration is 3% of the total capacity at the detection limit. Because the physical absorption is considered negligible, the density changes due to displacement of the CO_2 (i.e. swelling) are also ignored.

The extinction coefficient for the C-H stretch vibration (ε_{C-H}, cm/mol) can be determined from the initial spectrum of the TEtSA molecular liquid and taking Equation 3.8 for the case when ionic liquid mole fraction equals zero ($x_{IL} = 0$), valid when no CO_2 is present in the system,

$$\varepsilon_{C-H} = \frac{A_I^0 MW_{ML}}{b_I \rho_{ML}}$$

(3.9)

where A_I^0 (cm^{-1}) is the integrated absorbance area for Region I from the initial (no CO_2) spectrum and ρ_{ML} (g/cm^3) is the density of TEtSA at the temperature of the experiment.

The determination of the changing C-H stretch vibration with respect to TEtSA conversion can now be determined from

$$A_{C-H} = A_I^0 \left[(1 - x_{IL}) + (2x_{IL}) \left(\frac{\rho_{IL}}{\rho_{ML}} \right) \left(\frac{MW_{ML}}{MW_{IL}} \right) \right]$$

(3.10)

assuming that the effective pathlength and extinction coefficient for the C-H stretch remain constant over the full conversion range.

The pathlength is a function of the refractive index, and the refractive index change from the molecular liquid to the ionic liquid is about 0.02. This change in refractive index corresponds to a change in the effective pathlength of < 5%. We account for the change in pathlength by representing the b_I term as a function of composition (using the Lorentz-Lorenz mixing rule unless the trend is otherwise known

from an experimental calibration curve). This method was found to introduce a significant amount of rigor to the solution procedure. Due to the small change in pathlength, it will be considered constant. It will soon be shown that the error associated with this assumption will be minimized in the final determination of ionic liquid mole fraction, as the same deviation will manifest itself in the determination of the extinction coefficient of the ammonium stretch vibration (ε_{NH3+}, cm/mol).

In addition to the density changes affecting the C-H stretch vibration, the conversion from molecular liquid to ionic liquid also results in the appearance of the broad ammonium peak that appears in Region I. The integrated absorbance area for the ammonium stretch (A_{NH3+}, cm^{-1}) can be found from

$$A_{NH3+} = \varepsilon_{NH3+}b_I\left(\frac{\rho_{IL}}{MW_{IL}}\right)(x_{IL}).$$
(3.11)

The integrated absorbance area of Region I at an unknown conversion (A_I^s, cm^{-1}) is then found from adding the contributions of the C-H stretch vibration and the ammonium stretch vibration,

$$A_I^s = A_I^0\left[(1 - x_{IL}) + (2x_{IL})\left(\frac{\rho_{IL}}{\rho_{ML}}\right)\left(\frac{MW_{ML}}{MW_{IL}}\right)\right]$$
$$+ \varepsilon_{NH3+}b_I\left(\frac{\rho_{IL}}{MW_{IL}}\right)(x_{IL})$$
(3.12)

and the ε_{NH3+} value is determined from the spectrum of the ionic liquid, where the conversion is equal to one ($x_{IL} = 1$). Recall that the chemical absorption has been verified via *ex situ* experiments to react to completion at 35°C and 1 bar of CO_2 pressure. The spectrum of the fully formed ionic liquid is obtained by allowing sufficiently long time for the reaction to go to completion. As there is no stirring in the reactor, this time is affected by the diffusivity, reaction rate, and thickness of the sample. The reaction was determined to be completed when the spectra exhibited no change over a period of

71

several hours.

Using the integrated absorbance area for Region I at an "infinite time" (A_I^∞, cm^{-1}) where the conversion is equal to one, the value of ε_{NH3+} can be determined from

$$\varepsilon_{NH3+} = \frac{A_I^\infty}{b_I}\left(\frac{MW_{IL}}{\rho_{IL}}\right) - 2\left(\frac{A_I^0 MW_{ML}}{b_I \rho_{ML}}\right). \tag{3.13}$$

The assumption used in determining Equation 3.13 is that the pathlength remains constant for the molecular liquid and ionic liquid, where the value of b_I is determined using the refractive index of the molecular liquid form of TEtSA. However, it has been determined that over the course of the reaction the pathlength change is approximately 5%. This error is then compensated for in the term ε_{NH3+}. The implication then becomes that the pathlength change is linear with respect to ionic liquid mole fraction; for such a small change this is a good approximation.

The conversion of TEtSA from the molecular form to the ionic form was examined using this reflectance spectroscopic technique at 35°C and a CO_2 pressure of 1 bar, given in Figure 3.10.
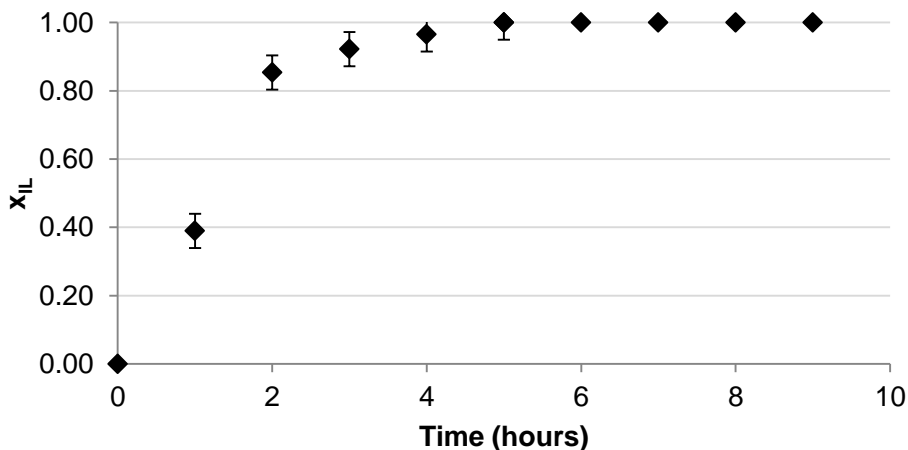
Figure 3.10. The conversion of TEtSA from the molecular liquid to ionic liquid at 35°C and a function of time.

The thickness of the TEtSA molecular liquid was approximately 2500 µm, and measurements were taken every 60 minutes. The chemical absorption uptake of CO_2 in the TEtSA molecular liquid appears to occur over several hours with no stirring.

The measurement of the chemical absorption of CO_2 in the TEtSA molecular liquid was compared to a gravimetric technique, where the mass uptake of CO_2 was examined over time. The gravimetric experiments used a Hiden Isochema IGA-001 Gas Sorption Analyzer, located in Dr. Krista Walton's research facilities at Georgia Tech. The experiment was performed at 35°C with 1 bar of CO_2, using a stainless steel cylindrical sample holder (diameter of 11 mm) and an equivalent amount of material to yield a sample thickness of 2500 µm. The Hiden IGA records mass uptake, and assuming that the physical absorption is negligible at the low pressure studied, the ionic liquid mole fraction was calculated and compared to the reflectance infrared spectroscopic technique (ATR FTIR), given in Figure 3.11.

Fair agreement between the spectroscopic technique and gravimetric technique were obtained, as evidenced by Figure 3.11. The data suggest that for a given time, the spectroscopic technique indicates a higher conversion relative to the gravimetric technique. A possible explanation is that the sample thickness is actually smaller in the spectroscopic technique, relative to the estimated thickness based on the sample volume and dimensions of the reactor. The uptake is likely limited by the diffusion of CO_2 into the sample, as opposed to the reaction of CO_2 with the amine. A plot of x_{IL} versus $(t/\ell^2)^{1/2}$ (where t is time in seconds and ℓ is sample thickness in centimeters) is given in Figure 3.12.
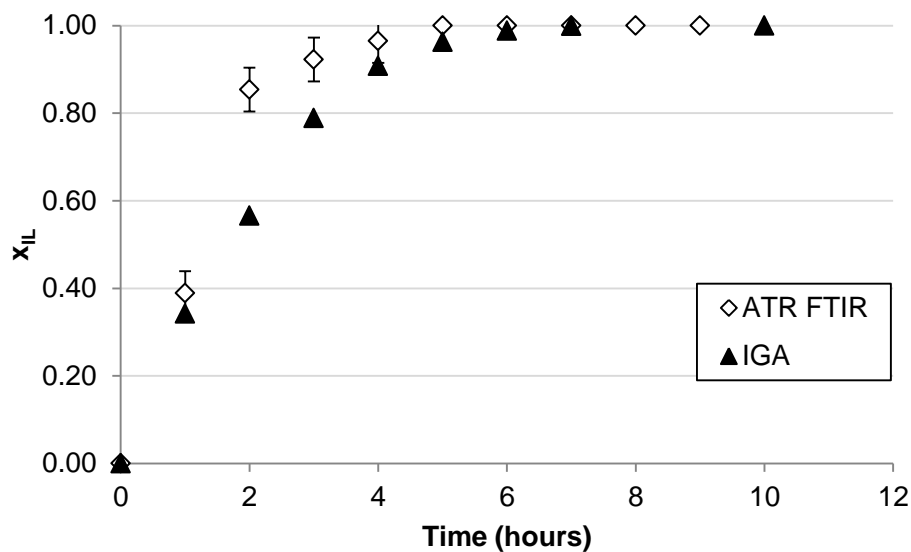
Figure 3.11. Comparison of the reflectance spectroscopic (ATR FTIR) and gravimetric (IGA) techniques for the determination of conversion in the CO_2 and TEtSA system at a temperature of 35°C.
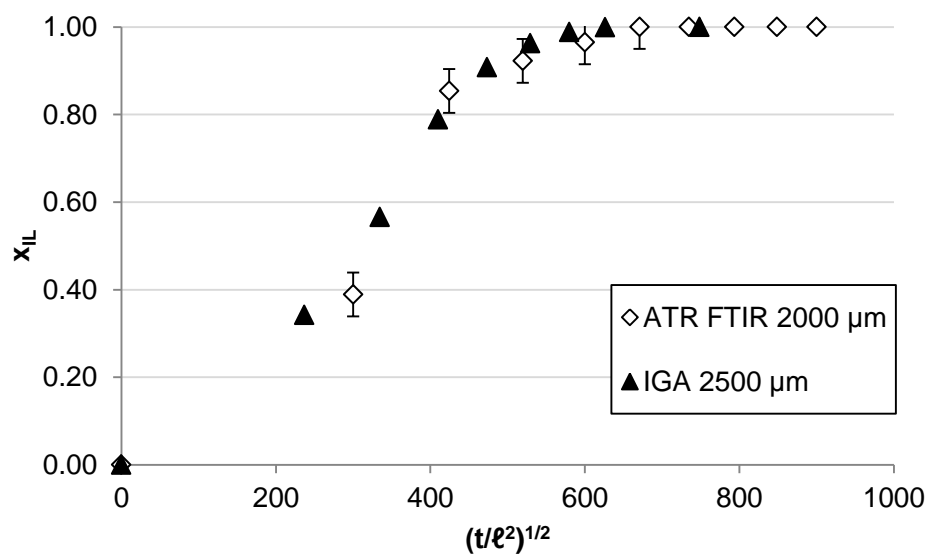
Figure 3.12. Comparison of the reflectance spectroscopic (ATR FTIR 2000 μm) and gravimetric (IGA 2500 μm) techniques, normalized by sample thickness, for the determination of conversion in the CO_2 and TEtSA system at a temperature of 35°C.

The thickness value used for normalization of the FTIR data was 2000 µm, giving good agreement with the IGA data normalized for a thickness of 2500 µm. Although the volume of TEtSA added corresponds to a thickness of 2500 µm, some sample is deposited onto the surface of the tubing that feeds to the reactor. This is a limitation of the reflectance experimental apparatus. The thickness of the sample used for the IGA experiments is well known as the sample is placed directly on the bottom of the pan, and the exact mass is determined at the start of the experiment. The error in the determination of sample thickness for the IGA experiment is ± 10 µm.

Using 2000 µm for the thickness of the spectroscopic sample, the results from Figure 3.12 indicate good agreement between the reflectance spectroscopic and gravimetric techniques for determining ionic liquid mole fraction. However, if the actual sample thickness were < 2000 µm for the reflectance experiments, the results would be lower than the IGA, indicating a concentration gradient in the sample. Due to the difficulty in measuring the actual sample thickness in the reflectance apparatus, it is not possible to draw any conclusions regarding the presence of a concentration gradient observed over the course of the experiment.

Conclusions

Reflectance infrared spectroscopy is a powerful tool at the disposal of researchers for the quantitative analysis of chemical reaction and physical absorption applied to a broad range of materials and systems. The accuracy of the technique, and the validity of assumptions made, is dependent on a strong understanding of the fundamental concepts regarding IR and ATR spectroscopy. Presented here is the application to the chemical and physical absorption of CO_2 in a novel amine solvent

TEtSA. However, sufficient information has been supplied to allow researchers the opportunity to apply the technique to a broad range of systems.

The physical absorption of CO_2 in the TEtSA ionic liquid has been validated against a known system of CO_2 and water, exhibiting excellent agreement. The reflectance spectroscopic technique yields the solubility and swelling information over a broad range of experimental temperatures and pressures, giving the pure component information necessary for the development of materials and design of an industrial scale process.

The chemical reaction of CO_2 with the TEtSA molecular liquid was investigated, and the results were compared with the common gravimetric technique. Although the results were consistent between the two techniques, the reflectance technique suffers from limited information on the thickness of sample contained in the reactor, ultimately limiting the benefit of the technique. Should the experimental apparatus or technique be improved to give accurate sample thickness information, the technique could be applied to effectively determining the diffusivity of CO_2 in reactive liquid solvents.

The utility of quantitative spectroscopy using reflectance infrared accessories is bound only by the creativity of the researcher. Spectroscopy enables *in situ* data collection on very small samples, increasing experimental efficiency and improving accuracy. Due to the high sensitivity of the technique, sample integrity can be ensured and competing mechanisms can be differentiated. As the popularity of the technique continues to grow, and researchers become more comfortable with the analysis, reflectance infrared spectroscopy will give valuable experimental data for the design and development of materials and processes to benefit future generations.

References

(1)   Babarao, R.; Jiang, J. W. *Langmuir* **2008**, *24*, 6270.

(2)   Fauth, D. J.; Frommell, E. A.; Hoffman, J. S.; Reasbeck, R. P.; Pennline, H. W. *Fuel Process. Technol.* **2005**, *86*, 1503.

(3)   Saghafi, A.; Faiz, M.; Roberts, D. *Int. J. Coal Geol.* **2007**, *70*, 240.

(4)   Anthony, J. L.; Maginn, E. J.; Brennecke, J. F. *Journal of Physical Chemistry B* **2002**, *106*, 7315.

(5)   Camper, D.; Scovazzo, P.; Koval, C.; Noble, R. *Industrial & Engineering Chemistry Research* **2004**, *43*, 3049.

(6)   Blanchard, L. A.; Gu, Z. Y.; Brennecke, J. F. *Journal of Physical Chemistry B* **2001**, *105*, 2437.

(7)   *Handbook of Instrumental Techniques for Analytical Chemistry*; Settle, F., Ed.; Prentive-Hall, Inc., 1997.

(8)   Blasucci, V.; Dilek, C.; Huttenhower, H.; John, E.; Llopis-Mestre, V.; Pollet, P.; Eckert, C. A.; Liotta, C. L. *Chemical Communications* **2009**, 116.

(9)   Blasucci, V.; Hart, R.; Mestre, V. L.; Hahne, D. J.; Burlager, M.; Huttenhower, H.; Thio, B. J. R.; Pollet, P.; Liotta, C. L.; Eckert, C. A. *Fuel* **2010**, *89*, 1315.

(10)   Flichy, N. M. B.; Kazarian, S. G.; Lawrence, C. J.; Briscoe, B. J. *Journal of Physical Chemistry B* **2002**, *106*, 754.

(11)   Chang, C. J.; Day, C. Y.; Ko, C. M.; Chiu, K. L. *Fluid Phase Equilibria* **1997**, *131*, 243.

(12)   Carroll, J. J.; Slupsky, J. D.; Mather, A. E. *Journal of Physical and Chemical Reference Data* **1991**, *20*, 1201.

(13)   Wiebe, R.; Gaddy, V. L. *Journal of the American Chemical Society* **1940**, *62*, 815.

CHAPTER 4   COUPLING OF REACTIONS AND SEPARATIONS USING REVERSIBLE IONIC LIQUIDS

Introduction

In academic research laboratories and commercial scale processing alike, reactions and separations are often times thought of as two separate unit operations. Commonly, chemists first develop an optimal set of reaction conditions for a given reaction, and then hand off the product mixture to an engineer to design the separation. The end result is that separations in industrial chemical production comprise a large fraction of the total production cost. Additionally, many multi-step synthetic procedures involve switching between polar and nonpolar solvents to create a homogeneous reaction phase, thereby increasing the number of separation steps required.   To eliminate the intermediate separation steps and final product purification stage, one would ideally want a solvent that switches polarity and solubility properties as desired. To ensure viability in commercial scale processing and to reduce further the environmental impact of the chemical industry, one would also want the ideal solvent system to be recyclable. The desire to combine a solvent that will facilitate a reaction and then offer a separation, combined with the ability to be reused for sustainable processing, led to the development of reversible ionic liquids as a specific class of "switchable solvents."[1-4]

Room-temperature ionic liquids (ILs) have received much attention from the scientific community in recent years. There is almost a limitless combination of anions and cations that can be used, and some say that ILs are the answer to all solution chemistry problems a chemist or engineer could face. However, the one issue most researchers do not address when dealing with reactions in ILs is the separation step.

ILs have proven to be very effective as reaction media, but isolating products or catalysts from the solvent remains difficult, except for very volatile products that can be easily stripped from the IL. This problem becomes even more severe if purification of the ILs for recovery or recycling is considered. It quickly becomes evident that when the separation step is considered in the overall processing scheme, the appeal of using ILs in organic synthesis is quickly diminished.

In recent years the Eckert-Liotta Research Group has examined many techniques to couple reactions and separations, including: supercritical fluids,[5-15] near-critical fluids,[11,16-20] phase-transfer catalysts,[21-23] gas-expanded liquids,[10,11,24-27] the organic aqueous tunable solvents process (OATS),[28-30] and piperylene sulfone (a recyclable DMSO substitute).[31-33] The most recent and exciting additions to the arsenal of novel solvent systems are reversible ionic liquids. Just like conventional ILs, reversible ionic liquids can be designed for a specific application, where the molecular architecture of the solvent system can be adjusted (or tuned) to achieve the desired solvent properties. Going beyond the synthesis and characterization of two-component reversible ionic liquids, the use of these unique solvent systems has been examined for a variety of industrially relevant applications. In addition to a discussion of the positive aspects of the switchable solvent systems in coupling reactions and separations, the challenges and limitations of these solvents will also be addressed.

Traditional ionic liquids, such as 1-butyl-3-methylimidazolium tetrafluoroborate ([bmim][BF_4]) and 1-butyl-3-methylimidazolium bis(trifluoromethanesulfonyl)amide ([bmim][BTA]) (to name just a few popular ones), have been widely explored during the past decade for synthetic transformations with marked success.[34,35] To this day however, efficiently achieving both reaction and separation in traditional ionic liquids remains a major challenge. The inherent ionic nature of molten salts and their relatively high

viscosity often precludes distillation of the IL itself or precipitation of the product. Commonly, the product is extracted from the IL with a nonpolar solvent such as hexane.[36] The extraction strategy is product-dependent, generates significant amounts of organic waste, and disposal or regeneration of the contaminated IL phase can be costly. Extraction of the product with $scCO_2$ has been shown to be a possible separation technique, and in many cases represents an environmentally benign alternative.[8,37-39] In all cases, separations from ILs are typically restricted to removal of very nonpolar and/or highly volatile components.

With the advent of switchable systems, this situation is fundamentally changed. For the case of reversible ionic liquids, the solvent can take two different forms – molecular and ionic – and each form exhibits considerably different properties as shown in Chapter 2. The resulting property change upon switching from one solvent form to another is so drastic that it opens up unique opportunities to address simultaneously reactions and separations. A general process flow diagram for the coupled reaction and separation in the two-component reversible ionic liquids is given in Figure 4.1.

This chapter discusses the applications of two-component reversible ionic liquids for integration of reaction and separation in the Claisen-Schmidt condensation reaction and the Heck reaction. Additionally, some limitations and challenges that have been observed using the two-component reversible ionic liquids as switchable solvents for coupling reaction and separations processes are discussed.
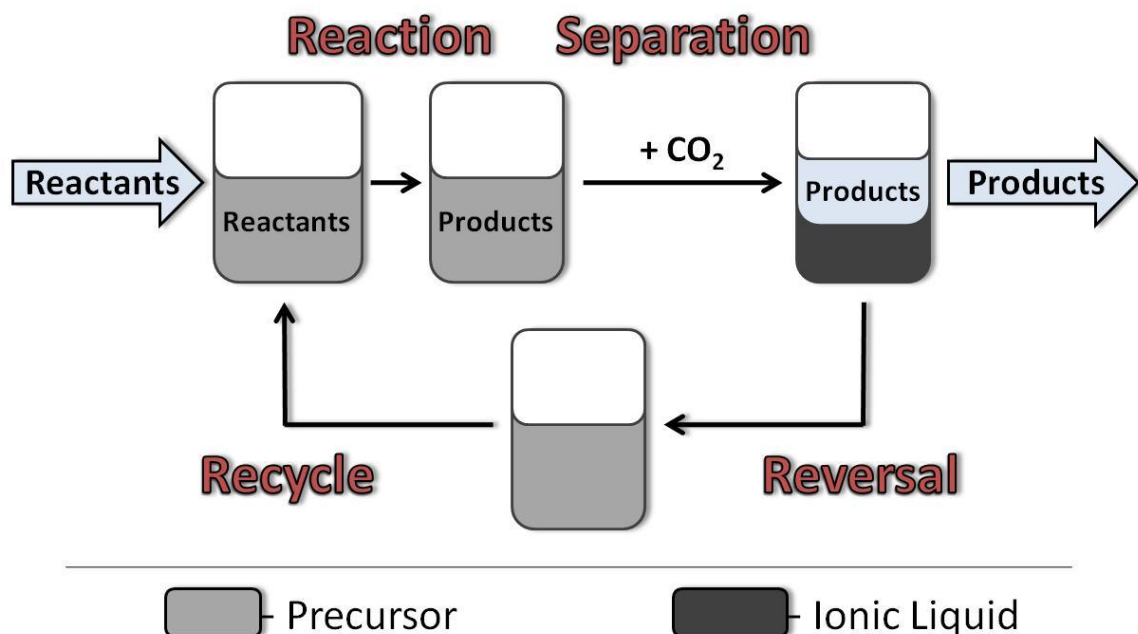
Figure 4.1. The general flow diagram for a sustainable processing using reversible ionic liquids.

Experimental Methods

GC-MS analyses to quantify the concentrations of reactants and products were conducted on an HP 6890 GC-MS. Standard calibration curves of all starting materials and products were prepared. If the reaction was recycled, the desired products were isolated, characterized by NMR and compared to literature values. All materials were reagent grade and purchased from Sigma-Aldrich, unless otherwise stated.

Claisen-Schmidt Condensation of Butanone and Benzaldehyde

The butanone (1.7 mL, 0.019 mol) and the benzaldehyde (2.03 mL, 0.019 mol) were added to TMBG (4.1 g, 0.024 mol). The reaction was then stirred at room temperature or at $80^{\circ}C$ for the desired amount of time. After cooling, $MgSO_4$ was added to the reaction mixture and stirred for ~30 min before being filtered. Methanol (1 mL) and

heptane (1 mL) were then added and CO_2 was bubbled through the mixture for ~1 hour. The heptane phase was analyzed by GC-MS. The products isolated from the hexane phase and from the ionic liquid phase were analyzed by ^{1}H NMR. *1-phenyl-pent-1-en-3-one*[40]: ^{1}H NMR: (CDCl$_3$): 1.16 (3H, t), 2.7 (2H, q), 6.7 (1H, d), 7.37-7.4 (3H, m), 7.5-7.6 (3H, m). *4-phenyl-3-methyl-3-buten-2-one:* ^{1}H(d$_6$-DMSO): 1.87 (d, 3H), 2.37 (s, 3H), 7.3-7.45 (m, 4H), 7.59 (s, 1H).

General procedure for the Heck Reaction

Styrene was distilled under reduced pressure, filtered through neutral alumina oxide and stored under argon at -20 °C. DBU was dried over CaH$_2$, distilled under reduced pressure and stored under argon. Acetonitrile was dried by molecular sieves and kept under argon.

The required amount of catalyst was introduced as a toluene solution into a 10 ml windowed autoclave. The solvent was removed under reduced pressure. DBU (2.00 mL, 13.2 mmol) and hexanol (1.68 mL, 13.2 mmol) were combined in a Schlenk flask under nitrogen atmosphere. CO_2 was sparged trough the solution until the exothermic reaction cooled down. The ionic liquid produced was added to the catalyst, followed by bromobenzene (0.21 mL, 2.0 mmol) and styrene (0.27 mL, 2.4 mmol). The reaction was pressurized with the required CO_2 pressure and stirred for 3 days at the respective reaction temperature. After cooling down and depressurizing, the reaction mixture was transferred to a Schlenk flask which was kept under CO_2 at atmospheric pressure. The reaction mixture was extracted with heptane. The heptane phase was evaporated under reduced pressure and analyzed by HP 5890 Series II GC, using tridecane as an internal standard. The reversible ionic liquid was sparged with argon and heated to convert to the molecular phase, precipitating the salt. The supernatant solvent was removed, converted to the ionic liquid and fresh ionic liquid was added. The ionic liquid, containing

the catalyst was charged with fresh substrates in the autoclave and treated as mentioned before. The precipitate was washed with pentane and dried under reduced pressure to be analyzed by NMR. *DBU·HBr salt:* ^{1}H (CDCl$_3$): d = 1.54-1.77 (6H, m), 1.88-2.00 (2H, m), 2.81 (2H, bs), 3.30-3.47 (6H, m), 4.82 (1H, bs). ^{13}C (CDCl$_3$) d = 20.3, 24.5, 27.4, 29.3, 33.5, 39.4, 48.8, 54.3, 165.3.

Cyanosilylation of Cyclohexanone

Trimethylsilyl cyanide (0.8 mL, 0.006 mol) was added to TMBG (0.003-0.006mol) at room temperature with stirring. Cyclohexanone (0.5 mL, 0.005 mol) was then added slowly at room temperature. After reaction completion, methanol (1 equivalent relative to TMBG) and heptane (0.8 mL) were added. CO_2 was bubbled through the mixture for 1 hour to form the ionic liquid. The heptane phase was analyzed by GC-MS and the ionic liquid phase and the isolated product by ^{1}H & ^{13}CNMR. *1-trimethylsilyloxy-1-cyclohexanecarbonitrile.* ^{1}H (d$_6$-DMSO): 0.2 (s, 9H), 1.48-1.7 (m, 8H), 1.9 (m, 2H). ^{13}C (d$_6$-DMSO): 1.4, 22.4, 23.8, 38.6, 70.5, 121. *TMBG/TMS-CN salt:* ^{1}H (d$_6$-DMSO): 0.1 (s, 9H), 0.82 (t, 3H), 0.98 (m, 2H), 1.25 (m, 2H), 2.8 (s, 12H). ^{13}C (d$_6$-DMSO): 1.1, 13.9, 18.8, 19.7, 31.7, 39.1, 123.4, 161.3.

Michael Addition of dimethyl malonate to 2-cyclohexenone

Cyclohexenone (0.17 mL, 1.75 mmol) was added to TMBG (0.3 g, 1.75 mmol). Dimethyl malonate (0.2 mL, 1.75mmol) was then added at room temperature. The reaction was heated to 80°C for 16 hours. After cooling, methanol was added (0.07 mL, 1.75 mmol) and CO_2 was bubbled through the mixture for approximately 1 hour. The heptane phase was analyzed by GC-MS and the ionic liquid phase by ^{1}HNMR. When HCl work up was performed, the reaction mixture was treated with aqueous HCl (10%) for ~1 hour. Ether was then added and the biphasic mixture was stirred for ~1 hour. The

ether phase was then analyzed by GC-MS. After removal of the ether, the isolated product was characterized by ^{1}H NMR. *3[bis(methoxycarbonyl)methyl]cyclohexanone.* ^{1}H (CDCl$_3$): 1.4-1.55 (m, 1H), 1.65-1.8 (m, 2H), 1.9-2.0 (m, 1H), 2-2.15 (m, 1H), 2.3-2.55 (m, 5H), 3.3 (d, 1H), 3.75 (s, 6H).

Michael Addition of aniline to 1,3-diphenyl-propenone

Aniline (0.05 mL, 0.5 mmol) and 1,3-diphenyl-propenone (0.11g, 0.5mmol) are added to the mixture methanol (0.5 mL) and heptane (2 mL). TMBG was then added (1.8 g, 0.01 mol) and the reaction mixture heated at 80°C for 16 hours. After cooling, methanol (0.5 mL) and heptane (0.5 mL) were added and CO_2 was bubbled through the mixture for ~1 hour. The heptane phase was analyzed by GC-MS. The ionic liquid phase and the isolated product characterized were analyzed by ^{1}H NMR. *3-(N-phenylamino)-1,3-diphenyl-1-acetone.* ^{1}H (CDCl$_3$): 3.46 (d, 1H), 3.49 (d, 1H), 5.02 (m, 1H), 6.57 (d, 2H), 6.67 (m, 1H), 7.05 (m, 2H), 7.25 (d, 1H), 7.3-7.34 (m, 2H), 7.78-7.59 (m, 5H), 7.92 (d, 2H).

Results and Discussion

Claisen-Schmidt Condensation—Reaction of Butanone and Benzaldehyde

The Claisen-Schmidt condensation of butanone and benzaldehyde yields three products: the internal enone (3-methyl-4-phenyl-but-3-en-2-one), the terminal enone (1-phenyl-pent-1-en-3-one) and water (Figure 4.2).[20,41] Under basic conditions, the terminal enone product is the predominant product formed.[42] The reaction of butanone and benzaldehyde was carried out in TMBG, which played the dual role of base catalyst and solvent.[43,44]
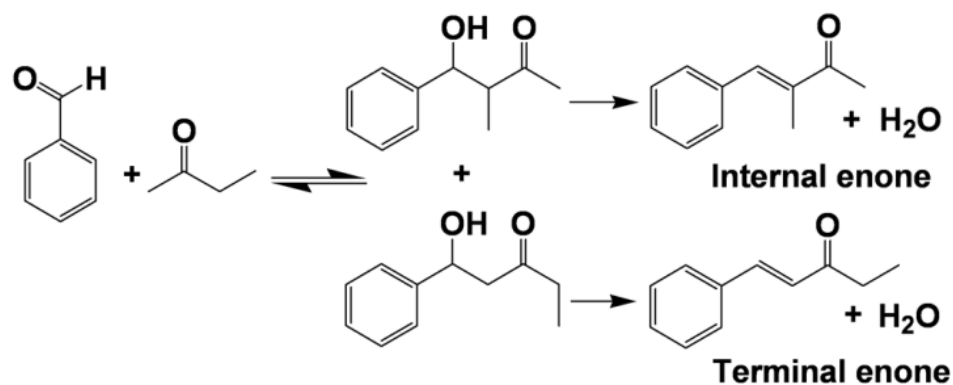
Figure 4.2. The Claisen-Schmidt Condensation reaction of 2-butanone and benzaldehyde.

The isolation of the enone products was performed by adding octane and methanol to the reaction mixture, followed by the addition of CO_2, which triggered the formation of the ionic liquid. Under these conditions an octane phase separated from the newly developed ionic liquid phase. The enone products were predominantly in the octane phase and were easily separated by decantation. After 24 hours at room temperature or 3 hours at 80°C, yields of 48% and 44% in enone products were obtained, respectively (Table 4.1).

Table 4.1. Reaction conditions and yields for the condensation of butanone and benzaldehyde in the presence of TMBG.

Temperature (°C)	Time (hours)	Yield (%)
Room Temp	24	48
80	1	13
80	2	24
80	3	44

The formation of the terminal and internal enone-products was also studied as a function of time at $80^{\circ}C$. As the reaction time increased, the yields first increased from 13% at 1 hour to 44% at 3 hours and then began to decrease after 4 hours (Table 4.1). The decrease was attributed to competing condensation processes between the enone products and the benzaldehyde, resulting in lower overall yields of the desired products. As a consequence, short reaction times to partial conversions were necessary in order to develop a process in which isolated yields were maximized and solvent recycle was possible (Figure 4.3).
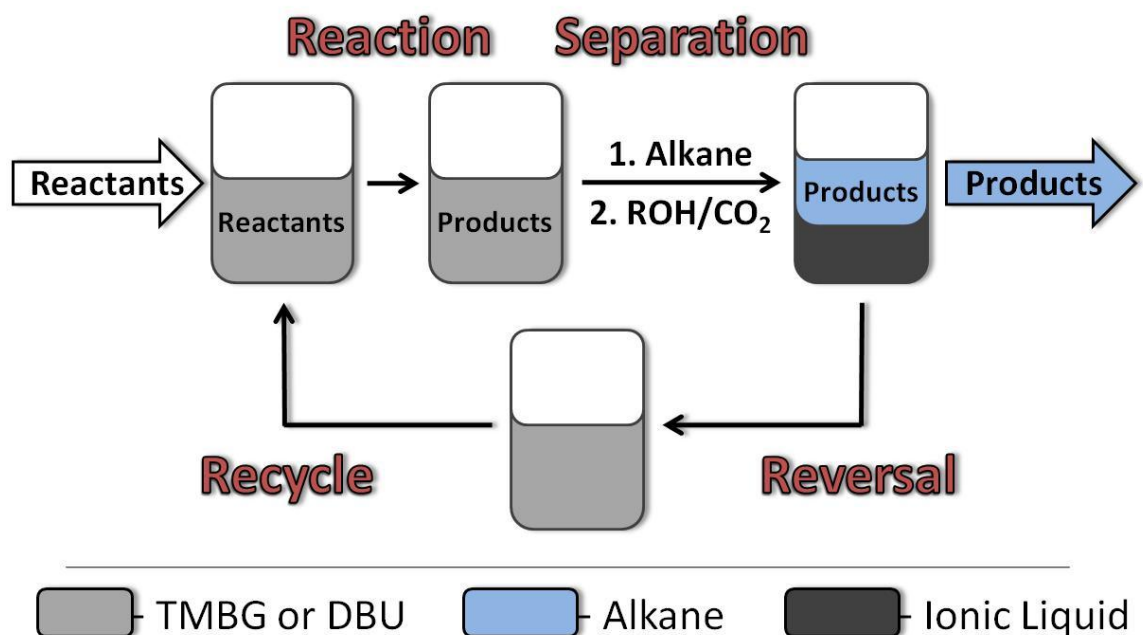
Figure 4.3. Process diagram for the coupled reaction and separation of the Claisen-Schmidt condensation of butanone and benzaldehyde.

The first attempt to recycle TMBG upon reversal of the ionic liquid failed. Water, a product from the condensation reaction, reacted with TMBG and CO_2 to form the N,N,N',N'-tetramethyl-N''-butylguanidium carbonate. The formation of the carbonate salt

86

resulted in a dramatic increase in the viscosity of the ionic liquid. This, coupled with the severe conditions for the reversal of the carbonate salt, precluded recycling. However, the reversal of the ionic liquid and recycle of TMBG were successful when the reaction mixture was dried over magnesium sulfate and filtered prior to reaction with CO_2. By introducing the drying step into the process, the TMBG was successfully recycled three times. The isolated yields in enone products were 34, 32 and 34% for each cycle with a consistent product distribution of 95% terminal enone product. Again, it should be emphasized that partial conversion was necessary in order to avoid the higher condensation products, thus providing recycle for the Claisen-Schmidt condensation in reversible ionic liquids.

Heck Reaction—Reaction of Bromobenzene and Styrene

Palladium catalyzed C-C coupling reactions between an aryl halide and a substituted alkene, also known as Heck reactions, are useful chemical transformations in many synthetic processes. Heck reactions inherently cause the formation of HX (X = halide; Figure 4.4), which needs to be neutralized by a base to recover the catalyst. Therefore, stoichiometric amounts of salt are formed as a by-product.
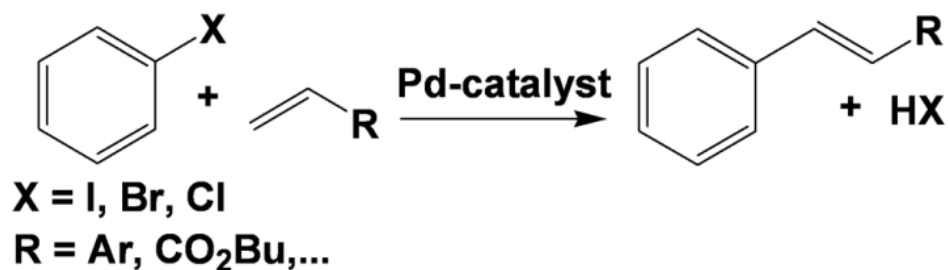
Figure 4.4. General reaction scheme for the Heck C-C coupling reactions.

In attempts to facilitate product isolation and recycle of the catalyst, ionic liquids have been widely explored to immobilize Pd complex catalysts for C-C bond formation.[35,45] In some cases, beneficial effects of the ionic environment on the efficiency and selectivity of the catalyst have been observed. It was also demonstrated that the organic products can be extracted and catalyst solutions can be reused. Some extractions have included the use of $scCO_2$ as an extraction medium.[46,47] In most cases, however, the accumulation of stoichiometric amounts of salts in the IL was not addressed. The presence of salts makes any continuous processing problematic and will ultimately limit batch-wise recycling. For a notable exception using a triphasic system of H_2O/IL/organic, see Perosa, *et al.*[48] The unique properties of the two-component reversible ionic liquids open new opportunities to make Heck processes more efficient as well as more environmentally-friendly by combining an efficient reaction with the ability to separate selectively the desired products, salt by-product, and catalyst.

Heck reactions were investigated in the two-component reversible ionic liquid mixture of DBU/hexanol. The overall process was designed to couple the reaction, which was carried out under ionic conditions, and a two-stage separation: first isolating the nonpolar product from the ionic liquid, and second by precipitating the salt by-product from the nonpolar solvent mixture. In principle, the reversible "switch" from ionic to molecular solvent should enable the separation of product and by-product sequentially, leading to a recycling of the solvent system and the catalyst (Figure 4.5).

As a benchmark reaction, the palladium catalyzed Heck reaction of bromobenzene and styrene was investigated (Figure 4.6). E-stilbene was produced as the major product. Other isomers (1,1-diphenylethylene and Z-stilbene) were obtained in yields of less than 5%.
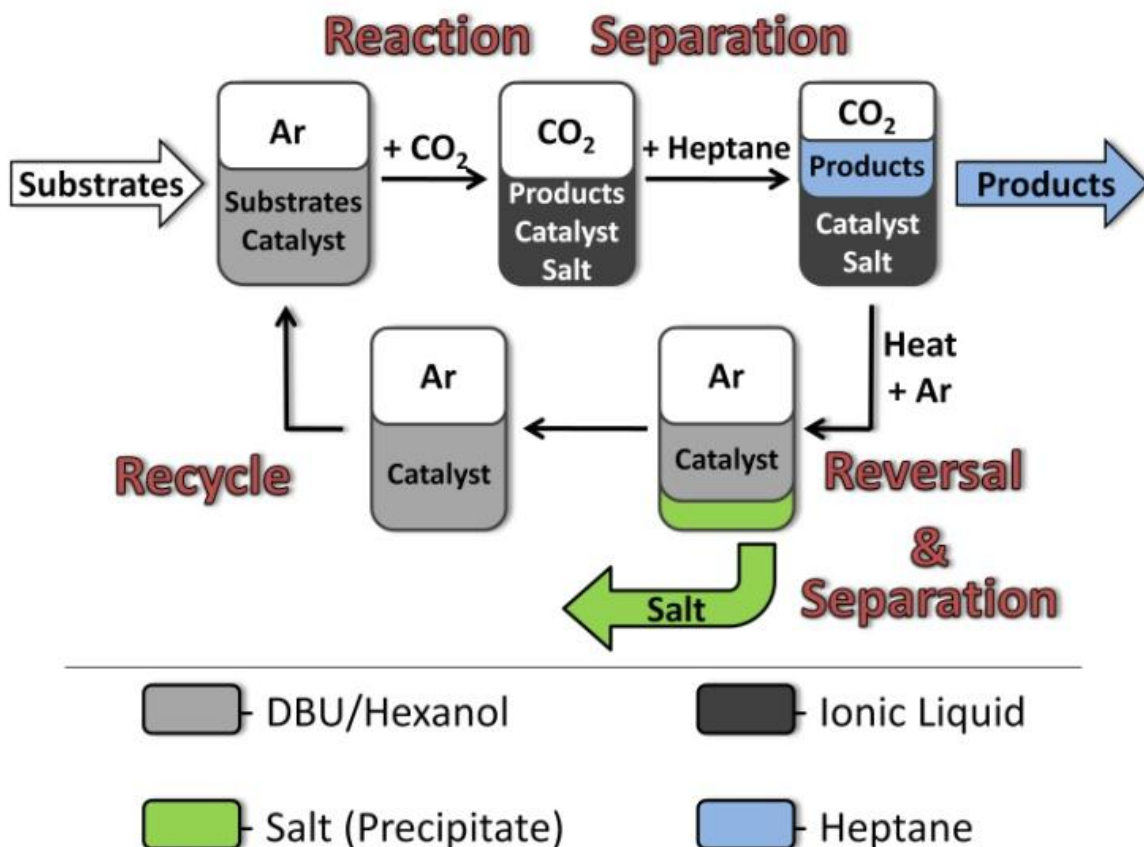
Figure 4.5. The process flow diagram for the Heck reaction in the DBU/hexanol reversible ionic liquid solvent system.
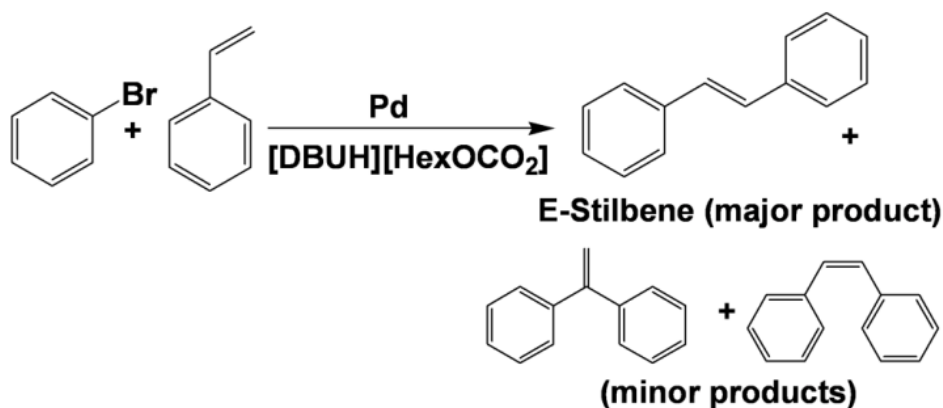
Figure 4.6. Heck reaction of bromobenzene and styrene in the reversible ionic liquid [DBUH]$^+$[HexOCO$_2$]$^-$.

Several forms of palladium were compared in the reaction process. Palladium acetate (Pd(OAc)$_2$) and palladium chloride (PdCl$_2$) in the presence and absence of triphenylphosphine ligand were compared. In addition, the preformed palladium chloride-triphenylphosphine complex was also investigated (Table 4.2). The following general procedure was employed. The required amount of palladium catalyst was introduced into the reaction vessel in a toluene solution. The solvent was then removed under reduced pressure, and the preformed reversible ionic liquid was added. The starting materials, bromobenzene (1 eq) and the styrene (1.2 eq), were introduced into the reaction vessel and the vessel pressurized with CO$_2$. The reaction mixture was kept at temperature for 3 days. After cooling and depressurization, the reaction products were extracted with heptane and analyzed via GC with tridecane as internal standard.

Table 4.2. Effect of catalyst type and concentration of the Heck reaction of bromobenzene and styrene at 115°C and 30 bar CO$_2$. (* - catalyst precursor and ligand were dissolved in acetonitrile and combined in the reaction vessel. After stirring for 20 minutes the solvent was removed under reduced pressure.)

Entry	Catalyst	Concentration (mol %)	Ligand	Yield (% E-stilbene)
1	Pd(OAc)$_2$	0.5	-	0
2	Pd(OAc)$_2$	0.5	TPP	2
3	PdCl$_2$	0.5	-	26
4	PdCl$_2$	0.5	TPP	31
5	PdCl$_2$(TPP)$_2$	0.5	-	87
6	PdCl$_2$(TPP)$_2$	1	-	83
7	PdCl$_2$(TPP)$_2$	2	-	97

The isolated complex $PdCl_2(TPP)_2$ (TPP = triphenylphosphine, PPh_3) was found to give the best performance, with up to a 97% yield of E-stilbene using a catalyst loading of 2 mol% (Table 4.2). The effects of temperature and CO_2 pressure on the yields of product were also investigated (Table 4.3).

Carrying out the coupling under 30 bar of CO_2 at 115°C was found to afford the higher yield in E-stilbene. No additional base was required in these experiments since free DBU, in equilibrium with the ionic species, was found to act as a scavenger for HBr.

Table 4.3. Effect of CO_2 pressure and temperature on the Heck reaction of bromobenzene and styrene. (* - 2 mol% $PdCl_2(TPP)_2$)

Entry	Temperature (°C)	Pressure (bar)	Yield (%)
1	100	30	9
2	115	30	87
3*	115	0	22
4	115	50	39
5	140	30	65

Extraction of the product(s) from the reaction mixture was carried out under a CO_2 atmosphere to ensure that the solvent remained in the ionic form. However, GC analysis indicated that some free DBU and hexanol were also extracted into the heptane phase. After phase separation, the ionic phase was heated and purged with argon to revert back to the DBU/hexanol molecular liquid. A colorless precipitate separated from the solution; it was filtered off and identified as the HBr salt of DBU by NMR

spectroscopy. The supernatant solution remained yellow, suggesting the presence of dissolved palladium catalyst.

The application of two component reversible ionic liquids to the Heck reaction offers a new and potentially effective solution for the problem of salt accumulation. The reaction was carried out in the ionic liquid form of the solvent, from which the nonpolar product could be isolated by extraction. Reversing the solvent to its molecular liquid state caused the salt by-product to precipitate. After separation of the salt, the solvent (containing the catalyst) was switched back to its ionic form and was used for another Heck reaction showing significant activity. The optimized recycle procedure for the Heck reaction using reversible ionic liquids is currently being investigated by our collaborators at RWTH Aachen University in Germany (Prof. Leitner and DJ Hahne).

Reversible Ionic Liquids: Challenges and Limitations

Realistically, reversible ionic liquids are not the solution to all reaction-separation problems. In this section, their limitations and challenges are discussed for three reactions and one processing issue: 1) the cyanosilylation of cyclohexanone, 2) the Michael addition of 2-cyclohexenone, 3) the Michael addition of aniline to 1,3-diphenyl-propenone and 4) viscosity of ionic liquid form.

<u>Cyanosilylation of Cyclohexanone</u>

The cyanosilylation of cyclohexanone with trimethylsilyl cyanice (TMSCN) was carried out in TMBG at room temperature (Figure 4.7). The isolation of the product was performed by adding heptane and methanol to the reaction mixture. The addition of CO_2 triggered the formation of the ionic liquid which resulted in a two-phase system, the ionic liquid and the heptane phases. The product 1-trimethylsilyloxy-1-cyclohexanecarbonitrile

partitioned predominantly into the heptane phase, thus facilitating its separation from the reaction mixture.
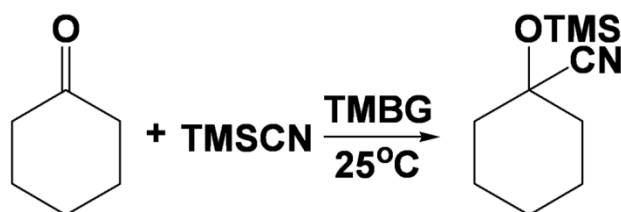
Figure 4.7. Cyanosilylation of cyclohexanone in TMBG.

The variation of reaction time (1.5 to 16 hours) as well as of the molar ratio of TMBG to cyclohexanone (0.02:1 to 1:1) had little or no effect on the reaction yields, which were essentially quantitative. However, the analysis of the ionic liquid phase (via NMR) indicates the formation of the ionic by-product N,N,N',N'-tetramethyl-N''-butyl-N''-trimethylsilylguanidinium cyanide (Figure 4.8).[49]
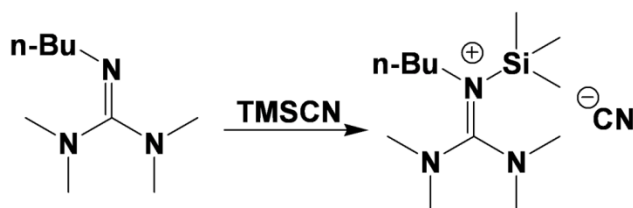
Figure 4.8. Formation of the by-product N,N,N',N'-tetramethyl-N''-butyl-N''-trimethylsilylguanidinium cyanide.

The formation of this ionic by-product is detrimental as it is irreversible and its presence drastically increases the viscosity of the ionic liquid phase, precluding the quantitative reversal of the ionic liquid for recycle. The formation of the silyl salt was minimized, but not eliminated, by adding heptane at the reaction stage as opposed to

the separation stage. The product yields were not affected; they remained quantitative (96 to 98%). Under these conditions, the recycling of TMBG upon reversal of the ionic liquid phase was investigated at two molar ratios of TMBG to cyclohexanone to TMSCN, 0.4:1:1.2 and 1:1:2 respectively (Table 4.4).

Table 4.4. Cyanosilylation of cyclohexanone coupled with the recycling of the ionic liquid phase.

Entry	Mole Ratio TMBG:Cyclohexanone:TMSCN	Time (hours)	Yield (%)
1-1	0.4:1:1.2	17	96
1-2	0.4:1:1.2	16	54
2-1	1:1:1.2	16	86
2-2	1:1:1.2	16	56

In the first cycle, the 1-trimethylsilyloxy-1-cyclohexanecarbonitrile product was isolated with 86 and 96 % yields (Table 4.4, entries 1-1 & 2-1 respectively). The ionic liquid phase was then reversed upon heating at 50^oC for 4 hours. The resulting TMBG was reused for a second cycle, yielding the desired product in 54% and 56% (Table 4.4, entry 1-2 & 2-2 respectively). The loss of yields upon recycle has been attributed to the contamination of the guanidine precursor with the by-product (N,N,N',N'-tetramethyl-N"-butyl-N"-trimethylsilylguanidinium cyanide).

Michael addition of dimethyl malonate to 2-cyclohexenone

The base-catalyzed Michael addition of dimethyl malonate to 2-cyclohexenone was carried out in TMBG at 80^oC. In all experiments, the ratio of TMBG to malonate to 2-cyclohexenone was 1:1:1. Upon addition of methanol, hexane and CO_2, the formation

of the ionic liquid yielded two phases, the ionic liquid and the hexane phase. The analysis by GC-MS of the hexane phase showed the complete disappearance of the starting materials. The ^{1}H NMR analysis showed that the product existed in the ionic form and was present exclusively in the ionic liquid phase. The reason for this is simply that in a basic medium like TMBG the α-carbon of the β-diester product is deprotonated resulting in the ionic product exclusively (Figure 4.9).

An acidic work-up with 10% aqueous HCl was performed yielding the neutral form of the product, which now partitioned predominantly into the hexane phase. The neutral product was subsequently isolated in 86 to 100 % yields. Although TMBG can be recovered and eventually recycled, the necessity of an acidic work-up complicates the overall process providing little advantage for coupling the reaction and separation.
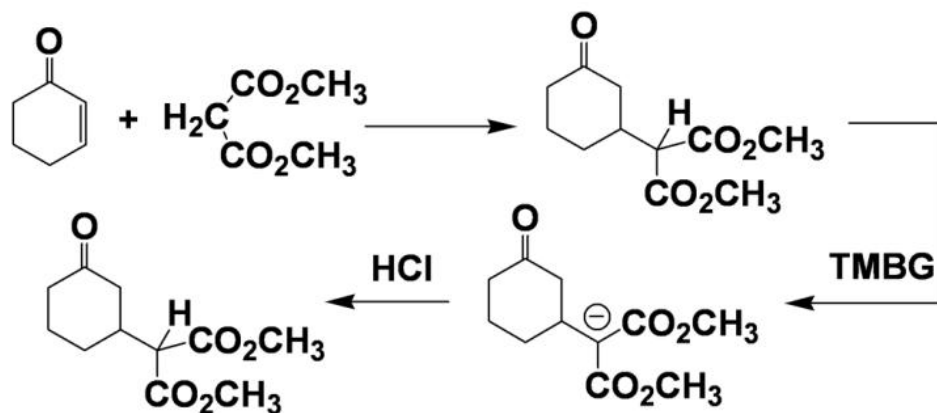
Figure 4.9. Base catalyzed Michael addition of dimethylmalonate and 2-cyclohexenone.

Michael addition of aniline to 1,3-diphenyl-propenone

The Michael addition of aniline to 1,3-diphenyl-propenone (chalcone) was carried out by first dissolving the reaction partners in a methanol:heptane mixture (1:4) followed by the addition of TMBG in an equimolar ratio relative to methanol (Figure 4.10).
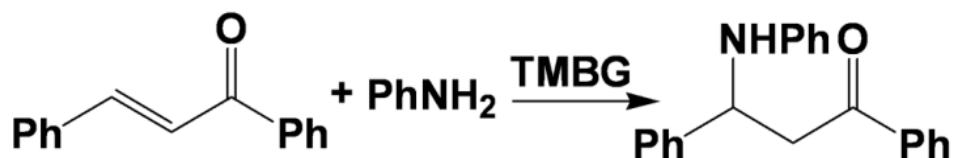
Figure 4.10. TMBG-catalyzed addition of aniline to 1.3-diphenyl-propenone.

The reaction was run at $80\,^{\circ}C$ for 18 hours. The isolation of the 1,3-diphenyl-3-phenylamino-propan-1-one product was performed by bubbling CO_2 throughout the mixture (forming the ionic liquid) resulting in a two-phase ionic liquid and heptane system. The 1,3-diphenyl-3-phenylamino-propan-1-one partitioned predominantly into the heptane phase, from which it was isolated in 86% yield. After reversal of the ionic liquid at $60\,^{\circ}C$ for 4 hours, the TMBG was recycled. In the second cycle, the isolated yield decreased to 45%. It is conjectured that the accumulation of organic materials in the ionic liquid phase changes the product partitioning in recycle attempts when compared to the first cycle.

Conclusions

While conventional room temperature ionic liquids are often cited as environmentally-friendly alternative solvents, current research continues to indicate that they will face severe limitations in applicability due to separation difficulties. In this chapter, two reactions (Claisen-Schmidt condensation and Heck coupling) were presented, illustrating the successful reaction in two-component reversible ionic liquids with the added benefits of easy separation of the product and recycling of the solvent system and catalyst. In addition, much emphasis was provided on the limitations and

challenges of coupling reactions and separations in two-component reversible ionic liquids for the cyanosilylation of cyclohexanone and two examples of Michael additions. For a more extensive study on the application of two-component reversible ionic liquids, readers should be directed to the PhD thesis of a former colleague, Ejae John (Prof. Liotta, Georgia Tech, 2007).

The ability to couple reaction and separation in a common solvent system allows for the development of sustainable processing in the chemical industry that is simpler, more efficient, and more environmentally-benign than solvents commonly used today. By treating a typical reaction/separation process inter-dependently rather than independently, the approach that research laboratories and commercial plants take in the design of processes is fundamentally challenged. With proper care and technique, it has been shown that reversible ionic liquids are capable of being recycled, completely eliminating the need to purify or dispose of waste. Additionally, they facilitate catalyst recovery, yielding efficient separations of expensive catalysts for reuse. Other systems where switchable solvent systems have much potential are being investigated, in an attempt to push the envelope of sustainable solvent systems.

References

(1)   Heldebrant, D. J.; Jessop, P. G.; Thomas, C. A.; Eckert, C. A.; Liotta, C. L. *Journal of Organic Chemistry* **2005**, *70*, 5335.

(2)   Jessop, P. G.; Heldebrant, D. J.; Li, X. W.; Eckert, C. A.; Liotta, C. L. *Nature* **2005**, *436*, 1102.

(3)   Phan, L.; Chiu, D.; Heldebrant, D. J.; Huttenhower, H.; John, E.; Li, X. W.; Pollet, P.; Wang, R. Y.; Eckert, C. A.; Liotta, C. L.; Jessop, P. G. *Industrial & Engineering Chemistry Research* **2008**, *47*, 539.

(4)   Blasucci, V.; Dilek, C.; Huttenhower, H.; John, E.; Llopis-Mestre, V.; Pollet, P.; Eckert, C. A.; Liotta, C. L. *Chemical Communications* **2009**, 116.

(5)   Dillow, A. K.; Brown, J. S.; Liotta, C. L.; Eckert, C. A. *Journal of Physical Chemistry A* **1998**, *102*, 7609.

(6)   Brown, J. S.; Lesutis, H. P.; Lamb, D. R.; Bush, D.; Chandler, K.; West, B. L.; Liotta, C. L.; Eckert, C. A.; Schiraldi, D.; Hurley, J. S. *Industrial & Engineering Chemistry Research* **1999**, *38*, 3622.

(7)   Thompson, R. L.; Glaser, R.; Bush, D.; Liotta, C. L.; Eckert, C. A. *Industrial & Engineering Chemistry Research* **1999**, *38*, 4220.

(8)   Brown, R. A.; Pollet, P.; McKoon, E.; Eckert, C. A.; Liotta, C. L.; Jessop, P. G. *Journal of the American Chemical Society* **2001**, *123*, 1254.

(9)   Nolen, S. A.; Lu, J.; Brown, J. S.; Pollet, P.; Eason, B. C.; Griffith, K. N.; Glaser, R.; Bush, D.; Lamb, D. R.; Liotta, C. L.; Eckert, C. A.; Thiele, G. F.; Bartels, K. A. *Industrial & Engineering Chemistry Research* **2002**, *41*, 316.

(10)   Jessop, P. G.; Stanley, R. R.; Brown, R. A.; Eckert, C. A.; Liotta, C. L.; Ngo, T. T.; Pollet, P.; Royal Soc Chemistry: 2003, p 123.

(11)   Eckert, C. A.; Liotta, C. L.; Bush, D.; Brown, J. S.; Hallett, J. P. *Journal of Physical Chemistry B* **2004**, *108*, 18108.

(12)   Koch, D.; Leitner, W. *Journal of the American Chemical Society* **1998**, *120*, 13398.

(13)   Furstner, A.; Ackermann, L.; Beck, K.; Hori, H.; Koch, D.; Langemann, K.; Liebl, M.; Six, C.; Leitner, W. *Journal of the American Chemical Society* **2001**, *123*, 9000.

(14)   Solinas, M.; Jiang, J. Y.; Stelzer, O.; Leitner, W. *Angewandte Chemie-International Edition* **2005**, *44*, 2291.

(15)   Maayan, G.; Ganchegui, B.; Leitner, W.; Neumann, R. *Chemical Communications* **2006**, 2230.

(16)   Chandler, K.; Deng, F. H.; Dillow, A. K.; Liotta, C. L.; Eckert, C. A. *Industrial & Engineering Chemistry Research* **1997**, *36*, 5175.

(17)   Chandler, K.; Liotta, C. L.; Eckert, C. A.; Schiraldi, D. *Aiche Journal* **1998**, *44*, 2080.

(18)   Lesutis, H. P.; Glaser, R.; Liotta, C. L.; Eckert, C. A. *Chemical Communications* **1999**, 2063.

(19)   Patrick, H. R.; Griffith, K.; Liotta, C. L.; Eckert, C. A.; Glaser, R. *Industrial & Engineering Chemistry Research* **2001**, *40*, 6063.

(20)   S. Nolen, C. L. L., C.A. Eckert, R. Glaser *Green chemistry* **2003**, *5*, 663.

(21)   Chandler, K.; Culp, C. W.; Lamb, D. R.; Liotta, C. L.; Eckert, C. A. *Industrial & Engineering Chemistry Research* **1998**, *37*, 3252.

(22)   Wheeler, C.; Lamb, D. R.; Jayachandran, J. P.; Hallett, J. P.; Liotta, C. L.; Eckert, C. A. *Industrial & Engineering Chemistry Research* **2002**, *41*, 1763.

(23)   Jayachandran, J. P.; Wheeler, C.; Eason, B. C.; Liotta, C. L.; Eckert, C. A. *Journal of Supercritical Fluids* **2003**, *27*, 179.

(24)   Chamblee, T. S.; Weikel, R. R.; Nolen, S. A.; Liotta, C. L.; Eckert, C. A. *Green Chemistry* **2004**, *6*, 382.

(25)   Xie, X. F.; Liotta, C. L.; Eckert, C. A. *Industrial & Engineering Chemistry Research* **2004**, *43*, 7907.

(26)   Weikel, R. R.; Hallett, J. P.; Liotta, C. L.; Eckert, C. A. *Industrial & Engineering Chemistry Research* **2007**, *46*, 5252.

(27)   Hallett, J. P.; Ford, J. W.; Jones, R. S.; Pollet, P.; Thomas, C. A.; Liotta, C. L.; Eckert, C. A. *Industrial & Engineering Chemistry Research* **2008**, *47*, 2585.

(28)   Lu, J.; Lazzaroni, J.; Hallett, J. P.; Bommarius, A. S.; Liotta, C. L.; Eckert, C. A. *Industrial & Engineering Chemistry Research* **2004**, *43*, 1586.

(29)   Broering, J. M.; Hill, E. M.; Hallett, J. P.; Liotta, C. L.; Eckert, C. A.; Bommarius, A. S. *Angewandte Chemie-International Edition* **2006**, *45*, 4670.

(30)   Hill, E. M.; Broering, J. M.; Hallett, J. P.; Bommarius, A. S.; Liotta, C. L.; Eckert, C. A. *Green Chemistry* **2007**, *9*, 888.

(31)   Vinci, D.; Donaldson, M.; Hallett, J. P.; John, E. A.; Pollet, P.; Thomas, C. A.; Grilly, J. D.; Jessop, P. G.; Liotta, C. L.; Eckert, C. A. *Chemical Communications* **2007**, 1427.

(32)   Jiang, N.; Vinci, D.; Liotta, C. L.; Eckert, C. A.; Ragauskas, A. J. *Industrial & Engineering Chemistry Research* **2008**, *47*, 627.

(33)   Donaldson, M. E.; Mestre, V. L.; Vinci, D.; Liotta, C. L.; Eckert, C. A. *Industrial & Engineering Chemistry Research* **2009**, *48*, 2542.

(34)   *Ionic liquids III : fundamentals, progress, challenges, and opportunities*; American Chemical Society :: Washington, DC :, 2005.

(35)   *Ionic liquids in synthesis*; 2nd, completely rev. and enl. ed. ed.; Wiley-VCH: Weinheim :, 2008.

(36)   Welton, T. *Chemical Reviews* **1999**, *99*, 2071.

(37)   Blanchard, L. A.; Hancu, D.; Beckman, E. J.; Brennecke, J. F. *Nature* **1999**, *399*, 28.

(38)   Leitner, W. *Accounts of Chemical Research* **2002**, *35*, 746.

(39)   Cole-Hamilton, D. J. *Science* **2003**, *299*, 1702.

(40)   Phillip Peac, D. J. C., Jennefer A. Kenny, Inderjit Mann, Ian Houson, Lynne Campbell, Tim Walsgrove, Martin Wills *Tetrahedron* **2006**, *62*, 1864.

(41)   Sunberg, F. A. C. a. R. J. *Advanced Organic Chemistry, Part B: Reactions and Synthesis*; 3rd ed ed.; Plenum Press: New York, NY, 1990.

(42)   M. Stiles, D. W., G. Hudson *JACS* **1959**, *81*, 628.

(43)   Costa, M.; Chiusoli, G. P.; Taffurelli, D.; Dalmonego, G. *Journal of the Chemical Society-Perkin Transactions 1* **1998**, 1541.

(44)   Toshio Isobe, K. F., and Tsutomu Ishikawa *Journal of Organic Chemistry* **2000**, *65*, 7770

(45)   Mo, J.; Xiao, J. L. *Angewandte Chemie-International Edition* **2006**, *45*, 4152.

(46)   Carmichael, A. J.; Earle, M. J.; Holbrey, J. D.; McCormac, P. B.; Seddon, K. R. *Organic Letters* **1999**, *1*, 997.

(47)   Yoon, B.; Yen, C. H.; Mekki, S.; Wherland, S.; Wai, C. M. *Industrial & Engineering Chemistry Research* **2006**, *45*, 4433.

(48)   Perosa, A.; Tundo, P.; Selva, M.; Canton, P. *Chemical Communications* **2006**, 4480.

(49)   L. Wang, X. H., J. Jiang, X. Liu, X. Feng *Tetrahedron Letters* **2006**, *47*, 1581.

CHAPTER 5   REVERSIBLE IONIC LIQUIDS FOR POST-COMBUSTION CO_2 CAPTURE

Introduction

The capture and sequestration of CO_2 promises to be one of the largest problems faced by the coming generation of scientists and engineers, in terms of economic impact and technical feasibility. CO_2 is one of the chief products of combustion, and combustion is at the heart of energy production, transportation, manufacturing, and nearly every other facet of the global infrastructure. Despite the debate over the magnitude of the effect of CO_2 on the global climate, the fact remains that the major developed nations of the world are actively developing political strategies for the mitigation of CO_2. As one of those leaders, the United States of America is taking an aggressive position towards the regulation of CO_2 released within its borders. This is evidenced by several bills introduced to Congress (most notable is H.R. 2454: American Clean Energy and Security Act of 2009; passed by House in 2009, currently stalled in Senate)[1] and significant federal funding for the development of carbon dioxide capture and storage projects ($3.4 billion from the American Recovery and Reinvestment Act of 2009 alone).[2] Receiving much attention as a potential point source for the development of CO_2 capture technologies is the coal fired power plant – responsible for approximately one-third of all the CO_2 emitted in the United States.

In addition to being a major contributor to the total CO_2 emissions in the US, coal fired power plants are strategically appealing due to the relatively close proximity to geological sequestration sites – a potential storage option for the permanent sequestration of CO_2. All coal fired power plants produce roughly the same flue gas streams from the combustion of coal using air as the oxidant, and the development of a

viable capture technology has the potential to apply to hundreds of these point sources with only minor changes in operating conditions. If only it were that simple. From a separation standpoint, the post-combustion flue gas stream serves as a monumental technical challenge due to the amount and conditions of the flue gas stream coupled with the dilute concentration of CO_2.

The CO_2 capture technologies currently being developed for a retro-fit application to post-combustion CO_2 capture include membranes, solid adsorbents, and liquid solvents.[3] Membrane technologies achieve separation primarily by means of size exclusion,[4,5] though some materials have been developed to incorporate chemical interactions.[6] Solid adsorbents and liquid solvents utilize chemical and/or physical mechanisms to achieve separation.[3] In general, chemical reaction mechanisms for separation processes involve the formation of strong bonds (e.g. covalent, ionic) and typically offer high separation efficiency due to a high selectivity of reactive species relative to unreactive species. Physical separation mechanisms, on the other hand, result from the formation of relatively weak bonds (e.g. van der Waals forces). The advantage of physical separation mechanisms is the low energy requirement for releasing the captured species, giving way to regeneration of the solvent for recycle. The regeneration energy requirement for chemical separation mechanisms is significantly higher relative to physical mechanisms.

Of the available technologies, chemical absorption is the most widely implemented for the recovery of CO_2 from coal powered electric generating facilities[7]. (It should be noted that the term *absorption*, as it is used here, refers to solvent based technologies. *Adsorption* is reserved for technologies using solid adsorbents.) The widespread use arises from the fact that chemical absorption processes are capable of recovering 75-90% of CO_2 from dilute feed streams, and producing a high purity (> 99%)

CO_2 product stream[8]. Chemical absorption processes take advantage of the acidic nature of the CO_2 feed stream, and removes CO_2 by use of amine based acid-base chemistry, shown in Figure 5.1. The equilibrium reaction requires two moles of amine per one mole of CO_2 captured, and is reversed when heated.
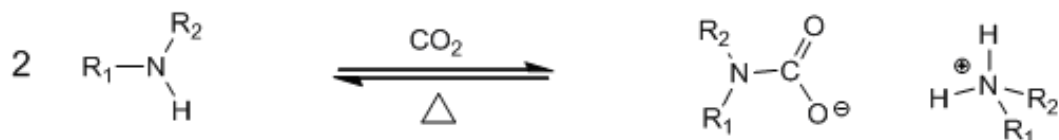
Figure 5.1. The general reaction scheme of an amine with CO_2, resulting in the formation of a carbamate (-) and ammonium (+). R_2 = H for primary amines.

Several mechanisms have been developed to describe the reaction of amines with CO_2, but the most respected and frequently used mechanism involves the formation of an unstable zwitterions,[9] an amine molecule containing both the positive and negative charge,

$$CO_2 + R_2NH \leftrightarrow R_2N^+CO_2^-$$ (5.1)
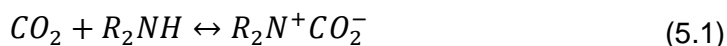
which then protonates a base to form the stable carbamate/ammonium salt,

$$R_2N^+CO_2^- + R_2NH \rightarrow R_2NCO_2^- + R_2NH_2^+.$$ (5.2)
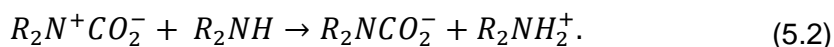
The second step is the rate determining step, and the zwitterionic product from step one is extremely unstable and is not found in appreciable concentrations.

The primary problem associated with using amine based chemical absorption processes is that the recovery of the CO_2 from the solvent requires much energy in the form of heat. The process flow diagram for typical liquid solvent CO_2 scrubbing systems is simple, as shown in Figure 5.2.
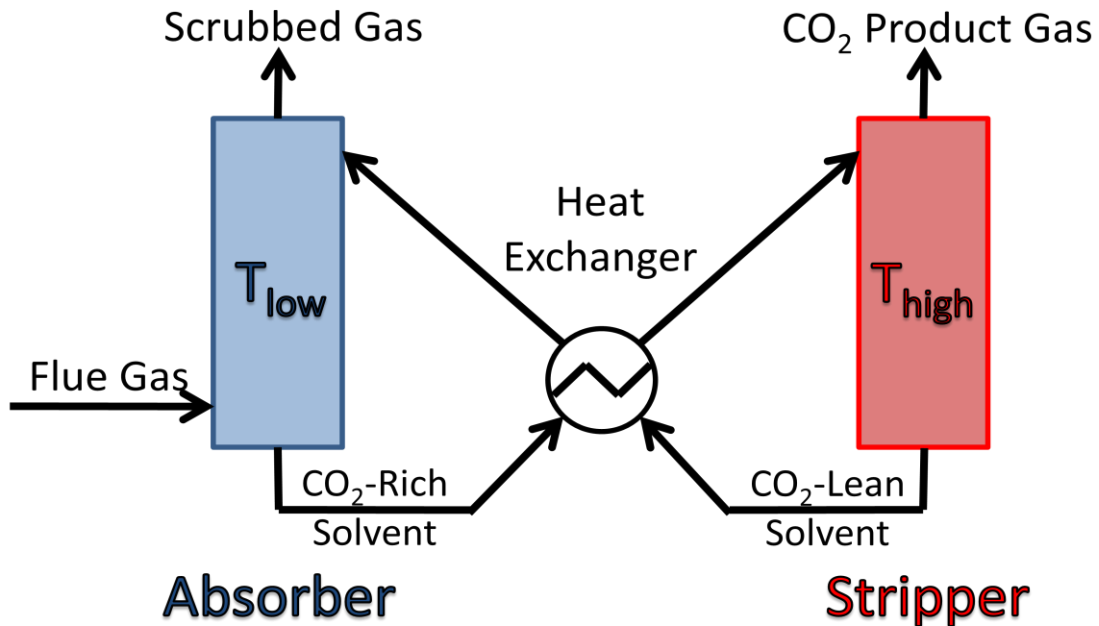
Figure 5.2. A typical process flow diagram for the CO_2 capture of power plant flue gas using chemical absorption solvents.

The main unit operations involved in the CO_2 capture process are an absorber tower, a stripper column, and a heat exchanger to recover heat from the hot regenerated solvent. The flue gas enters from the bottom of the absorber while the cooled lean solvent is pumped in from the top of the tower. The gas contacts the solvent and CO_2 is absorbed; the remaining flue gas leaves out the top of the tower, and the CO_2 rich solvent leaves out the bottom. From there, the solvent passes through the heat exchanger, where it is heated slightly before entering the stripper column. A reboiler at the bottom of the stripper column heats the solvent using steam to reverse the absorption reaction and regenerate the solvent. The hot lean solvent is recycled back through the heat exchanger and a cooler before it is pumped back to the top of the absorber. The CO_2 product stream from the top of the stripper column is saturated with water at nearly atmospheric pressure, and must be dehydrated and compressed before

it is sent to a pipeline for transport to a consumer or sequestration site. Chemical absorption CO_2 recovery processes, when applied to post-combustion CO_2 capture from power plants, are innately integrated into the steam cycle. The result is a 40% loss of power output from the power generating facility.[10]

Physical absorption processes are also attractive for the post-combustion recovery of CO_2 from large point source emitters. Physical absorption uses non-reactive liquid solvents that have some acid gas affinity. Because physical absorption processes are typically pressure driven (as opposed to thermally driven chemical absorption), they are ideally used for feed streams with high partial pressures of CO_2. With available technology, physical absorption processes for the application to post combustion CO_2 recovery are not economically feasible due to the low energy efficiency that arises from the compression of a feed stream that is mostly nitrogen. Some common types of physical absorption solvents include chilled methanol, N-methylpyrrolidone (NMP), and recently, room-temperature ionic liquids.[11] Research has shown that ionic liquids as physical absorbents have much promise, with CO_2:N_2 selectivities reported as high as 127[12] and with CO_2 absorption capacities nearing 3% (molar) at CO_2 partial pressures of only 1 bar.[13]

One-component reversible ionic liquids for CO_2 capture are examined here in an attempt to utilize a selective chemical absorption process coupled with the high CO_2 capacity offered by physical absorption. A structure-property relationship associating solvent structure with fundamental thermodynamic properties of separation has been used to gather the information necessary to design an optimal one-component reversible ionic liquid solvent for CO_2 capture. In addition to a study on enhancing the CO_2 capacity of reversible ionic liquids, the viscosity of the solvents and the apparent chemical absorption uptake rates were examined; leading to an overall assessment for the

application of these novel solvents to CO_2 capture using absorption processing technology.

Viscosity Measurements

The viscosities of the materials used were thoroughly investigated as viscosity represents one of the major limitations in applying ionic liquids to industrial processes. The viscosity, or flowability, is often ignored when designing processes utilizing traditional organic solvents as the viscosities are well within the limits of available processing technology. A good rule of thumb for an upper limit of viscosity in absorber-like processes is 100 cP, which is approximately the viscosity of low molecular weight polyethylene glycols successfully used in industrial processing.[14] Although the viscosities of ionic liquids can be altered by adjusting the molecular structure, they are generally very high relative to organic solvents and fall in the 50 to 10,000 cP range.[15] In addition to posing a risk for process-ability, the high viscosity of ionic liquids can also dramatically influence the diffusivity of gases into the liquids.[16-18]

The viscosity measurements of the one-component molecular and ionic liquids were conducted using a Rheosys Merlin II rotational viscometer with an integrated Peltier temperature controller capable of measuring at temperatures of -10 to 120°C and rotational speeds of 1 to 2000 rpm. The geometry used was a 5.44° cone and plate system. Because the cone is truncated to prevent damage to the plate, standard viscosity samples (Brookfield Engineering Laboratories, Inc., 1000 cP and 100 cP) were used to calibrate the gap setting. After calibration, the gap was checked with the standards weekly to ensure proper alignment.

The viscometer method used for the measurement of molecular liquid samples consisted of 10 samples at varying rotational speeds from 50 to 2000 rpm, and then back from 2000 to 50 rpm to eliminate the possibility of hysteresis (due to momentum). The measured viscosities for the molecular liquids exhibited identical values for increasing and decreasing shear rates, suggesting no hysteresis. Additionally, the viscosities of the molecular liquids were observed to remain constant (within experimental error) at varying shear rates, verifying that these materials are Newtonian fluids.

The viscosities of the molecular liquids were determined from 25 to 55°C, and are given in Figure 5.3. The measurements were run in triplicate, with the error bars representing the standard deviation of the values. The error of the viscosity for the molecular liquids is considerable, and is a function of the rheometer accuracy. The accuracy of the rheometer is a function of the full scale torque load, and is ideally suited for higher viscosity samples. For example, at 25°C the viscosity of all materials is between 5-20 cP; at the maximum rotational speed of 2000 rpm the percentage of maximum torque being measured by the rheometer is less than 1%. Therefore, for low viscosity samples (<100 cP) the viscometer is only appropriate for determining order-of-magnitude approximations of the viscosity.

Despite the error associated with the viscosity measurements of the molecular liquid samples, it can be seen that all materials fall below the 100 cP threshold. However, there appears to be a trend of increasing viscosity with respect to temperature; an observation that is contradictory to widely accepted trends. Therefore, there must be some other process that is altering the viscosity of the samples. A likely culprit is the accumulation of water, as water and amines are known to react and form hydroxides. The hydroxides can hydrogen bond with surrounding amines, causing a network of

relatively strong intermolecular interactions that result in an observed increase in viscosity.
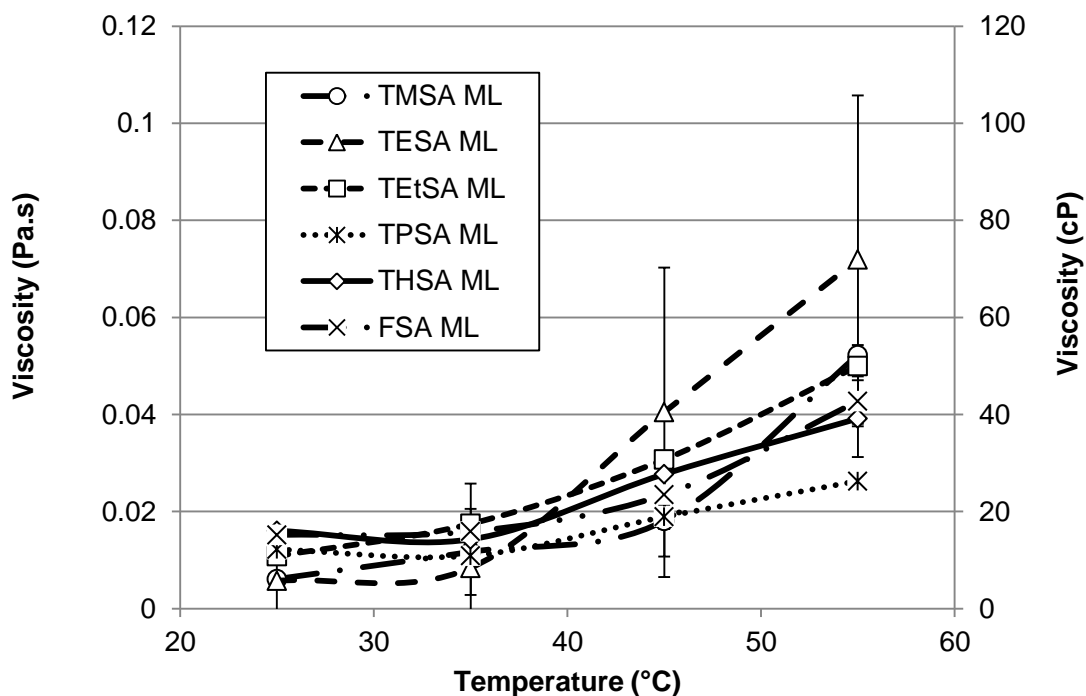
Figure 5.3. The viscosity measurements of the one-component molecular liquids from 25 to 55°C.

More important than the molecular liquids are the viscosity measurements of the one-component ionic liquids, given in Figure 5.4. The viscometer method used for the ionic liquid samples is more ambiguous than the method used for the molecular liquid samples where a constant method was used for all samples. Due to the high viscosity, the maximum torque load could easily be reached. Therefore, the samples were prepared and the rotational speed was altered manually until the maximum torque percentage was observed. The method then consisted of 5 measurements at increasing rotational speeds from 50 rpm to the maximum, then 5 measurements at decreasing

rotational speeds. The stability of the ionic liquids was a concern, particularly at higher

temperatures, so the overall method was designed to be completed with several

minutes. As with the molecular liquid samples, no hysteresis was observed and the

materials were confirmed to be Newtonian (i.e. no shear thinning was observed).
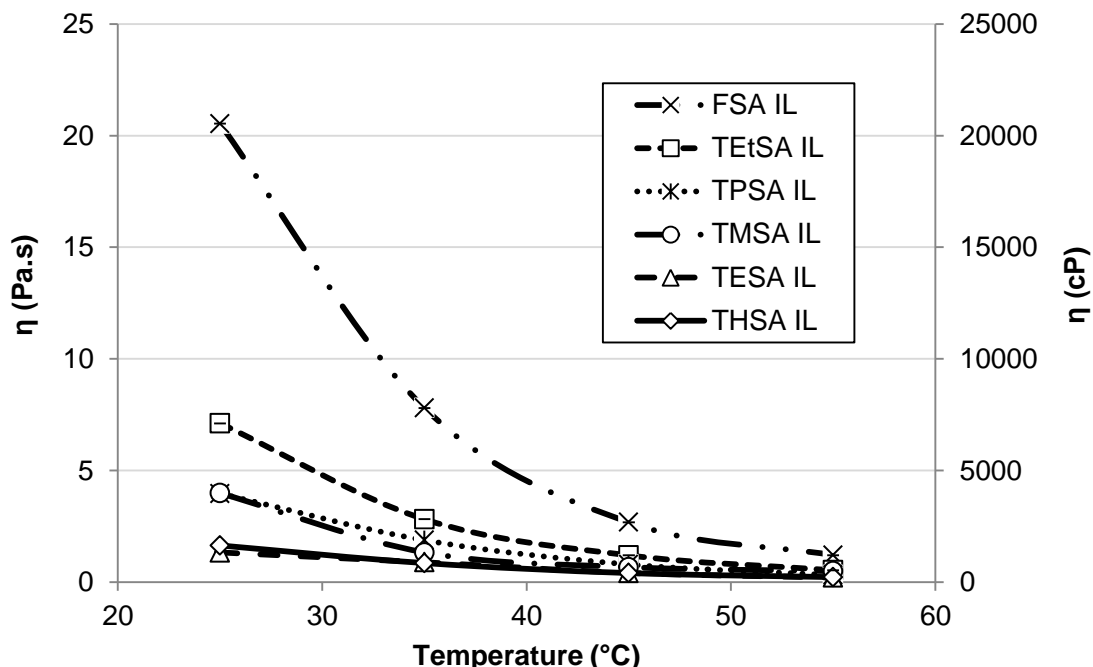
Figure 5.4. The viscosity measurements of the one-component ionic liquids from 25 to 55°C.

The viscosity measurements for the ionic liquids were again run in triplicate with

the error bars representing the standard deviation of the measurements. Here, the error

bars are covered by the data points, reflecting the high accuracy of the viscometer for

highly viscous samples. The trend of viscosity with respect to temperature follows the

accepted trend of decreasing viscosity with increasing temperature.

The conversion of the molecular liquid to the ionic liquid results in a viscosity

change of 3 orders-of-magnitude for all the materials examined; problematic for absorber

110

processing. In regards to the structure dependency of the viscosity, the viscosity is observed to decrease as more carbons are placed on the silicon. Therefore, TEtSA has the highest ionic liquid viscosity of any of the trialky- materials (THSA being the lowest) and TMSA has a higher viscosity than TESA. The TESA and THSA exhibit nearly identical viscosities, suggesting the addition of electron donor groups to the silicon can also have a strong effect on decreasing viscosity. The fluorinated material FSA exhibits the highest viscosity of all, being almost a gel (i.e. extremely low flow characteristics); consistent with electron withdrawing groups on silicon resulting in considerably higher ionic liquid viscosities.

To confirm the stability of the ionic liquids over the course of the experiment and at especially at the high temperatures an Arrhenius plot for the natural log of viscosity (ln η, where η has units of Pa.s) versus inverse temperature (1/T, where T is in units of K) was examined, Figure 5.5.
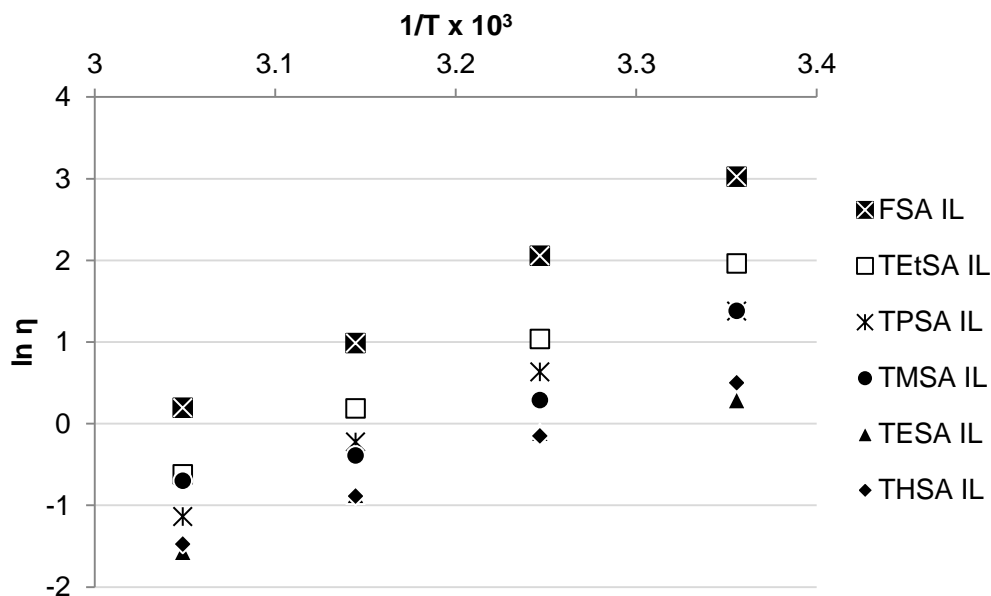
Figure 5.5. The Arrhenius plot for the ionic liquid viscosities.

For the case of ionic liquid reversion and subsequent viscosity decrease due to the presence of the molecular liquid, one would expect the Arrhenius plot to deviate from linearity, especially at higher temperatures where the slope would be decreased. The Arrhenius plot has commonly been used to describe the temperature dependence of ionic liquids, and Figure 5.5 indicates that it also applies to the ionic liquid form of reversible ionic liquids presented here. All ionic liquid materials examined appear to follow a linear trend, suggesting that the reversion of the ionic liquid was minimal over the course of the reaction. However, the TMSA appears to deviate from this trend, likely due to the reaction of the amine with ambient water.

Lastly, the viscosity as a function of conversion was investigated for the TPSA system at 25°C, shown in Figure 5.6, by preparing samples of intermediate conversion (addition of CO_2 for short periods of time) and using the refractive index of the mixture to determine the composition (see Chapter 2 for more details).
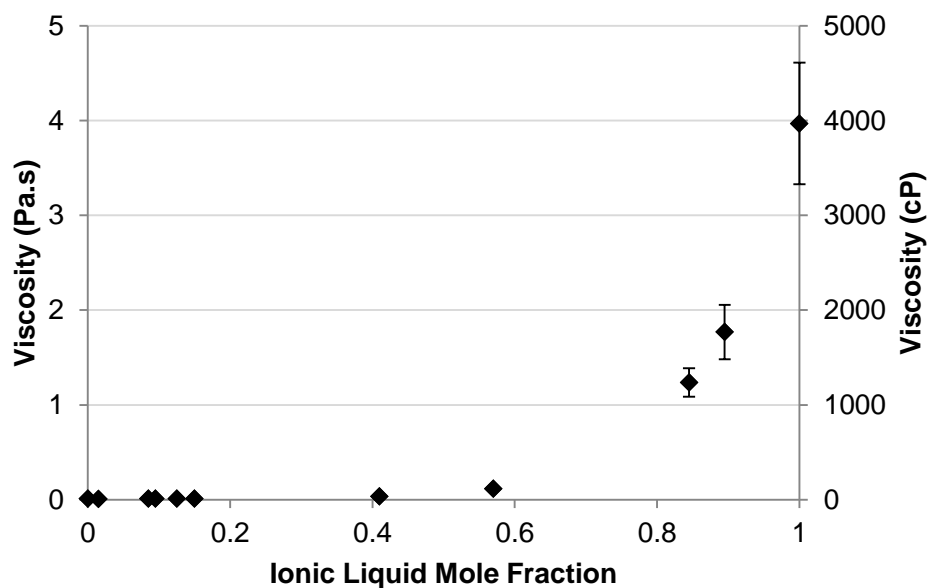
Figure 5.6. The viscosity of TPSA as a function of ionic liquid mole fraction, 25°C.

From Figure 5.6 two regions can be identified: (1) at ionic liquid mole fractions from 0 to approximately 0.6 the viscosity is relatively independent of composition, and (2) at ionic liquid mole fractions from 0.6 to 1 indicate a very composition dependent region of viscosity. In the low ionic liquid mole fraction region, the unreacted amine behaves as a solvent and solvates the salt causing dissociation of the ions. Take for example the system of sodium chloride (NaCl) and water, where the viscosity of the water changes very little with the addition of salt up to the saturation concentration.

The region exhibiting a strong dependence of viscosity on composition is consistent with published reports of small amounts of co-solvents (or contaminants) result in large changes in the viscosity of ionic liquids.[19] Thus, a change occurs near an ionic liquid mole fraction of 0.6; indicating the ionic liquid changing from the solute to the solvent. For the ionic liquid solvent, small changes in composition (on the order of 1%) can cause drastic changes in viscosity (on the order of 100 cP).

It is apparent that the high ionic liquid mole fraction region is problematic for processing of the reversible ionic liquids in an absorber configuration. A better examination of the low ionic liquid mole fraction region is offered in Figure 5.7.

Assuming an upper limit of viscosity of 100 cP, it is shown that ionic liquid mole fractions of this material up to 0.5 will yield a usable liquid for the application to industrial absorber processes. An ionic liquid mole fraction of 0.5 corresponds to a conversion of the molecular liquid of equal to 67%. This is a considerable conversion to yield a processable fluid; considering the viscosity of the fully formed ionic liquid is near 4000 cP. Although high conversions can be achieved while maintaining low viscosity, as the concentration dependent region of the viscosity plot is approached, small increases in

conversion result in drastic increases in viscosity which could be detrimental to the operation of flow processes using reversible ionic liquids as the solvent.
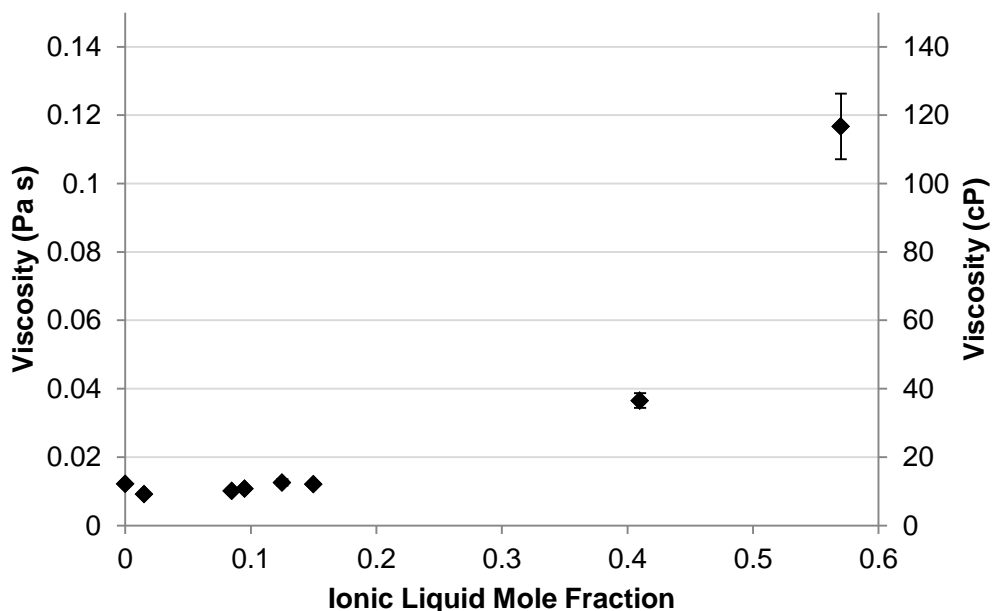
Figure 5.7. The composition independent region of the viscosity of TPSA as a function of ionic liquid mole fraction, 25°C.

Physical Absorption

The physical absorption capacities of the ionic liquid forms of the six one-component reversible ionic liquids were investigated using the reflectance infrared spectroscopic technique described in Chapter 3. The physical absorption of CO_2 is an attractive alternative to the chemical absorption because of the low thermal requirement of regeneration, where the enthalpy of desorption for physical absorption is a fraction of the enthalpy of desorption for the chemical absorption. Additionally, when combined with the chemical absorption, the physical absorption increases the total capture capacity of the solvent thereby increasing the efficiency of the absorption process. First presented

by Higbie more than 75 years ago is the argument that on short time scales (ms) industrial absorber processes configured with either trays or packing materials are effectively thin film absorption processes.[20] This is also the case examined with the custom built reflectance infrared reactor apparatus, described in Chapter 3. Presented in this section is a discussion on the diffusivity and solubility of CO_2 in the ionic liquid forms of the reversible ionic liquids, the swelling of the ionic liquid phase upon absorption of CO_2, and predictive techniques for approximating the solubility of CO_2.

Diffusivity of CO_2 in the Ionic Liquids

It follows that with respect to both the design of experiments and the application of the solvent to an industrial process, more important than the equilibrium absorption (or solubility) of CO_2 in the ionic liquids is the uptake rate of CO_2 into the stagnant ionic liquid film. The time dependent concentration profile of CO_2 (C_{CO2}, mol/mL) in the ionic liquid can be described by Fick's Second Law, given here for the one-dimensional diffusion in the x-direction,

$$\frac{dC_{CO2}}{dt} = D_{CO2}\frac{d^2C_{CO2}}{dx^2}. \tag{5.3}$$

The estimated diffusion coefficient of CO_2 in the ionic liquid (D_{CO2}, cm^2/s) scales with the inverse of the ionic liquid viscosity (η_{IL}, cP) following the Wilke-Chang equation,

$$D_{CO2} = \frac{7.4 \times 10^{-8}\sqrt{\varphi MW_{IL}}T}{\eta_{IL}V_{CO2}^{0.6}} \tag{5.4}$$

where MW_{IL} is the molecular weight of the ionic liquid, T is the temperature (K), V_{CO2} is the molar volume of CO_2 at the boiling point (34 cm^3/mol)[21], and φ is the association factor of the solvent.[22] The association factor is determined experimentally; for common organic solvents (including water) the range of association factors is from 1.0 - 2.6 where the association constant increases with the polarity of the solvent (i.e. φ = 2.6 for water

and 1.0 for aliphatic hydrocarbons).[23] The Wilke-Chang equation has been used to compare the experimental diffusivities of various gases in ionic liquids with a broad range in viscosity, and the association factors found from the experimental data have ranged from 15 to 33.3.[24] It should be noted that a considerable exception to this range was presented, at $\varphi = 0.15$.[18]

Given that the diffusion coefficient for CO_2 in traditional organic solvents ($\eta < 50$ cP) is on the order of 10^{-5} cm^2/s, the diffusion coefficient in ionic liquids ($\eta \sim 1000$ cP) would be on the order of 10^{-7} cm^2/s as described by the Wilke-Chang equation. However, this is not the case. Several studies have been conducted to examine the relationship between diffusivity and viscosity in gas/ionic liquid systems, and because the Wilke-Chang equation has not been found to effectively capture the relationship, other simple models have been developed.[18,24] The findings indicate that the diffusivity of CO_2 in ionic liquids scales with $\eta^{-0.6}$. Therefore, for the ionic liquid forms of the reversible ionic liquids studied here, the approximate diffusion coefficient is $D_{CO2} \sim 10^{-6}$ cm^2/s.

The solution to Fick's Second Law (Equation 5.3) for the case of one-dimensional diffusion into a slab of thickness "ℓ" and constant surface concentration has been rigorously performed.[23] For the time dependent determination of CO_2 uptake relative to the maximum (M_t/M_∞), the solution takes the form

$$\frac{M_t}{M_\infty} = 1 - \frac{8}{\pi^2} \sum_{n=0}^{\infty} \frac{1}{(2n+1)^2} exp\left[-\frac{(2n+1)^2 \pi^2 D_{CO2} t}{4\ell^2} \right]. \tag{5.5}$$

To examine the physical absorption uptake of CO_2 into the highly viscous ionic liquids studied here, the capacity of CO_2 at a pressure of 10 bar in the FSA ionic liquid (thickness of approximately 500 µm) was monitored, given in Figure 5.8. The FSA compound was chosen because it exhibits the highest viscosity of all materials presented here, 7500 cP at 35°C. Comparison of the absorbance spectra at 10 minutes

and 60 hours by application of the Beer-Lambert Law is trivial in this case because both the molar absorptivities and pathlengths are identical for the two cases. Thus, assuming the CO_2 concentration at 60 hours is the maximum uptake at infinite time (M_∞), the percentage of maximum uptake (M_t/M_∞) at 10 minutes is > 95%.
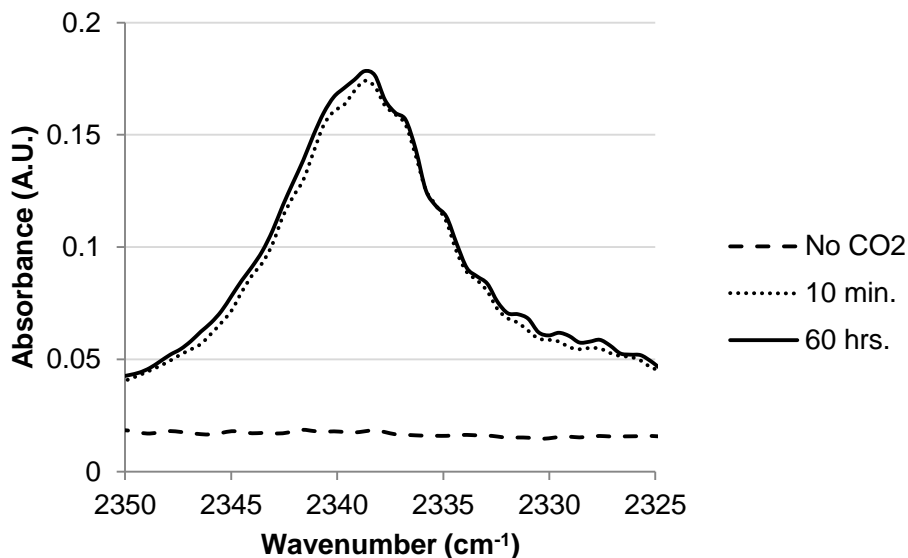
Figure 5.8. The infrared spectra of the FSA ionic liquid under 10 bar CO_2, showing the change in the asymmetric stretch vibration of physically absorbed CO_2 over time.

Upon application of Equation 5.3, truncated to n = 0 (valid for "long times") and using ℓ = 0.05 cm, M_t/M_∞ = 0.95, and t = 600 seconds, the solution for D_{CO2} is found to be 5 x 10^{-6} cm^2/s at 35°C. By comparison, the Wilke-Chang equation (using an association factor of 25) approximates a diffusivity of CO_2 in the FSA ionic liquid of 5 x 10^{-8} cm^2/s at 35°C; two orders-of-magnitude lower than the experimentally observed value. For application to the design of the reflectance infrared spectroscopic experimental technique, a relatively short time for maximum uptake is desired, t < 1 hour. Using the D_{CO2} determined from the FSA uptake experiment (5 x 10^{-6} cm^2/s), the sample thickness

to offer > 95% uptake in 1 hour was found to be approximately 1300 μm. For the reflectance analytical technique to be valid, the minimum samples thickness must exceed approximately 120 μm (refer to Chapter 3 for more details). Thus, a valid range of samples thicknesses that will allow for rapid uptake of CO_2 into the ionic liquids and application of the reflectance infrared technique has been determined (120 μm < ℓ < 1300 μm); all measurements were performed using samples thicknesses within this range. To ensure equilibrium, measurements were compared at 60 minutes and 75 minutes, and deemed to be at equilibrium if the change observed was < 1%.

The diffusivity of CO_2 in the FSA ionic liquid presented here is the "worst case scenario" in regards to the physical absorption uptake in the ionic liquids for two reasons: (1) FSA has the highest viscosity of any of the materials tested, therefore the diffusivity in the other materials is higher relative to FSA, and (2) as CO_2 absorbs in the ionic liquid the viscosity is drastically reduced, hence an increase in transport properties would be observed for subsequent data points. Baker and coworkers published a study that utilized fluorescence spectroscopy in order to determine the effect of CO_2 on the viscosity of ionic liquids.[25] The results of the paper indicate that for CO_2 pressures up to 150 bar, the viscosity of the ionic liquid was cut by a factor of 5. A decrease in ionic liquid viscosity would suggest an increase in diffusivity; therefore, as the concentration of CO_2 increases in the ionic liquid phase the relative time to reach equilibrium solubility would decrease.

Physical Absorption Capacity of CO_2 in the Ionic Liquids

Now that the uptake of the physically absorbed CO_2 in the ionic liquids has been discussed, the examination of equilibrium solubilities of CO_2 can be initiated with confidence. Using the quantitative technique described in Chapter 3, the solubility of CO_2

in the ionic liquid can be calculated. The CO_2 mole fraction (x_{CO2}) in the ionic liquids TMSA, TESA, and FSA at 35°C is given as a function of CO_2 pressure (bar), Figure 5.9.
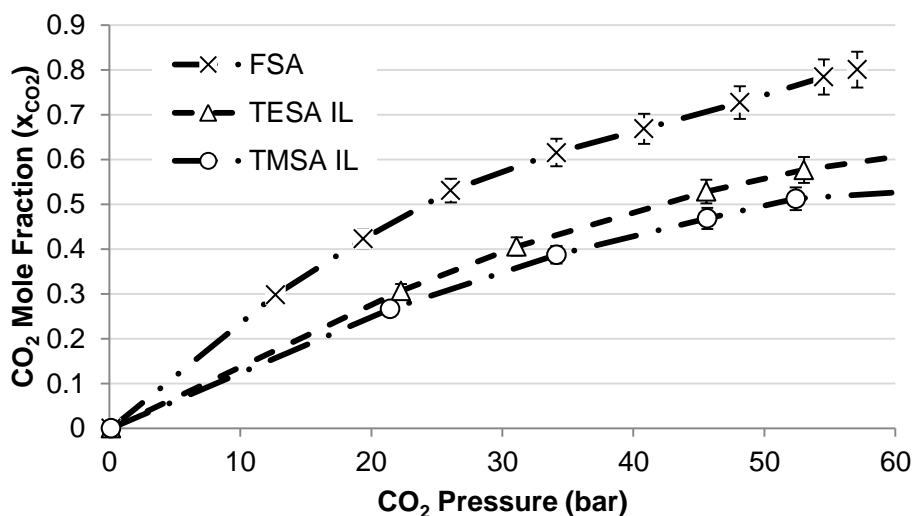
Figure 5.9. The solubility of CO_2 in the ionic liquid form of TMSA, TESA, and TMSA as a function of CO_2 pressure (bar) at 35°C.

It is evident from Figure 5.9 that the fluorinated material has superior CO_2 solubility than the alkoxy- substituted materials, as expected. In fact, the FSA compound was identified and synthesized in order to determine the effect of fluorination on physical absorption capacities in the reversible ionic liquids. CO_2 is well known to be fluoro-philic, and fluorinated materials have been shown to exhibit high CO_2 solubilities.

The CO_2 mole fraction (x_{CO2}) in the alkyl- substituted ionic liquids TEtSA, TPSA, and THSA at 35°C is given as a function of CO_2 pressure (bar), Figure 5.10. It can be seen that the solubility of CO_2 in the THSA ionic liquid is much higher at a given pressure than for either TEtSA or TPSA. Additionally, the mole fraction of CO_2 in the ionic liquid is very similar for the TESA/TMSA and TEtSA/TPSA materials; while the THSA and FSA materials exhibit considerably higher capacities. The data indicate that

119

the equilibrium solubility increases with the increasing bulkiness of the ionic liquid. Prof. Brennecke at Notre Dame first postulated that the solubility of CO_2 in ionic liquids is directly related to the void volume of the ionic liquids.[26]
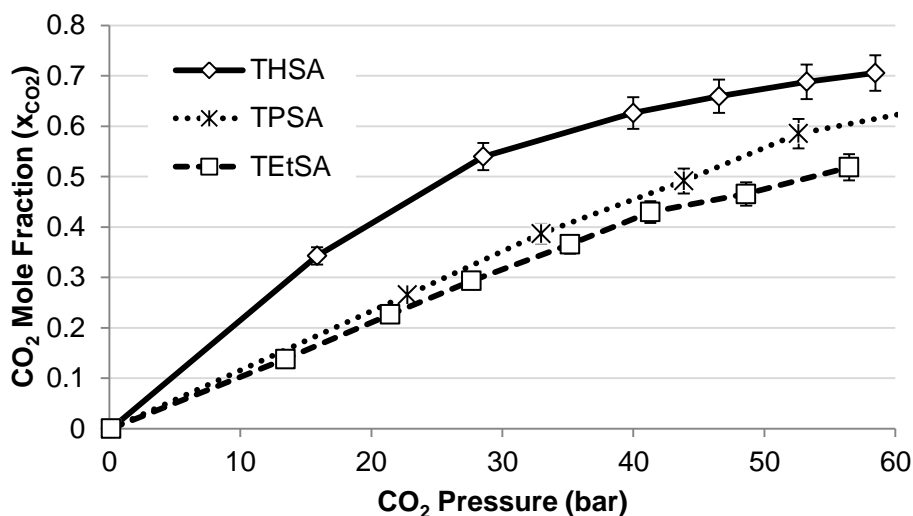
Figure 5.10. The solubility of CO_2 in the ionic liquid form of TEtSA, TPSA, and THSA as a function of CO_2 pressure (bar) at 35°C.

The void volume (V_V) of the ionic liquid is the "empty" space between the molecules, and is found by subtracting the theoretical van der Waals volume (V_{vdW}) from the experimentally determined molar volume (V_M). The vdW volume is the theoretical volume the molecule occupies assuming the atoms are hard spheres, one of van der Waals postulates in developing the vdW equation of state. In reality, molecules do not behave as strong spheres. It should be noted that the vdW volume of a molecule is not the addition of the vdW volumes of the atoms that constitute the molecule. Another postulate of van der Waals was that the volume of individual atoms overlap when a bond is formed; hence, the vdW volume of a molecule is always less than the sum of vdW volumes of the individual atoms.

Many methods are available to approximate the vdW volume of materials, including simulation software and group contribution methods. A group contribution method developed by Bondi was released nearly 50 years ago, and provides a simple way for determining vdW volumes of complex molecules by adding the contributions of each individual segment.[27] The vdW volume contributions relevant to the materials studied here are provided in Table 5.1 for the straightforward comparison of future work to the results provided here.

Table 5.1. The vdW volume contributions presented by Bondi and used in this study.

Segment	V_{vdW} (cm^3/mol)
CH_3-	13.67
$-CH_2-$	10.23
$>CH-$	6.78
CF_3-	20.49
$-CF_2-$	15.73
$-O-$	5.2
$>Si<$	6.82
Ion Pair	38.36

The vdW volume of the "Ion Pair" refers to the volume occupied by the carbamate and ammonium ions. Although Bondi's work did not include values for ion pairs, it was assumed to involve a secondary amine bound to a carboxylic acid plus a primary amine. Although there is likely to be some error in this assumption, the value is

consistent for every ionic liquid reported here. The vdW volumes of several ionic liquids were compared between the Bondi contribution method and a molecular model simulation software program, Spartan '08, and the values were within good agreement (< 5% difference).

The ionic liquid molecular weights (MW_{IL}, g/mol), densities at 25°C (ρ_{IL}, g/cm^3), molar volumes (V_M, cm^3/mol), vdW volumes (V_{vdW}, cm^3/mol), and void volumes (V_V, cm^3/mol) are given in Table 5.2.

Table 5.2. The void volumes of the ionic liquid forms of the reversible ionic liquids.

Compound	MW_{IL} (g/mol)	ρ_{IL} (g/cm^3)	V_M (cm^3/mol)	V_{vdW} (cm^3/mol)	V_V (cm^3/mol)
TMSA	402	1.126	357	227	130
TESA	486	1.043	466	288	178
TEtSA	390	0.922	423	257	166
TPSA	474	0.912	520	318	202
THSA	727	0.884	822	502	320
FSA	783	1.193	656	395	261

The relationship between void volume and solubility of CO_2 in the six ionic liquids was examined by first calculating the Henry's Law constant (H_{CO2}, bar) of CO_2 in the ionic liquids. Henry's Law is a limiting case of vapor-liquid equilibrium, valid for systems at low solubility, stating that the solubility of a gas in equilibrium with a liquid phase is directly proportional to the partial pressure of the gas in the vapor phase,

$$H_{CO2} = \lim_{x_{CO2} \to 0} \left(\frac{P_{CO2}}{x_{CO2}} \right) \qquad (5.6)$$

where x_{CO2} is the mole fraction of CO_2 in the liquid phase and P_{CO2} is the partial pressure of CO_2 in the vapor phase. The detection limit of the reflectance infrared spectroscopic technique precludes the direct measurement of the solubility of CO_2 in the ionic liquids at low pressure as a discernable asymmetric CO_2 vibration generally was not observed for pressures < 10 bar. Henry's Law constants were determined by the straight-line fit (through the origin) of the data points for which P_{CO2} < 35 bar. A plot of H_{CO2} (bar, at 35°C) versus V_V (cm^3/mol) is given in Figure 5.11. It should be noted that the errors bars for TESA, TEtSA, TPSA, and FSA are all within the data point.
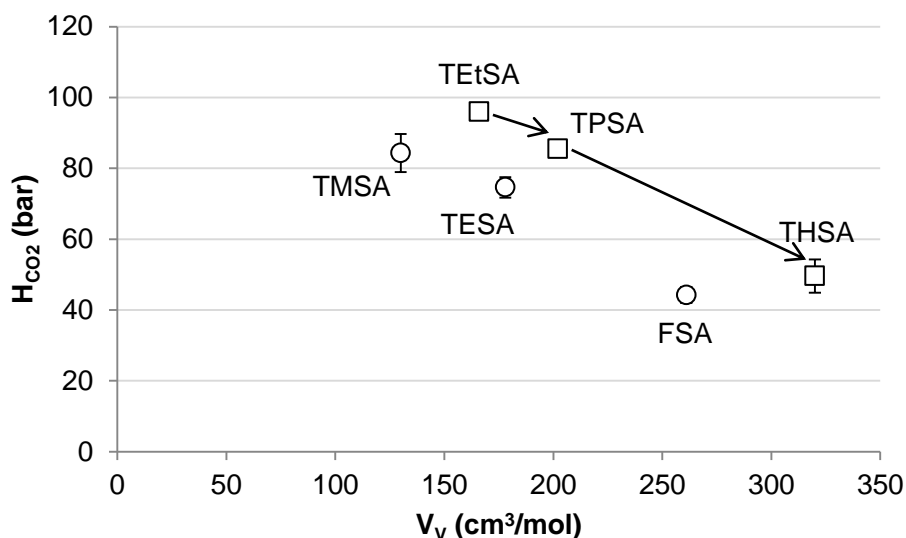
Figure 5.11. Plot of Henry's Law constants (H, bar) versus void volumes (V_V, cm^3/mol) for the ionic liquid forms of TMSA, TESA, TEtSA, TPSA, THSA, and FSA at 35°C.

It is seen in Figure 5.11 that H_{CO2} does correlate with V_V in an apparent linear fashion within a "class" of compounds. The two classes of compounds are (1) trialkyl-substituted materials (represented by the open squares) and (2) the trialkoxy-

substituted and fluorinated materials (represented by the open circles). This information is crucial for the design of reversible ionic liquid materials with enhanced physical absorption capacities. The 35°C H_{CO2} values found for the reversible ionic liquids reported here are comparable to the 35°C H_{CO2} values of conventional ionic liquids. For example, the H_{CO2} values of the well studied ionic liquid 1-butyl-3-methylimidazolium hexafluorophosphate [bmim][PF_6] were reported to be 53.4 ± 0.3 bar and 81.3 ± 0.5 bar at temperatures of 25°C and 50°C, respectively.[28]

Another important consideration for the design of reversible ionic liquid is how the solubility of physically absorbed CO_2 in the ionic liquid phase changes with temperature. Because the experimental apparatus is only heated and not cooled, temperature control near room temperature is difficult. Additionally, at high temperatures the ionic liquid is susceptible to reversion back to the molecular liquid, which would skew the resulting solubility information. A benefit of the infrared technique for probing CO_2 solubilities in the ionic liquids is the ability to monitor the composition of the solvent, where reversion of the ionic liquid is easily detectable and could thusly be avoided. Nevertheless, at 50°C and P_{CO2} > 10 bar, the ionic liquids appeared to remain stable and the x_{CO2} information could be collected, shown in Figure 5.12 for TMSA and TEtSA comparing the solubility data collected at 35°C and 50°C.

The information of the Henry's Law constants as a function of temperature can be used to determine the enthalpy of absorption (ΔH_{abs}, kJ/mol) and entropy of absorption (ΔS_{abs}, J/mol·K) for CO_2 in the ionic liquids by application of the equations,

$$\Delta H_{abs} = R \left(\frac{d(\ln P)}{d(1/T)} \right)_{x1} \tag{5.7}$$

$$\Delta S_{abs} = -R \left(\frac{d(\ln P)}{d(\ln T)} \right)_{x1} \tag{5.8}$$

where R is the gas constant (8.314 J/mol·K), T is the temperature (in K), and x_1 is the mole fraction of CO_2 in the ionic liquid phase.[29]
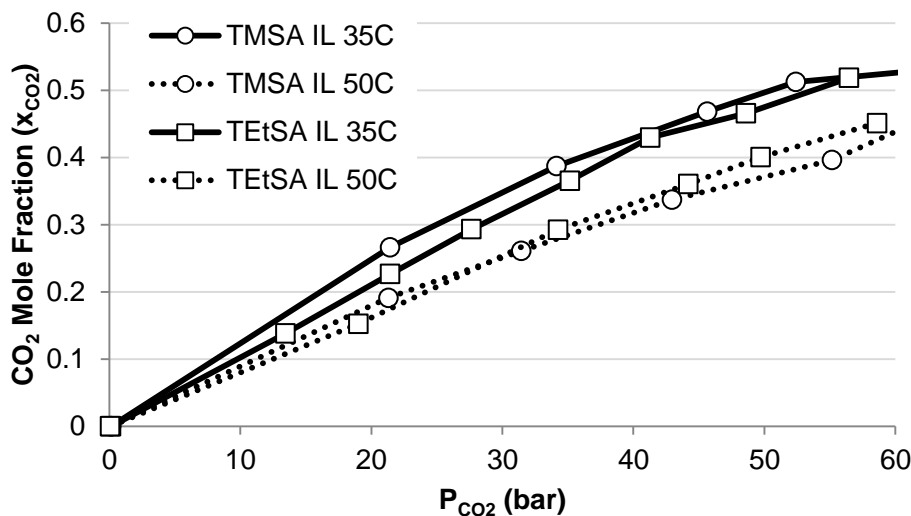
Figure 5.12. Plot of CO_2 solubilities (x_{CO2}) as a function of CO_2 pressure (P_{CO2}) for TMSA (open circles) and TEtSA (open squares) at 35°C (solid lines) and 50°C (dashed lines).

The enthalpy of absorption for CO_2 in the ionic liquids is indicative of the strength of the interactions between the ionic liquid and CO_2 dissolved in solution, while the entropy of absorption is related to the ordering that occurs in the liquid phase of the ionic liquid and CO_2 mixture. The enthalpy/entropy values calculated for TMSA and TEtSA are given in Table 5.3, along with the reported values of [bmim][PF$_6$].

The thermodynamic values reported here for TMSA and TEtSA agree well with ΔH_{abs} and ΔS_{abs} reported for the well-studied ionic liquid [bmim][PF$_6$]. It can be inferred from the thermodynamic properties of absorption that there are stronger solvent-solute interactions present for CO_2 in TMSA relative to TEtSA based on the enthalpy values calculated. This observation is consistent with the Nile Red polarity measurements (refer

to Chapter 2, in summary the polarity of the alkoxy- materials is higher than for the alkyl-substituted materials) and CO_2 solubility reported here, where the alkoxy-materials show significantly higher solubilities of CO_2 at a given temperature than the alkyl- substituted materials. The entropic effects of absorption indicate a higher degree of ordering for the alkoxy- solvent TMSA relative to TEtSA.

Table 5.3. The calculated enthalpies of absorption (ΔH_{abs}, kJ/mol) and entropies of absorption (ΔS_{abs}, J/mol·K) for CO_2 in the ionic liquids, compared with [bmim][PF$_6$].

Compound	ΔH_{abs} (kJ/mol)	ΔS_{abs} (J/mol·K)
TMSA	-17.5 ± 1.8	-55.7 ± 5.9
TEtSA	-12.7 ± 1.3	-40.3 ± 4.1
[bmim][PF$_6$][28]	-16.1 ± 2.2	-53.2 ± 6.9

Liquid Phase Swelling

The liquid phase swelling information was also obtained from the reflectance infrared spectroscopic data of the physical absorption of CO_2 in the ionic liquids. As CO_2 is absorbed in the liquid, some of the ionic liquid is displaced by the gas, resulting in a decrease in the density of the liquid phase. Swelling is defined here as the difference in densities of the CO_2 swollen ionic liquid (ρ_S) and ionic liquid with no CO_2 present (ρ_{IL}), divided by ρ_{IL}. A plot of swelling (%) versus CO_2 pressure (P_{CO2}, bar) is given in Figure 5.13.
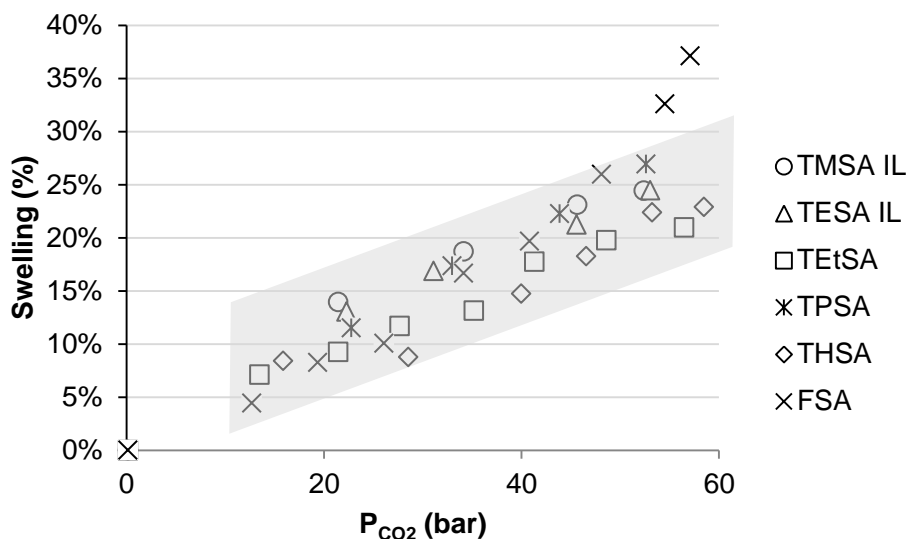
Figure 5.13. Plot of the CO$_2$ induced swelling (%) of the ionic liquids as a function of CO$_2$ pressure (P$_{CO2}$, bar).

The swelling information is critical for both the design of experiments and for application of the solvents to industrial processing. In regards to experimental design, the experimental apparatus must have ample headspace to allow for the expansion of the liquid phase volume. This case is also true for industrial applications, with the caveat that higher swelling implies a larger solvent volume must be processed. From the graph in Figure 5.13, it is shown that over the pressure range studied the swelling for most of the ionic liquids is < 30% (i.e. the density of the liquid phase is 70% of the ionic liquid density with no CO$_2$ present) at the maximum pressure (60 bar). And for all ionic liquids, save the fluorinated compound FSA, the swelling appears to taper off; consistent with the x$_{CO2}$ data provided in Figure 5.9 and Figure 5.10 indicating saturation of the gas in the liquid is being approached at higher pressures. The FSA ionic liquid appears to swell considerably at higher pressures, where x$_{CO2}$ is approximately 0.8 at 60 bar.

Predictive Techniques for Approximating CO_2 Solubility in Ionic Liquids

Estimation of CO_2 solubilities in ionic liquids can be very helpful in regards to the design of experiments intended to measure such properties, as well as for determining economic viability of industrial scale processes utilizing ionic liquids for which the solubilities are not known. For the approximation of gas solubility (especially CO_2) in ionic liquids at low pressures (i.e. Henry's Law constant), Regular Solution Theory (RST) has been used with some success.[30,31] In short, RST assumes that the molecules in a fluid mixture are oriented randomly and the solute-solvent interactions in a mixed solution are dominated by short-range forces that results in a simple predictive model requiring knowledge of only pure component properties. Practically, RST relates the solubility to the energy required to create a space for the solute within the "regular" solvent.

The equation of RST for the Henry's Law constant of CO_2 in an ionic liquid (H_{CO2}) is given,

$$\ln H_{CO2} = \ln f_{CO2}{}^0 + \frac{V_{CO2}\Phi_{IL}{}^2}{RT}(\delta_{IL} - \delta_{CO2})^2 \qquad (5.9)$$

where $f_{CO2}{}^0$ (bar) is the fugacity of pure CO_2 at the standard state, V_{CO2} (cm^3/mol) is the theoretical molar volume of CO_2 at the temperature and pressure of the solution (determined from phase behavior data), Φ_{IL} is the volume fraction of the ionic liquid (defined in Chapter 2), R is the gas constant, T (K) is the temperature and the δ_i (J/cm^3)$^{1/2}$ term is the solubility parameter.

The solubility parameter is related to the cohesive energy density of a substance, where the cohesive energy density is defined as the amount of energy required to remove a molecule from the bulk, given

$$\delta = \sqrt{\frac{-\mathrm{E}}{V_M}} \qquad (5.10)$$

where E (J/mol) is the energy required to vaporize the solvent and V_M (cm^3/mol) is the pure component molar volume.

Because ionic liquids have extremely low vapor pressure, the experimental determination of vaporization energies is difficult and often times unknown. Recently, it has been suggested that for the application to ionic liquids, the energy of vaporization can be replaced by the activation energy of viscosity (E_a^{vis}, J/mol) times a factor of four.[32]

$$\delta = \sqrt{\frac{4\mathrm{E}_a^{vis}}{V_M}} \qquad (5.11)$$

The relationship between energy of vaporization and activation energy of viscosity for viscous liquids was first proposed by Eyring in the development of an absolute reaction rate theory.[33] Eyring's theorem was developed with the following assumptions:

1. The energy of vaporization is equal to the energy required to make a hole in the liquid the size of the molecule being vaporized; which is the sum of the energies required for the vaporizing molecule to separate from the surrounding molecules and leave the surface and enter the gas phase.

2. In viscous flow, for a molecule to move from one site to another a hole having the size of the molecule must be created.

Thus, Eyring predicted there must be a relationship between the energy of vaporization and the energy required for viscous flow; acknowledging that the energy for viscous flow would be lower than the energy for vaporization due to the absence of the work required for expansion to the vapor state. The relationship between activation energy of viscosity and enthalpy of vaporization was offered in a later report where

Eyring found the energy of vaporization to be approximately a factor of four larger than activation energy of viscosity; hence, the development of Equation 5.11.[34]

The use of Equation 5.11 for the estimation of ionic liquid solubility parameters has been found to work well for conventional ionic liquids.[32] For the solubility of CO_2 in reversible ionic liquids, the relationship between Henry's Law constants and the solubility parameter determined from the activation energy of viscosity is given in Figure 5.14, where the solubility parameter for CO_2 was determined from:[35]

$$\delta_{CO2} = -0.0535T + 28.26 \tag{5.12}$$

It can be seen from the plot that good agreement exists between the experimentally determined H_{CO2} values and the δ_{IL} values found using E_a^{vis}. A general relationship for determining the solubilities of CO_2 in the silyl-amine based reversible ionic liquids from the temperature dependent viscosity data is now available, given in Figure 5.14.
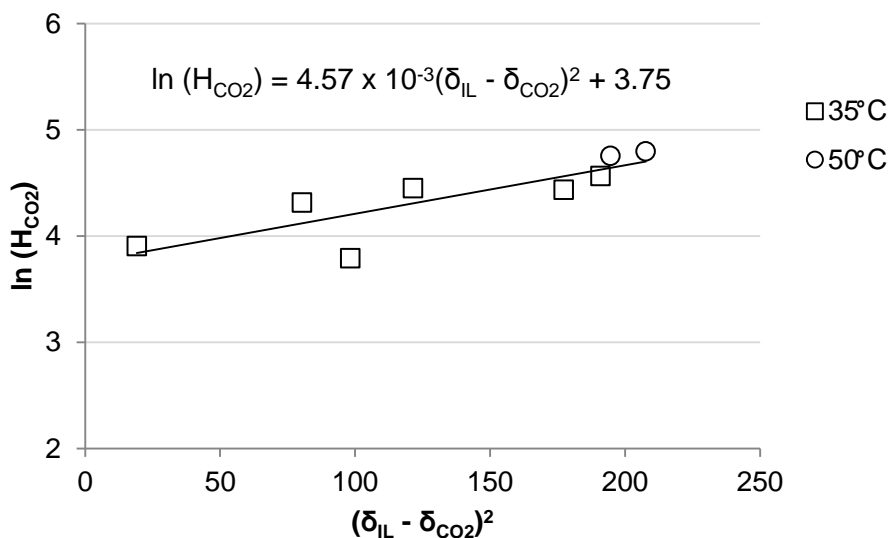
Figure 5.14. The relationship between experimentally determined Henry's Law constants for CO_2 in the reversible ionic liquids (H_{CO2}, bar) and solubility parameter (δ_{IL}, $J^{1/2}/cm^{3/2}$) calculated using the activation energy of viscosity.

Although relatively trivial, the treatment of using RST with the Eyring-modified treatment of the ionic liquid solubility parameter gives some insight into the relationship between the highly viscous nature of ionic liquids and the high CO_2 capacities observed. The implication from this modified-RST prediction technique is that Eyring's conclusions regarding a relationship between viscous flow and vaporization energy hold true for ionic liquids within the scope of solubility parameters applied to RST. Hopefully this information will lead to the development of a better understanding of the diffusivity and flow in ionic liquids, ultimately yielding in improved predictive techniques applied to ionic liquid systems.

Chemical Absorption

The chemical absorption of CO_2 in the one-component reversible ionic liquids was confirmed to approach the stoichiometric limit, two moles of amine per one mole of CO_2, at temperatures up to 35°C and CO_2 pressures of 1 bar (described in Chapter 2). Therefore, all materials exhibited a maximum molar capacity of CO_2 equal to 0.5 (moles CO_2/moles amine). A more appropriate definition of CO_2 capture capacity for the discussion of solvent based absorption processes is given as the moles of CO_2 captured per mass of solvent (mol CO_2/kg solvent). Using this definition of CO_2 capture capacity, the capacity versus molecular weight of amine (MW_{ML}, g/mol) for the one-component reversible ionic liquids is given in Figure 5.15.

Even without the aid of Figure 5.15, it is readily apparent that increasing the molecular weight of the amine reduces the CO_2 capture capacity, considering only the chemical absorption. The importance is to illustrate that relative to TEtSA, a small reduction in molecular weight yields a significant increase in chemical absorption capacity. The bulkier materials, THSA and FSA, exhibit much smaller changes in

131

chemical absorption capacity relative to the molecular weight of the amine molecular liquid. An attempt at lowering the molecular weight of the amine, beyond TEtSA, was presented in Chapter 2 as the synthesis of (3-aminopropyl)ethyldimethylsilane (EMSA). The characterization of EMSA showed that a solid was formed upon the reaction with CO_2, and the DSC results indicated that the release of CO_2 occurred at the melting point of the solid (approximately 40°C); detrimental for the application to CO_2 capture using the pure compound. However, a mixture of EMSA with a cosolvent could provide a eutectic that would allow for its successful application to CO_2 capture. Thus, using the symmetric (3-aminopropyl)silane substructure for the development of reversible ionic liquids for CO_2 capture, the TEtSA material represents the lowest molecular weight and highest chemical absorption capacity available.
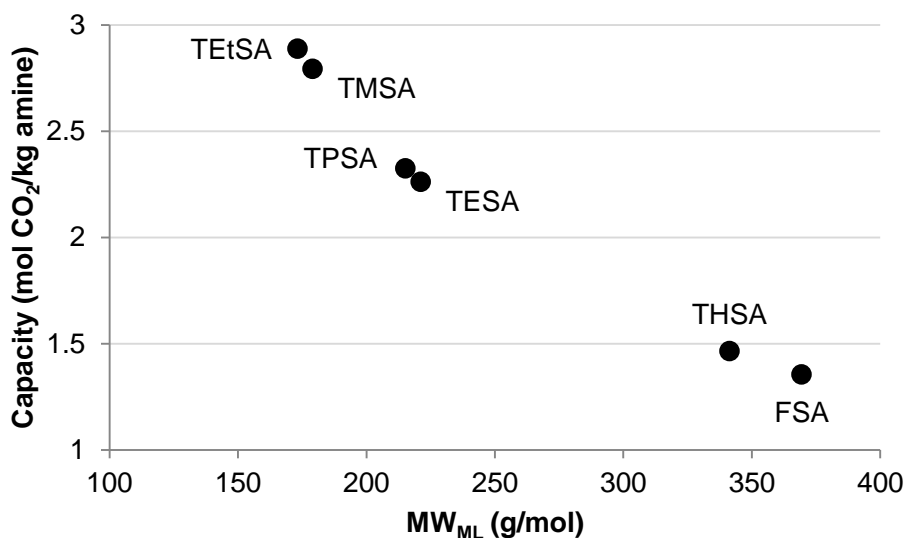
Figure 5.15. The relationship between amine molecular weight (MW$_{ML}$, g/mol) and the theoretical maximum chemical absorption CO_2 capture capacity (mol CO_2/kg amine) for the one-component reversible ionic liquids.

Although the one-component reversible ionic liquids are capable of capturing the stoichiometric limit of CO_2 through the chemical absorption mechanism, the rate of CO_2 uptake is an important parameter in the design of the materials for industrial processing. An accurate model of the rate of chemical absorption of CO_2 in liquid solvents must consider the reaction mechanism (especially complicated for the case when water is present, where as many as 10 steps have been proposed[36]) and the vapor-liquid equilibrium, other effects such as stirring rates are difficult to capture.

For the case of CO_2 reacting with primary amine solutions at low temperatures (< 50°C), the reaction rate greatly exceeds the mass transfer rate.[37] Countless studies have been conducted to limit the mass transfer limitations and provide and accurate representation of the overall kinetic rate constant. Elegant experimental apparatuses have been developed for the CO_2/amine system to limit the mass transfer to the point where the reaction kinetics could be experimentally observed. Most notable are the laminar jet absorber[38] and wetted wall column.[39] However, the experimentally determined rate constants have been found to be in poor agreement, where the results typically correlate with the apparatus and model used.[36] Ultimately, the rate of CO_2 absorption that would be observed in an industrial process is unique to the operating conditions and design of the process.

The chemical absorption uptake of CO_2 in a stagnant film of the TEtSA molecular liquid was examined using a gravimetric technique. The gravimetric experiments used a Hiden Isochema IGA-001 Gas Sorption Analyzer, located in Dr. Krista Walton's research facilities at Georgia Tech. The experiment was performed at 35°C with 1 bar of CO_2, using a stainless steel cylindrical sample holder (diameter of 11 mm) and the amount of sample was varied to give insight into the uptake as a function of the film thickness. After the sample was loaded in the experimental chamber, the pressure was reduced to 200

mbar to remove a majority of the air. With liquid samples, the sample is lost at low pressures due to evaporation, and pressures < 200 mbar were found to cause the initial mass to fluctuate. The Hiden IGA records mass uptake, and assuming that the physical absorption is negligible at the low pressure studied, the chemical absorption uptake was determined as a function of time. The maximum uptake of CO_2 was determined to equal the mass of the sample once stabilized for long periods of time (about 4 hours).

The percentage of the maximum uptake (M_t/M_∞) was calculated from the IGA experimental results at three samples thickness: 570 µm, 1100 µm, and 1600 µm. The results, plotted against $t^{1/2}$ (where t is time in seconds) are given in Figure 5.16.
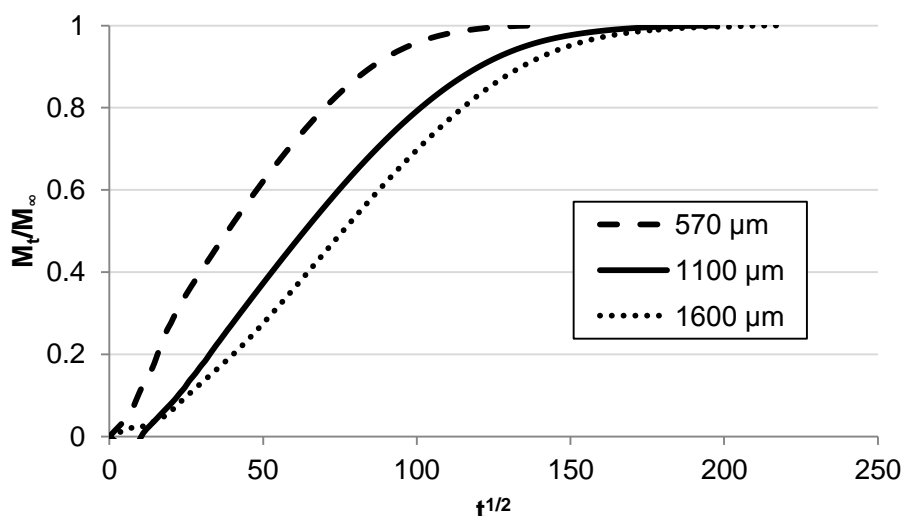
Figure 5.16. The chemical absorption uptake of CO_2 in TEtSA with varying sample thicknesses.

Assuming instantaneous reaction of CO_2 with TEtSA at the surface of the film (and the concentration of the ionic species is constant at the surface), the transient chemical absorption uptake of CO_2 in the TEtSA molecular liquid was examined using Fick's Second Law for the ionic species assuming constant concentration of CO_2 at the

surface of the stagnant film. The calculated apparent diffusion coefficients (D_{mean}, cm^2/s) at 35°C for the CO_2 chemical absorption in TEtSA are given in Table 5.4.

Table 5.4. The calculated apparent diffusion coefficients of CO_2 in TEtSA at 35°C and 1 bar of CO_2 pressure with varying film thicknesses.

Film Thickness (μm)	D_{mean} (cm^2/s)
1600	$1 \times 10^{-6} \pm 20\%$
1100	$0.9 \times 10^{-6} \pm 15\%$
570	$0.4 \times 10^{-6} \pm 10\%$

The mean diffusivity of CO_2 is the observed diffusivity of CO_2 into the reactive solvent assuming the uptake follows the Fickian Diffusion Model, in the absence of stirring. Assuming the chemical absorption uptake of CO_2 in TEtSA follows the Fickian Diffusion Model appears to give fair agreement with the experimentally determined values for a given sample thickness, as evidenced by the low errors associated with the calculated D_{mean} values over the entire range of experimental data for each sample thickness. However, for proper application of Fick's Law, the diffusion coefficients would be constant regardless of film thickness; clearly not the case observed here. To illustrate the agreement between the uptake predicted by Fickian Diffusion and the experimentally obtained values, a plot of M_t/M_∞ versus $t^{1/2}$ (where t is in seconds) for the 570 μm sample is given in Figure 5.17. The predicted values were obtained from solution of Equation 5.5 (truncated to n = 3) using $D_{mean} = 0.4 \times 10^{-6}$ cm^2/s.

Regarding traditional chemical absorption solvents used for CO_2 capture (namely aqueous amines), the presence of a reaction in the solvent results in an increase in the

flux of CO_2; termed the "enhancement factor."[40] Using the non-reactive N_2O as a substitute for CO_2, the diffusion coefficient of CO_2 in aqueous amine solvents has been estimated at 35°C to be 1.5 x 10^{-5} cm^2/s, which is in agreement with the Wilke-Chang estimation[41]. The enhancement factor due to reaction of CO_2 in aqueous amines has been found to be anywhere from 10 – 100, implying that the mass transfer of CO_2 into the liquid is improved greatly.[42] This is clearly not observed for the one-component reversible ionic liquids in the stagnant film uptake experiments.
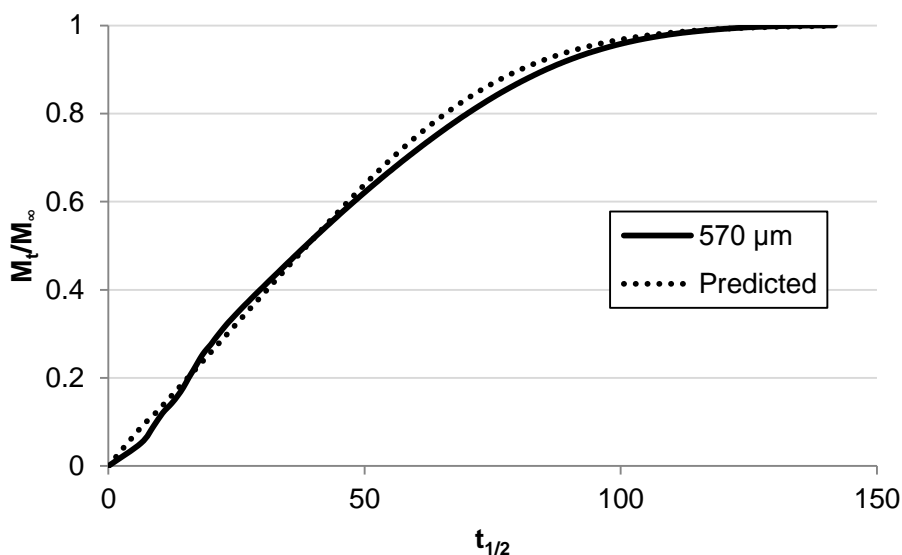
Figure 5.17. Comparison of the experimentally determined chemical absorption uptake of CO_2 into a stagnant film of TEtSA and the uptake predicted by the solution of Fick's Second Law for the case of constant CO_2 concentration at the surface. Temperature of 35°C and CO_2 pressure of 1 bar.

Although the actual process for the chemical absorption uptake of CO_2 in TEtSA is much more complicated than predicted by the simple Fickian Diffusion Model used here, the low D_{mean} values calculated can be used to shed light on the real uptake mechanism. The calculated D_{mean} values are in agreement with the estimated diffusivity of CO_2 in the ionic liquid, 10^{-6} cm^2/s. At lower conversions ($x_{IL} < 0.5$, or $M_t/M_\infty < 0.7$), the

viscosity of the bulk solvent is less than 100 cP and the expected diffusivity would be 10^{-5} cm^2/s as predicted by Wilke-Chang. One possible explanation could be that the reaction rate in the reversible ionic liquids is actually less than the diffusivity, in contradiction to widely accepted behavior for the reaction of CO_2 with primary amines. To test this hypothesis, a 2500 μm film of the TEtSA molecular liquid was examined at 35°C using the reflectance spectroscopic technique described in Chapter 3 at a CO_2 pressure of 50 bar. At such a high pressure, physically absorbed CO_2 would surely be observed. However, over the course of the experiment no physically absorbed CO_2 was observed until the formation of the ionic liquid had been completed. Because the spectroscopic technique measures the bottom-most layer of the film, the reaction rate of CO_2 in the TEtSA molecular liquid has been experimentally determined to be much faster than the diffusivity. Again, this is expected.

The formation of a transport resistant layer is a potential explanation for the low apparent diffusivities reported here. Recall that the conversion of the molecular liquid to the ionic liquid results in a viscosity change over three orders of magnitude. If the reaction of CO_2 with TEtSA is instantaneous relative to the transport, a highly viscous ionic film is formed on the surface of the TEtSA molecular liquid upon contact with CO_2. The diffusivity of CO_2 would then be greatly dampened, as the CO_2 would now be diffusing through a highly viscous film to access the remaining reactive sites. Therefore, the reaction would be a stepwise process from the surface of the film to the boundary, and the apparent diffusivity would follow the diffusivity of CO_2 in the ionic liquid form ($\sim 10^{-6}$ cm^2/s) with an ever expanding thickness of the boundary layer, even though the bulk viscosity is much lower.

An alternative explanation to the step-wise reaction-absorption mechanism just discussed is the possibility that the reaction occurs solely at the surface, and the rate

limiting step of absorption is the counter-diffusion of the ionic liquid in the transport resistant film layer with the unreacted amine in the bulk. The self-diffusion coefficients of ionic liquids have been found to be on the order of 10^{-6} cm^2/s,[43] which is consistent with the D_{mean} values found here. However, it seems unlikely to be the sole limiting factor as the diffusivity of the ionic liquid in the bulk unreacted amine is on the order of 10^{-5} cm^2/s (using the Nernst approximation for the diffusivity of dilute electrolytes),[23] and the thickness of the ionic liquid film layer is likely to be much smaller than the thickness of the bulk solvent.

The actual mechanism for the chemical absorption of CO_2 in the one-component reversible ionic liquids is likely some combination of the two theories presented here. Regardless, the D_{mean} value of 10^{-6} cm^2/s is at least one order-of-magnitude lower than for typical chemical absorption solvents. The low diffusivity can be overcome by vigorous mixing or the addition of a co-solvent. The addition of co-solvent would lower the chemical absorption capacity, which is unfavorable, and vigorous mixing is not feasible on large scale commercial absorber processes where the mixing is inherently poor due to the laminar flow of films in the tower. The local viscosity changes observed upon reaction of CO_2 with the reversible ionic liquids presents a challenge for the implementation of the technology to industrial scale processing.

Assessment of One Component Reversible Ionic Liquids for CO_2 Capture

The goal of this project is to design and develop a viable one-component reversible ionic liquid, utilizing both chemical and physical absorption, for the application to CO_2 capture. Many factors play a role in determining industrial scale viability, such as material synthesis and usable liquid properties, as well as improved efficiency related to

current technology. An overall assessment of the current state of one-component reversible ionic liquids for CO_2 capture is offered.

The synthesis of the one-component reversible ionic liquids was given, in detail, in Chapter 2. The hydrosilation reactions for the product synthesis are attractive for both industrial and laboratory levels. From a research standpoint, the structures of the materials can easily be altered by changing the structure of the silane; allowing for extensive structure-property relationships to be efficiently developed. From an industrial standpoint, the reaction is fast and efficient, and uses materials that are relatively inexpensive. Predicting the cost of the final material produced in large scale quantities (i.e. tons) is difficult for academics. However, the most expensive components in the synthesis are likely to be the silane and platinum catalyst. The laboratory scale reactions have shown to consume all silane, and due to the low vapor pressure fugitive losses on a large scale are expected to be minimal. Currently, there is no information regarding the efficiency of the catalyst; this will likely be a large contributor to the cost of the final product. Although more research must be conducted, the cost effective synthesis of one-component reversible ionic liquids on an industrial scale is promising.

For the performance comparison to an industrially relevant chemical absorption solvent for CO_2 capture, a 30% (by weight) monoethanolamine (MEA) solution was chosen. Aqueous MEA serves as the benchmark solvent in nearly all comparative studies, and a 30% solution is commonly used given the high corrosivity of the solution at higher concentrations. The maximum theoretical chemical absorption capacities (mol CO_2/kg solvent) are given in Table 5.5.

It is shown that the TMSA and TEtSA compounds both have maximum theoretical capacities exceeding the MEA benchmark. The alkoxy- substituted reversible ionic liquid materials were shown in Chapter 2 to react readily with water, and therefore

139

wouldn't be suitable for the application to CO_2 capture where water is present. For flue gas streams, therefore, the TEtSA compound exhibits an enhanced chemical absorption capacity relative to MEA and has the potential to serve as a viable substitute. In addition to the chemical absorption, the reversible ionic liquids benefit from the additional physical absorption capacity of CO_2 in the ionic liquid.

Table 5.5. The maximum theoretical chemical absorption capacities of the one-component reversible ionic liquids and a 30% MEA solution.

Compound	Capacity (mol CO_2/kg amine)
TMSA	2.79
TESA	2.26
TEtSA	2.89
TPSA	2.32
THSA	1.46
FSA	1.35
30% MEA	2.46

The physical absorption capacities in the one-component reversible ionic liquids were shown to correlate with the void volumes, and enhanced capacities were successfully achieved by manipulation of the molecular structure. However, an increase in physical absorption results in a sacrifice of some chemical absorption capacity. To ascertain the tradeoff of improving physical absorption capacity by sacrificing chemical absorption capacity, the total capacity (physical capacity plus chemical capacity, mol CO_2/kg solvent) was calculated as a function of CO_2 partial pressure (P_{CO2}, bar)

assuming the maximum theoretical chemical absorption capacity had been achieved and using the Henry's Law constants to determine the physical absorption capacity, given in Figure 5.18.
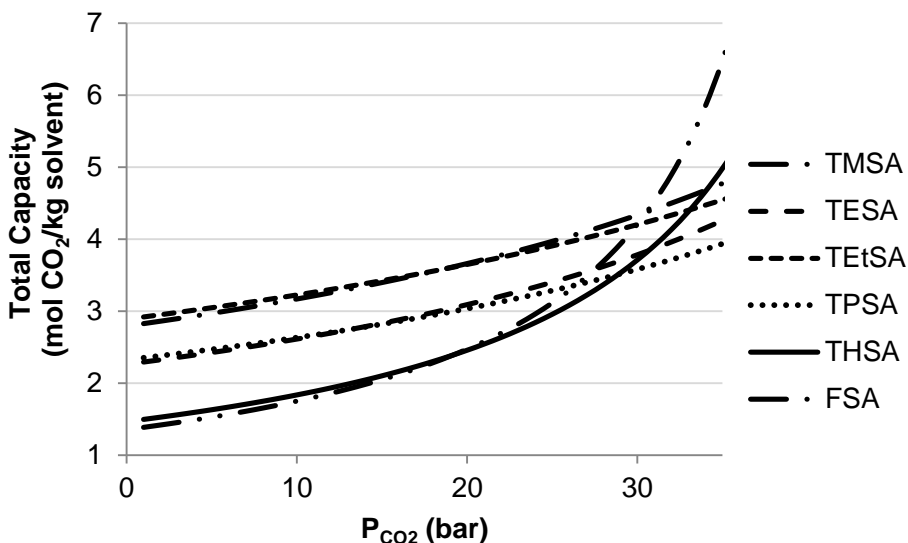
Figure 5.18. The combined physical and chemical absorption capacities (mol CO_2/kg solvent) as a function of CO_2 pressure (P_{CO_2}, bar).

It is apparent that the tradeoff between chemical absorption capacity and physical absorption capacity is not beneficial for P_{CO_2} < 30 bar. Even though the physical absorption capacities were greatly enhanced by manipulation of the molecular structure, for the purpose of CO_2 capture at low partial pressures, a capacity benefit would not be observed. The CO_2 partial pressure in typically coal fired power plant flue gas is ~ 0.2 bar, and the physical absorption capacity in the fully formed ionic liquid is < 3% of the total capacity for all the materials studied. For the treatment of gas stream with larger partial pressures of CO_2 (e.g. natural gas reservoirs), the benefit may be observed.

Lastly, the high viscosity ionic liquids could be problematic, if not detrimental, for the application of these materials to industrial scale absorbers. To operate up to the

maximum chemical absorption capacity would require the development of improved processing technology. However, this potential limitation can be avoided if the concentration of ionic liquid is maintained below 50% (molar). This corresponds to a 70% conversion of the molecular liquid, or 70% of the maximum theoretical capacity. This could be done by adjusting the absorption temperature of the tower, where higher temperatures will result in limiting the capacity. Again, these operating conditions are a unique function of the process design, but operating at higher absorption temperatures is beneficial minimizing the ΔT of the absorption/desorption cycle.

Conclusions and Path Forward

The one-component reversible ionic liquids presented here for application to CO_2 capture show much promise as viable candidates for replacing the benchmark solvent MEA. In addition to the highly selective chemical absorption mechanism, the reversible ionic liquids are capable of physically absorbing CO_2 in the ionic liquid form of the solvent. The understanding of molecular structure to physical absorption capacities was thoroughly examined, and the information provided the opportunity to modify the structure to enhance the physical absorption capacity by a factor of 2. Although the contribution of the physical absorption to the total capacity under normal flue gas conditions is small, it has shown to have a low enthalpy of absorption; advantageous for minimizing the energy requirement of the process. The enhanced physical absorption presents a benefit for the application to higher CO_2 partial pressure feed streams.

This fundamental study revealed some challenges for the application to industrial scale processing, namely the high viscosity of the ionic liquid form and the slow CO_2 uptake in the stagnant molecular liquid films. An understanding of composition versus viscosity gave insight into avoiding the detrimental viscosity, and the chemical

absorption uptake data provides a foundation for understanding the mechanism of uptake. The chemical absorption uptake, once better understood, presents an opportunity for engineers and chemists to enhance transport properties through molecular or processing modifications. One possibility is the use of atomizer technology for the chemical absorption uptake, where the interfacial area could be greatly enhanced and the uptake times could be drastically reduced.

The presence of water is likely in nearly all CO_2 capture applications, as combustion represents the primary source of CO_2 emissions. Water will surely have a positive impact on the capacities via carbonate formation that frees up some amine for further reaction, and will complicate the understanding of chemical absorption uptake. The presence of water in the system will definitely impact the transport rates and viscosities. The effect is likely positive for the transport rates, but the predicted impact on viscosity is a "mixed bag." The viscosity of the ionic liquid form will be decreased by the presence of water, but the formation of the carbonate salt could offset the benefits. Carbonates are stable solids, and it is difficult to predict the behavior of the ionic liquid, carbonate, and water mixture.

The one-component reversible ionic liquids explored to date represent only a small fraction of the potential molecular structures that could be developed through an ever-growing collaboration between engineers and chemists. Presented here are fundamental details that will guide the future development of these materials.

References

(1)   www.govtrack.us 2010; Vol. 2010.

(2)   www.netl.doe.gov 2010; Vol. 2010.

(3)   Aaron, D.; Tsouris, C. *Separation Science and Technology* **2005**, *40*, 321.

(4)   Powell, C. E.; Qiao, G. G. *Journal of Membrane Science* **2006**, *279*, 1.

(5)   Brunetti, A.; Scura, F.; Barbieri, G.; Drioli, E. *Journal of Membrane Science* **2010**, *359*, 115.

(6)   Lively, R. P.; Chance, R. R.; Kelley, B. T.; Deckman, H. W.; Drese, J. H.; Jones, C. W.; Koros, W. J. *Industrial & Engineering Chemistry Research* **2009**, *48*, 7314.

(7)   Anderson, S.; Newell, R. *Annual Review of Environment and Resources* **2004**, *29*, 109.

(8)   Rao, A. B.; Rubin, E. S. *Environmental Science & Technology* **2002**, *36*, 4467.

(9)   Danckwerts, P. V. *Chemical Engineering Science* **1979**, *34*, 443.

(10)   Rubin, E. S.; Chen, C.; Rao, A. B. *Energy Policy* **2007**, *35*, 4444.

(11)   Sanchez, L. M. G.; Meindersma, G. W.; de Haan, A. B. *Chemical Engineering Research & Design* **2007**, *85*, 31.

(12)   Baltus, R. E.; Counce, R. M.; Culbertson, B. H.; Luo, H. M.; DePaoli, D. W.; Dai, S.; Duckworth, D. C. *Separation Science and Technology* **2005**, *40*, 525.

(13)   Baltus, R. E.; Culbertson, B. H.; Dai, S.; Luo, H. M.; DePaoli, D. W. *Journal of Physical Chemistry B* **2004**, *108*, 721.

(14)   Schuette, G., RevIL Proposal_CoP Revisions.

(15)   Huddleston, J. G.; Visser, A. E.; Reichert, W. M.; Willauer, H. D.; Broker, G. A.; Rogers, R. D. *Green Chemistry* **2001**, *3*, 156.

(16)   Condemarin, R.; Scovazzo, P. *Chemical Engineering Journal* **2009**, *147*, 51.

(17)   Ferguson, L.; Scovazzo, P. *Industrial & Engineering Chemistry Research* **2007**, *46*, 1369.

(18)   Morgan, D.; Ferguson, L.; Scovazzo, P. *Industrial & Engineering Chemistry Research* **2005**, *44*, 4815.

(19)   Seddon, K. R.; Stark, A.; Torres, M. J. *Pure and Applied Chemistry* **2000**, *72*, 2275.

(20)   Higbie, R. *Transactions of the American Institute of Chemical Engineers* **1935**, *31*, 365.

(21)   Hayduk, W.; Cheng, S. C. *Chemical Engineering Science* **1971**, *26*, 635.

(22)   Poling, B. E. *The properties of gases and liquids*; 5th ed. ed.; McGraw-Hill: New York :, 2001.

(23)   Hines, A. L. *Mass transfer : fundamentals and applications*; Prentice-Hall: Englewood Cliffs, N.J. :, 1985.

(24)   Hou, Y.; Baltus, R. E. *Industrial & Engineering Chemistry Research* **2007**, *46*, 8166.

(25)   Baker, S. N.; Baker, G. A.; Kane, M. A.; Bright, F. V. *Journal of Physical Chemistry B* **2001**, *105*, 9663.

(26)   Blanchard, L. A.; Gu, Z. Y.; Brennecke, J. F. *Journal of Physical Chemistry B* **2001**, *105*, 2437.

(27)   Bondi, A. *J. Phys. Chem.* **1964**, *68*, 441.

(28)   Anthony, J. L.; Maginn, E. J.; Brennecke, J. F. *Journal of Physical Chemistry B* **2002**, *106*, 7315.

(29)   Anthony, J. L.; Maginn, E. J.; Brennecke, J. F. *Journal of Physical Chemistry B* **2001**, *105*, 10942.

(30)   Camper, D.; Scovazzo, P.; Koval, C.; Noble, R. *Industrial & Engineering Chemistry Research* **2004**, *43*, 3049.

(31)   Scovazzo, P.; Camper, D.; Kieft, J.; Poshusta, J.; Koval, C.; Noble, R. *Industrial & Engineering Chemistry Research* **2004**, *43*, 6855.

(32)   Moganty, S. S.; Baltus, R. E. *Industrial & Engineering Chemistry Research* **2010**, *49*, 5846.

(33)   Kincaid, J. F.; Eyring, H.; Stearn, A. E. *Chemical Reviews* **1941**, *28*, 301.

(34)   Hirschfelder, J.; Stevenson, D.; Eyring, H. *Journal of Chemical Physics* **1937**, *5*, 896.

(35)   Barton, A. F. M. *CRC handbook of solubility parameters and other cohesion parameters*; CRC Press: Boca Raton, Fla. :, 1983.

(36)   Aboudheir, A.; Tontiwachwuthikul, P.; Chakma, A.; Idem, R. *Chemical Engineering Science* **2003**, *58*, 5195.

(37) Versteeg, G. F.; Van Dijck, L. A. J.; Van Swaaij, W. P. M. *Chem. Eng. Commun.* **1996**, *144*, 113.

(38) Astarita, G. *Chemical Engineering Science* **1961**, *16*, 202.

(39) Emmert, R. E.; Pigford, R. L. *Aiche Journal* **1962**, *8*, 171.

(40) Wellek, R. M.; Brunson, R. J.; Law, F. H. *Can. J. Chem. Eng.* **1978**, *56*, 181.

(41) Ko, J. J.; Tsai, T. C.; Lin, C. Y.; Wang, H. M.; Li, M. H. *Journal of Chemical and Engineering Data* **2001**, *46*, 160.

(42) Dang, H. Y.; Rochelle, G. T. *Separation Science and Technology* **2003**, *38*, 337.

(43) Noda, A.; Hayamizu, K.; Watanabe, M. *Journal of Physical Chemistry B* **2001**, *105*, 4603.

CHAPTER 6   CONCLUSIONS AND RECOMMENDATIONS

The reversible ionic liquids presented here represent novel solvents with unique properties capable of improving upon the generally negative environmental impact encumbered by conventional solvents in the chemical industry. Though not a panacea, select applications were presented to showcase the potential of reversible ionic liquids in industrially relevant processes. Given here are the conclusions and recommendations to shed light on the advantages of using reversible ionic liquids, potential limitations of their use, and a guide for the design and development of next generation reversible ionic liquid solvents.

Chapter 2 – Synthesis and Characterization of Reversible Ionic Liquids

Most important for the design and development of sustainable materials, the conductivity measurements indicated the complete, repeatable formation of the ionic liquid species and effective reversal to molecular liquid. The synthesis of the reversible ionic liquids was efficient for both subsets, but the silyl-amine moieties proved much simpler. The synthesis of the one component materials is ideal for industrial scale processing due to the robust and efficient reaction, and the stability tests of the alkyl-substituted precursors indicated a relatively long shelf life – favorable for industrial scale synthesis and storage.

The characterizations presented here reflect the primary application of the two subsets of reversible ionic liquids. The Nile Red polarity experiments suggested that the two component materials exhibited a more significant polarity switch upon transformation from the molecular liquid to the ionic liquid, relative to the one component materials.

Their use as solvents for the coupling of reactions and separations was detailed in Chapter 3. For the case of the THSA compound, the observed polarity between the molecular and ionic forms was almost identical, indicating limited potential for application to coupled reaction and separation processes.

The DSC results indicated a cleaner separation between the loss of CO_2 and evaporation of the solvent for the one component materials. In contrast, the two component materials containing low molecular weight alcohols exhibited significant solvent loss concurrent with the loss of CO_2. For large scale applications, the switch of the one component materials is superior to the two components by avoiding significant solvent loss. Solvent losses in the reversion step would have to be reclaimed by subsequent separations, increasing process complexity and cost. The capture of CO_2 from power plant effluent is on a massive scale, and the one component materials were investigated for the application in Chapter 5 due to the clean reversal.

Pertaining to the design of future reversible ionic liquid materials, the one component materials are superior to the two components due the simplicity of altering the molecular structure. To date, only the silicon side of the molecule has been modified, and the relationship between the substitution on the silicon for symmetric molecules was investigated in much detail. Asymmetry on the silicon may have favorable effects on the melting points of the resulting ionic forms and should be investigated, potentially allowing for the design of lower molecular reversible ionic liquids. Additionally, substitutions between the nitrogen and silicon segment should also be investigated. In particular, substitution on the carbon atom adjacent to the nitrogen should be examined. Steric bulk near the nitrogen is likely to affect both the stability and solvent properties of the ionic form.

Chapter 3 - A Spectroscopic Technique for the Decoupled Measurement of Chemical and Physical Absorption in Reactive Solvent Systems

Reflectance infrared spectroscopy is a useful quantitative tool for probing the complimentary chemical and physical absorption of CO_2 in reactive amine based solvents. The versatility of the technique to other systems can be achieved with a thorough understanding of the fundamentals governing reflectance infrared spectroscopy and subsequent application of the Beer-Lambert Law, provided in Appendix A. The technique affords a molecular level insight into a complex reaction/absorption system, ideal for ensuring sample integrity and gaining a microscopic understanding of the studied system. The *in situ* sampling reduces errors associated with phase disruption.

When coupled with a commercially available heated diamond ATR accessory and custom design stainless steel reactor, high temperature and pressure process conditions could be safely and efficiently monitored. The design of the reactor limits sample sizes to several hundred milligrams, ideal for laboratory scale investigations of materials synthesized in-house. Additionally, the small sample size allows for rapid equilibrium to be achieved in the case of gas uptake into liquid and solid samples.

The technique was validated for the case on CO_2 absorption in water, and the experimentally determined extinction coefficients were compared to previously reported values (Appendix B). The physical absorption of CO_2 in the ionic form of TEtSA was accomplished at several temperatures, allowing for the determination of the thermodynamic properties associated with the absorption process. The technique was validated for several investigators spanning the course of several months, and errors between experiments were found to be within experimental error of the technique. Thus,

the technique is highly reproducible and intuitive, attractive for use in academic research laboratories where investigators are routinely substituted.

The chemical absorption of CO_2 in the molecular form was successfully monitored, and results indicated complete conversion of the molecule form to ionic form at a temperature of 35°C and CO_2 pressure of 1 bar; consistent with *ex situ* experiments. However, a limitation of the custom designed reactor was identified – without precise knowledge of sample thickness in the reactor chamber, the determination of diffusivities and uptake rates is precluded. Modifications to the experimental procedure or reactor, allowing for the accurate determination of sample thickness, would allow for such investigations. An available option in the Eckert-Liotta Laboratory is the commercially available Specac, Inc. Golden Gate Reactor Cell, with a removable reactor top that allows for samples to be directly placed in the reactor chamber; eliminating sample loss to the interior walls of the reactor.

The application of the technique to CO_2 sorption and swelling in polymeric thin films was presented in Appendix D, giving the reader another example of the reflectance infrared spectroscopic technique successfully applied to gas/solid phase systems. The only practical limitation of the technique is to systems where distinct spectral changes are observed. Hence, a detailed understanding of the spectral changes in a specific system must be understood before application of the quantitative technique can be pursued.

Chapter 4 – Coupling of Reactions and Separations Using Reversible Ionic Liquids

Exploiting the drastic polarity change observed for the molecular to ionic switch in the two component reversible ionic liquid systems, the application of coupling reactions

with separations was presented. Because the reaction-based switch of the solvent system can lead to complications in some reaction/separation systems, the application must be carefully chosen. However, several successful systems were reported. Namely the Claisen-Schmidt condensation and Heck reactions.

Although adding to the complexity of the process, the presence of water does not preclude the use of reversible ionic liquids for coupling reactions and separations in processes where water is created or required. For the Claisen-Schmidt condensation reactions, the water was a byproduct of reaction and the removal was required from the solvent system prior to activation of the ionic form. In addition to providing an adequate solvent, the TMBG played the role of catalyst for the reactions. The system was successfully recycled three successive times with no loss in yields or product distribution.

The Heck reaction provides an example of a successful organometallic reaction being performed in the DBU/hexanol solvent. Additional benefits were observed where the DBU acted as an acid scavenger (eliminating the need for an added base to neutralize the acid product) and the salt was also successfully removed from the system by taking advantage of the switchable polarity. Two separations were successfully achieved in the Heck reactions, illustrating the benefits of switchable solvents for promoting sustainable technology development.

The successful use of reversible ionic liquids for other reaction/separation systems is not without limitations, as described. However, as information is gained on the limitations, the probability of successful application to other systems is increased. Stemming from the Heck reaction, Sonogashira reactions would be another organometallic catalyzed process that could potentially utilize the acid scavenging ability

of the two component reversible ionic liquids, coupled with the benefits of a switchable solvent to yield facile separation of products from the reaction mixture for recycle.

Chapter 5 – Reversible Ionic Liquids for Post-Combustion CO$_2$ Capture

The capture of CO$_2$ from combustion effluent represents a huge technological and economic hurdle for coming generations. Liquid amine-based solvent systems are attractive due to the selectivity of a reaction mechanism for capture, but the intense energy requirements for solvent regeneration are troublesome. The energy requirements can be lessened by improving solvent capacities. The appeal of using one component reversible ionic liquids is the elimination of added co-solvent, resulting in an improvement in the maximum theoretical chemical absorption capacity over aqueous MEA by as much as 20%.

In addition to the highly selective chemical absorption, the resulting ionic form of the one component reversible ionic liquids is capable of physical absorption, at a fraction of the energy cost of chemical absorption. The physical absorption capacities were investigated for a broad range of one component molecular structures, and found to correlate with the void volume of the ionic liquid. The resulting structure-property relationships lead to the development of the highly branched THSA and fluorinated FSA compounds, which were shown to exhibit significant increases in physical absorption capacities; THSA exhibiting an improvement in the Henry's Law constant by a factor of 2 relative to the TEtSA and TPSA analogues.

The highly viscous nature of ionic liquids precludes their use in many industrial processes, and was investigated here as a function of solvent structure and molecular/ionic composition. The results were encouraging. The viscosities of the ionic

liquids forms could be drastically decreased by increasing the alkyl- substitution on the silicon, improving processability and mass transfer for gaseous uptake. However, the resulting ionic liquids exhibited viscosities still too high for industrial implementation with existing technology. The study of molecular/ionic composition on viscosity revealed startling results – chemical absorption capacities of nearly 70% of the maximum theoretical value resulted in mixture viscosities below the upper limit for absorption using existing technology. Thus, the knowledge of solvent structure on viscosity results in a usable fluid that circumvents the need for advancements in existing processing equipment.

The chemical absorption capacity inherently correlates with the molecular weight of the solvent, and attempts at furnishing higher capacity solvents by minimizing the alkyl- content on silicon were unsuccessful. However, all molecules examined were symmetric, and incorporating asymmetry on the silicon has the potential to decrease melting points. Additionally, mixtures of one component reversible ionic liquids may effectively reduce the average molecular weight of the solvent (beyond TEtSA) and yield a usable solvent for CO_2 capture.

Molecular modifications to the propyl- linkage between silicon and the amine were not attempted, and would like affect the properties of the reversible ionic liquid. Spartan simulations were performed to examine the effect of altering the silyl- amine substructure on the electronics on the amine. It was found that modifications to the silicon substituent had little to no effect, consistent with the DSC results in Chapter 2 that showed similar enthalpies of desorption (when normalized to moles of CO_2) for the TEtSA, TPSA, and THSA compounds. However, the addition of even a small neutral attachment (methyl group) to the carbon adjacent to the amine revealed significant changes in the charge on the amine, due to steric affects. This is encouraging for using

the structural modifications to alter the thermodynamics of the reaction of the one component reversible ionic liquids with CO_2.

The benefits of using the reversible ionic liquids for CO_2 capture have been shown for cases of pure CO_2. The next evolution of the project would be to examine simulated flue gas streams, where much nitrogen and water are present. Regarding chemical absorption, nitrogen is nothing more than a diluent, and the successful capture of CO_2 partial pressures below 1 bar needs to be confirmed. And then there's water. The effect of water is difficult to predict and must be examined experimentally. Although bicarbonate formation will lead to higher capacities, the resulting product is a solid and will likely affect viscosity and melting point of the product mixture. An offsetting phenomenon is likely, where unreacted water will reduce the viscosity and melting points. Additionally, the accumulation of water in the system is problematic for aqueous amine based solvents. The lipophilic nature of the one component reversible ionic liquids may limit the water accumulation, which would be a big economic advantage by eliminating the need for energy intensive solvent reconstitution.

APPENDIX A THEORY AND BACKGROUND ON QUANTITATIVE REFLECTANCE INFRARED SPECTROSCOPY

Introduction

The first reported application of reflection to measure absorption was in 1933,[1] but the development of an IR technique utilizing internal reflection wasn't reported until the 1950's. Popularity of the technique, combined with increasing availability of commercially available infrared reflectance accessories, has resulted in an explosion of its use in quantitative applications in the past two decades. The proper analysis of reflectance spectroscopy is complicated, and many errors have been observed in literature. To eliminate erroneous treatments, researchers must understand the theory of the technique.

Infrared Spectroscopy

Infrared spectroscopy (IR) is a versatile technique used regularly in academia and industry for the rapid, cost-effective, and accurate analysis of pure compounds or mixtures. Nearly all researchers in the world have access to a Fourier Transform Infrared Spectrophotometer (FT-IR), and the possibilities of its application are limited only by the creativity of the investigator. There are no practical limitations regarding the sample that can be examined; liquids, gases, solids, bases, acids, solutions, or suspensions. And with the advent of rapid data acquisition systems, aka computers, there has been an explosion of the use and application of IR spectroscopic techniques in both qualitative and quantitative analytical chemistry. Recently, the use of infrared spectroscopy has allowed researchers to identify preservation techniques used on priceless works of art,[2]

examine the three-dimensional diffusion of drugs through skin,[3] identify the composition of complex mixtures[4,5] and measure reaction rates/equilibria.[6-8]

Spectroscopy is the study of how molecules respond upon exposure to radiation. The types of radiation used are found in the *Electromagnetic Spectrum.* The most common electromagnetic classifications utilized in spectroscopy are (in order of increasing wavelength): x-ray, ultraviolet, visible, IR, and radio waves. Discussed here is the use of IR radiation, which can be split into three regions: far (1000-30 μm), mid (30-2.5 μm), and near (2.5-0.8 μm). The mid-IR region is used in this study and is by far the most commonly utilized region of IR spectroscopy as it reveals the fundamental vibrations, most useful for identifying specific functional groups. The near-IR region exposes the "overtone" vibrations, which occur at discrete multiples of the fundamental vibrations.

Fourier-transform infrared (FT-IR) spectrophotometers are used to generate IR radiation and detect the signal after it has been absorbed by the sample, producing the IR spectra. Most manufacturers provide FT-IR spectrophotometers in different configurations for applications ranging from general to highly specialized. The detection wavelength range is determined by the detector material. The standard deuterated L-alanine doped triglycene sulphate (DLaTGS) detector is accurate, highly reproducible, and inexpensive; though it is useful only for examining the mid- and near-IR regions. Detectors that provide access to the far-IR region are considerably more expensive.[9]

Molecules, at temperatures above absolute zero, vibrate and rotate at specific frequencies corresponding to the unique conformation of atoms and bonds that make up the structure. IR radiation is absorbed when the frequency of vibration matches the IR frequency. This unique relationship between molecular structure and vibrational frequency has led to the predominant use of IR spectroscopy: qualitative analysis. To

describe the wavelength of IR radiation absorbed in spectroscopy, wavenumbers (cm^{-1}) are frequently used in place of wavelength. The mid-IR region can then be classified as two distinct regions used for qualitative analysis: fingerprint (400-1500 cm^{-1}) and functional group (1500-4000 cm^{-1}). The response or output is then described as either transmission (T, % of radiation transmitted) or absorbance (A, with arbitrary units A.U.), and the two are related by the equation A = log$_{10}$(1/T). Figure A.1 is an illustration of the mid-IR spectrum of (3-aminopropyl)triethylsilane (TEtSA) that highlights the two regions, and provides peak identification[10] and the structure of TEtSA.
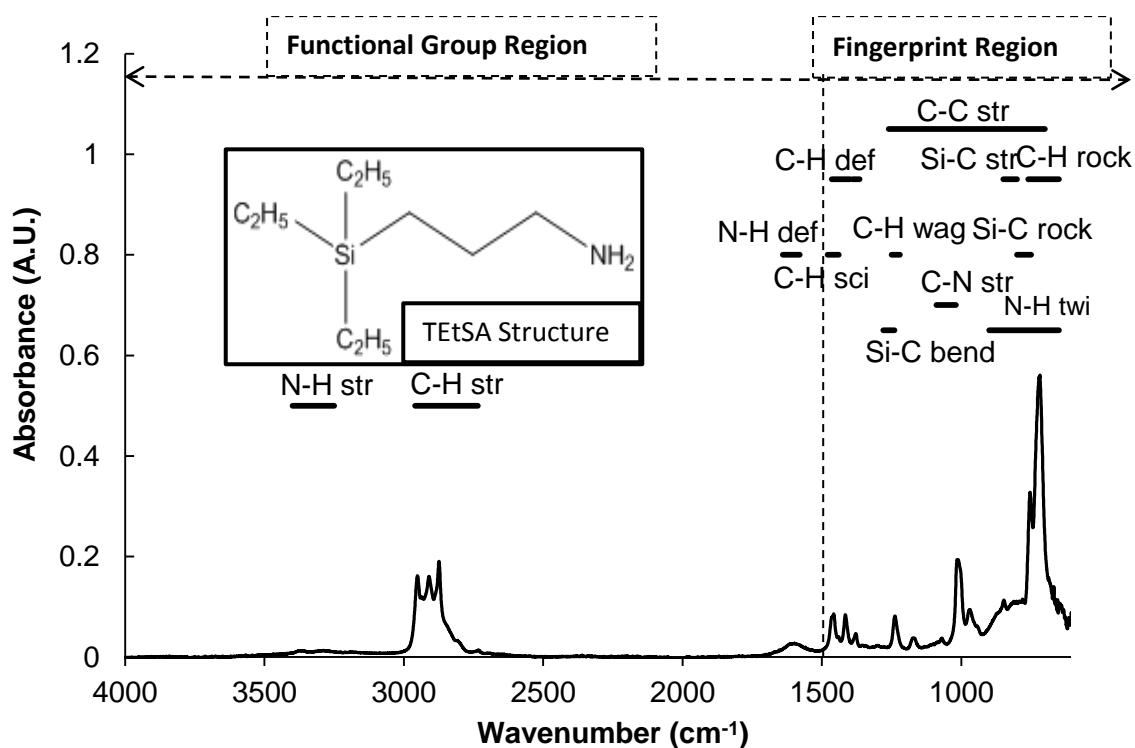
Figure A.1. The IR spectra of TEtSA, showing the molecular structure and corresponding absorption bands.

There are primarily six vibrational modes observed in the mid-IR region of organic compounds: symmetric and asymmetric stretching (str), scissoring (sci), rocking

(rock), wagging (wag), bending (bend), and twisting (twi).[11] As evidenced by the spectrum shown in Figure A.1, most vibrational modes appear in the fingerprint region, making it difficult to interpret. However, symmetric and asymmetric stretching vibration frequencies are more disparate and are primarily located in the functional group region. These are the vibrational frequencies used for the diagnostic interpretation in qualitative analysis.

Because the vibrational frequency observed is unique to a specific segment of a molecule, it is possible to predict frequencies knowing the bond strength and mass of connected atoms. If we think of a bond between two molecules as a spring, then Hooke's Law (which relates the force on a spring to the displacement multiplied by a spring constant) can be used to estimate the frequency of vibration for a bond between two atoms,

$$\upsilon = \frac{1}{2\pi c}\sqrt{f\,\frac{(m_1+m_2)}{m_1 m_2}} \qquad\qquad (A.1)$$

where v is vibrational frequency (cm^{-1}), c is the velocity of light (cm/s), f is the bond force constant (dyne/cm), and m_1 and m_2 are the masses (g) of atom 1 and atom 2, respectively.[12]

Hooke's Law is an idealized interpretation of IR spectroscopy and real systems are much more complicated, as evidenced in Figure A.1. Vibrational frequencies are represented as bands, not lines, because the molecular vibrations are also accompanied by rotational energy changes. The rotational energy is key to observing a response with IR. The fundamental vibrations must result in a rotation (or change in dipole) in order to be observed, referred to as "IR active." This is not the case of diatomic gases (N_2, H_2, O_2, etc.) and the symmetric stretch vibration of carbon dioxide, which are said to be "IR inactive."

Three distinct bands are observed in the C-H stretching region for TEtSA, indicating the C-H bonds in TEtSA are not all energetically equivalent. Coupled interactions as well as both inter- and intra-molecular interactions (such as hydrogen bonding) alter the vibrations and can result in band shifting or broadening. As a result, IR interpretation charts and tables list vibrational frequencies as a range of values. Table A.1 gives the *Force Constants* for common bonds, and compares the observed vibration bands to those calculated using Hooke's Law.

Table A.1. Force constants used in Hooke's Law and the calculated versus observed vibrational frequencies for common bonds.[12]

Bond Type	Force Constant (f) [dyne/cm]	Absorption Region (cm^{-1})	
		Calculated	Observed
C - O	5.0 x 105	1113	1300-800
C - C	4.5 x 105	1128	1300-800
C - N	4.9 x 105	1135	1250-1000
C = C	9.7 x 105	1657	1900-1500
C = O	12.1 x 105	1731	1850-1600
C ≡ C	15.6 x 105	2101	2150-2100
C - D	5.0 x 105	2225	2250-2080
C - H	5.0 x 105	3032	3000-2850
O - H	7.0 x 105	3553	3800-2700

The fact that specific bond vibrations can occur over a range of values, unique to a specific system, gives a hint to the utility of IR spectroscopy – molecular level insight. The presence of certain bands in the Functional Group Region can be used to readily identify specific functional groups in a molecular structure. Conversely, the

disappearance of said bands can be used to indicate chemical transformations. And the Fingerprint Region can be used to positively identify a pure compound. The diagnostic power gained from this "molecular level insight" is evidenced by comparing the IR spectra of TEtSA to the n-propyl substituted analogue (3-aminopropyl)tripropylsilane (TPSA), Figure A.2.
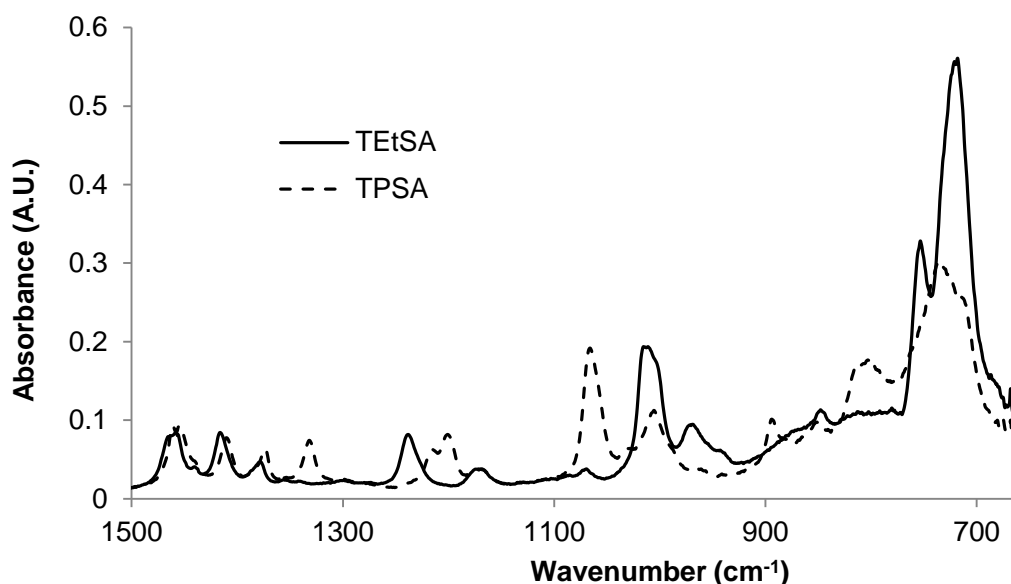
Figure A.2. Fingerprint Region of TEtSA (solid line) and TPSA (dashed line).

Although the molecular structures of TEtSA and TPSA are similar, *the Fingerprint Region* shows distinct differences. When the IR spectrum is available for a pure substance, a comparison of the *Fingerprint Regions* between an unknown and the reference can be used to positively identify the unknown. In most cases, however, IR spectroscopy is used as a qualitative tool to identify specific functionalities that appear in the *Functional Group Region*.

In addition to being a very powerful and sensitive technique for qualitative analysis, IR spectroscopy has also been used in quantitative analysis by application of the Beer-Lambert Law,

$$A = \log(1/T) = \varepsilon bc = \alpha b \qquad \text{(A.2)}$$

where A is absorbance (A.U.), T is transmittance (%), ε is the extinction coefficient (cm^2/mol), b is pathlength (cm), c is concentration (mol/cm^3), and α is the absorption coefficient (cm^{-1}).

The Beer-Lambert Law is used to relate the absorption of radiation to the material the radiation has traveled through. Seemingly simple, much care must be taken when applying the Beer-Lambert Law in quantitative IR spectroscopy. These considerations are discussed in much detail later in this chapter.

Attenuated Total Reflectance Spectroscopy

Attenuated Total Reflectance (ATR) spectroscopy is a sampling technique used to expose a sample to IR radiation. Transmission IR spectroscopy was the sampling technique utilized with the advent of IR spectroscopy, and remains the prominent technique used today. By direct application of the Beer-Lambert Law, a sample absorbs IR radiation proportional to the pathlength and concentration. In the case of transmission, the pathlength is the thickness of the sample through which the light travels and the concentration is related to the density. If the sample is too dense or too thick, then it will absorb all the IR radiation and the resulting spectrum will be observed as a flat line. This phenomenon is referred to as "detector saturation."

Transmission is very useful for examining samples where the thickness or density can be easily adjusted to avoid detector saturation. Controlling the pathlength

161

can easily be done with solid thin films by adjusting film thickness, or in the case of gases, by changing the pressure or width of the gas cell. Powder samples are commonly mixed with a non-absorbing salt (potassium bromide is commonly used for this purpose) and pressed into pellet form. The ratio of sample to salt is altered to give acceptable IR spectra. Liquid samples are prepared by sandwiching the sample between two salt pellets. Typical pathlengths used in transmission IR spectroscopy for gases is on the order of centimeters (cm); for solids and liquids it is on the order of microns (μm).

The principle laws governing the reflection and propagation of light were documented by Sir Isaac Newton more than three centuries ago. Reflection is a phenomenon that arises when light contacts the interface of two materials that have different refractive indices. Internal reflection is defined as the case when the radiation travels first through an optical crystal of high refractive index (n_1) and then through the sample with a lower refractive index (n_2). Refractive index is a dimensionless term that is the ratio of the speed at which light travels through the sample divided by the speed of light in vacuum. With all types of reflection, there is a minimum angle for which the radiation must contact the interface. This is called the "critical angle (θ_c)," and it is found from the relationship $\theta_c = \sin^{-1}(n_2/n_1)$.[13] Total internal reflection is the case when θ is greater than θ_c, resulting in complete reflection of the propagating wave and no refraction.

Internal reflection results in a wave of radiation perpendicular to the interface that extends into the lower refractive index material, Figure A.3. The intensity of the wave decays exponentially with respect to the distance traveled from the interface, giving it the name "evanescent wave." The rate at which the wave decays, i.e. attenuates, is related to n_2.

162
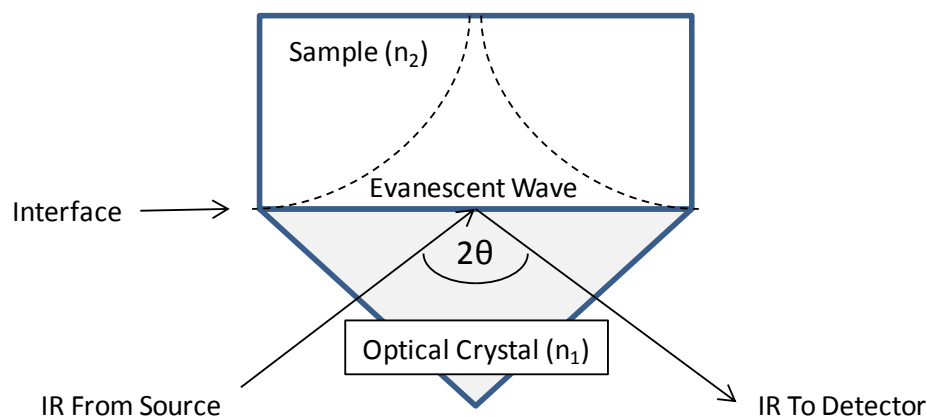
Figure A.3. A schematic of single reflection ATR IR spectroscopy.

Theoretically infinite, there is an effective distance that the wave travels into the absorbing material. This is an ambiguous concept and has resulted in much confusion in the literature. The intensity of the evanescent wave (E) at some distance from the interface (Z) is related by the equation: $E = E_0 \exp(-\gamma Z)$, where E_0 is the intensity at the surface and γ is the electric field amplitude decay coefficient.[14] Harrick and Dupre go on to define "depth of penetration (d_p)" as the distance (Z) for which Z equals $1/\gamma$, or the energy of the wave is about a third of the energy at the surface, Equation A.3. It should be emphasized that the intensity of the evanescent wave and the magnitude of d_p are dependent on the wavelength of radiation that is absorbed (λ_1).

$$d_p = \frac{1}{\gamma} = \frac{\lambda_1}{2\pi(\sin^2\theta - (n_2/n_1)^2)^{1/2}} \qquad (A.3)$$

Experimentally, ATR IR produces spectra nearly identical to transmission IR. For qualitative purposes, ATR can be viewed as a simple method to limit the pathlength to several microns (μm) which is ideal for examining solid and liquid samples. The difference between ATR and transmission spectroscopy is the treatment of pathlength. As shown in Equation A.3, the distance the evanescent wave travels into the sample is

dependent on the wavelength of vibration. Thus, the ATR IR signal intensity decreases as the wavelength decreases (or wavenumber increases). To account for this artifact in ATR IR, modern FT-IR spectrophotometers have an "ATR Correction" function to allow for direct comparison of ATR IR spectra to those collected via transmission. In some cases, this reduction in pathlength at low wavelengths will result in a loss in sensitivity. If the sample is weakly absorbing and/or the density is low, the resulting spectrum will exhibit poor signal-to-noise (S/N) ratio. This can be improved by using a multiple reflection crystal.

There are many ATR IR sample accessories that are commercially available, and many descriptions exist in the literature on the design of custom built cells. Some designs are capable of measuring only ambient conditions, while others offer high temperature and pressures capabilities. Besides the choice between multiple or single reflection designs, the biggest decision to be made regarding ATR IR sample accessories is the type of optical crystals used.

There are about a dozen types of materials that have favorable properties for use as ATR IR optical crystals, but four materials are prominently used: (1) zinc selenide (ZnSe), (2) germanium (Ge), (3) KRS-5 (a blend of thallium(I) iodide and thallium(I) bromide) and (4) diamond (C). The differences between the four materials include cost, stability, hardness, refractive index, and spectral interference. For the application to mid-IR spectroscopy, spectral interference isn't a concern. These four materials have become popular because they are free of interference in the mid-IR region. ATR IR can also be used to probe the near-IR region (14000-4000 cm^{-1}) as all materials but germanium exhibit minimal interference in the near-IR region. However, significant interference occurs in the far-IR region (400-10 cm^{-1}) for all of these materials and they should not be used in such investigations.

KRS-5 is cheap and abundant, and although it was designed to overcome the water sensitivity of common salts, it is a relatively soft material that can be etched by aqueous solutions. Germanium is also cheap, and because of its high refractive index value (n_1 = 4.0 at 1000 cm^{-1}) it has been widely used for strongly absorbing samples. ZnSe has become a preferred yet costlier replacement for KRS-5 because it has a similar refractive index (n_1 = 2.4 for ZnSe and n_1 = 2.37 for KRS-5, both measured at 1000 cm^{-1}) but lacks the problems with water.[13] There is only one material that is impervious to water, acids, bases and resists even the harshest mechanical stresses – diamond. Diamond is by far the most expensive, and because of its gemological value has had limited application in ATR IR spectroscopy until the late 1990's when the cost-effective manufacture of lab grown diamonds increased availability and decreased cost.

Application of the Beer-Lambert Law to ATR IR Spectroscopy

IR spectroscopy is a useful qualitative tool at the disposal of most, if not all, researchers. An often overlooked use of IR spectroscopy is quantitative analysis, and this is likely attributed to a lack of understanding or confidence in the treatment of the Beer-Lambert Law (Equation A.2) to the IR spectrum. In general, IR is most useful in quantitative applications because it's an in situ sampling technique leaving the system undisturbed. Considering the relatively low cost of FT-IR spectrophotometers combined with the high sensitivity and molecular level insight they afford, the value of IR is unparalleled. When the proper precautions are taken, quantitative IR can be used to probe reaction kinetics, phase behavior, and equilibria accurately. The considerations for using the Beer-Lambert Law to quantify ATR IR experiments are given in detail.

Absorbance (A)

The magnitude of absorbance readings is the major constraint when applying the Beer-Lambert Law to any spectroscopic technique, whether it be UV-Vis or IR. The Beer-Lambert Law assumes that at a fixed pathlength, linearity exists between the absorbance and concentration of a particular species. This definition gives rise to the practical meaning of the extinction coefficient. This assumption holds true for values of the absorption coefficient less than 10,000 (cm^{-1}).[13] Absorption coefficients are rarely reported. Therefore, a more useful criteria for ensuring linearity of the Beer-Lambert Law is defined as an absorbance value of less than 0.7 A.U., although good agreement has been shown for select cases up to absorbances of 2.0 A.U.[9]

The peaks in IR spectra exhibit varying degrees of intensity and broadness, relative to the specific group absorbing the radiation and the surrounding environment. For example, the O-H stretch vibration for alcohols in dense phases (i.e. liquids) is very broad and covers the range from 3000 to 3500 cm^{-1}. This is due to hydrogen bonding. When the IR spectrum is taken for the same alcohol in the gas phase, the O-H stretch vibration appears very sharp. This is due to the intense hydrogen bonding that takes place in the dense phase but is absent in the gas phase. Inter- and intra-molecular interactions have a large effect on both the shape and location of IR peaks.

Absorbance values are generally applied to the Beer-Lambert Law by using the maximum value of the peak at a fixed wavelength. Because IR peaks can be influenced so strongly by the environment surrounding the molecule, it is a better practice to use the area of the peak rather than the maximum. This is especially important in quantitative analyses when the changes in peaks are monitored over time. It is not uncommon for peaks to shift several wavenumbers or broaden as reactions proceed or compositions are altered, especially for dense phase examinations.

<u>Extinction Coefficient (ε)</u>

The extinction coefficient, or molar absorptivity, is defined as the measure of how strongly a species absorbs radiation. As mentioned earlier, the extinction coefficient is found from the experimental absorbance data when the linearity of the Beer-Lambert Law holds true and the concentration and pathlength of the sample are known. Because the extinction coefficient is found only from experimental data for a specific compound, it is not usually known. Most extinction coefficients reported in the literature are determined via transmission techniques. Applying extinction coefficients determined from transmission spectroscopy to ATR spectra adds much more complexity to the validity of the Beer-Lambert Law via the treatment of pathlength.

For quantitative spectroscopic techniques utilizing the Beer-Lambert Law, the extinction coefficient serves as a measure of the irradiation response of a particular species in a unique experimental setup. Whenever possible, the most accurate determination of extinction coefficient is found from a calibration curve obtained for one's unique experimental apparatus. Researchers have developed elegant methodologies in order to circumvent the lack of information available on extinction coefficients. The most popular treatment is to carefully select a system where the analysis method results in the disappearance of the extinction coefficient (and frequently pathlength) from the Beer-Lambert Law. This can be done by relating the measured absorbances of unknown samples to the absorbance spectrum of a solution with a known concentration such as the initial or final concentrations if a reaction is analyzed.[7,15,16] This is akin to generating a calibration curve that relates concentration to absorbance, except only a single point is used.

Even when proper care is taken to describe accurately the pathlength used in ATR IR spectroscopy, serious error can arise if researchers blindly use extinction

coefficients taken from published reports. When using extinction coefficient values taken from literature, one should also be cognizant of the assumptions made in the analytical method and how absorbance values were analyzed. As discussed in the previous section, peak maxima are commonly used to represent the absorbance that is used for the calculation of extinction coefficients (cm^2/mol) and subsequent quantitative analysis. If the peak areas are used for absorbance instead of maxima, the extinction coefficient (cm/mol) could be more than an order of magnitude different. Great care must be taken to ensure validity of the extinction coefficient used in analysis.

Pathlength (*b*)

The treatment of the pathlength in ATR IR spectroscopy is cumbersome. For transmission IR methods, pathlength is easily definable as either the distance the radiation travels through a closed cell (common in gas samples) or the thickness of the sample (typical when analyzing films). Recall that internal reflection spectroscopy results in the complete reflection of the propagating wave that generates an evanescent wave traveling an infinite distance into the sample. The pathlength would then be theoretically infinite regardless of wave intensity or refractive index of the crystal and sample. The ambiguity associated with the definition of ATR pathlength is what led to the definition of d_p (Equation A.3) by Harrick, where d_p correspond to the distance at which the intensity of the evanescent wave has decreased to 37% of its magnitude at the surface. Though somewhat arbitrary, Harrick intended for d_p to serve as a standard method for evaluating the effects of n_1, n_2, θ, and λ_1 on the measured spectra.

Much effort has gone into determining the proper definition of pathlength used in ATR IR that will give identical results to similar transmission IR experiments. Such an expression would allow for the direct application of extinction coefficients reported for transmission techniques to ATR IR experiments analyzing the same absorption band.

Harrick developed an expression for effective thickness (d_e) by examining absorption coefficients reported in literature for transmission IR, and working backwards until agreement was found with the ATR IR spectra.[17]

In all treatments of pathlength used for ATR IR analysis, the sample thickness should be much greater than d_p. In cases where the sample thickness is approximately equal to d_p, the spectra obtained can fluctuate greatly in magnitude and peak maxima.[18] The treatment of d_e that follows is limited exclusively to the case where the sample thickness is much greater than d_p.

Harrick had originally proposed that for an expression of d_e that would allow for direct translation to transmission IR, the polarization of the evanescent wave must be considered[19]. The evanescent wave is actually made up of two waves: one that is parallel to the plane of incidence (P) and another that is perpendicular to the plane of incidence (S; for senkrecht). The equation to determine the effective thickness traveled by the S polarized wave $(d_e)_S$ follows a similar expression to d_p.

$$(d_e)_S = \frac{(n_2/n_1)\lambda_1 \cos\theta}{\pi(1-(n_2/n_1)^2)(\sin^2\theta - (n_2/n_1)^2)^{1/2}}$$ (A.4)

The treatment of the P polarized wave $(d_e)_P$ is much more rigorous by comparison.

$$(d_e)_P = \frac{(n_2/n_1)\lambda_1 (2\sin^2\theta - (n_2/n_1)^2)\cos\theta}{\pi(1-(n_2/n_1)^2)[(1+(n_2/n_1)^2)\sin^2\theta - (n_2/n_1)^2](\sin^2\theta - (n_2/n_1)^2)^{1/2}}$$ (A.5)

The effective thickness for the unpolarized wave is given as the average of the two, $d_e = (0.5)(d_e)_S + (0.5)(d_e)_P$. The definition of d_e, just like the definition of d_p, relies only on the knowledge of n_1, n_2, θ, and λ_1.

The validity of using d_e to represent pathlength in the Beer-Lambert Law for the comparison of reflection to transmission is contingent upon achieving consistent

"intimate" contact of the sample with the optical crystal. Mirabella showed excellent agreement between the experimental and theoretical values of d_e for solid ethylene-vinyl acetate copolymer samples.[20] Mirabella examined three sample preparation techniques (pressed film, sheet film, and melt film) and discovered that the melt film samples exhibited nearly perfect fits between experiment and theory using both KRS-5 and germanium crystals with a range of incident angles from 40° to 65°. Although much care must be given to ensure consistent "intimate" contact for solid samples in ATR IR spectroscopy, it is much easier to attain with liquid samples.

To reiterate, the equation for d_p does not capture accurately the effects of differing sample refractive indices. The values of d_e and d_p were calculated and plotted versus changing sample refractive index, assuming all other parameters remained constant, given in Figure A.4.
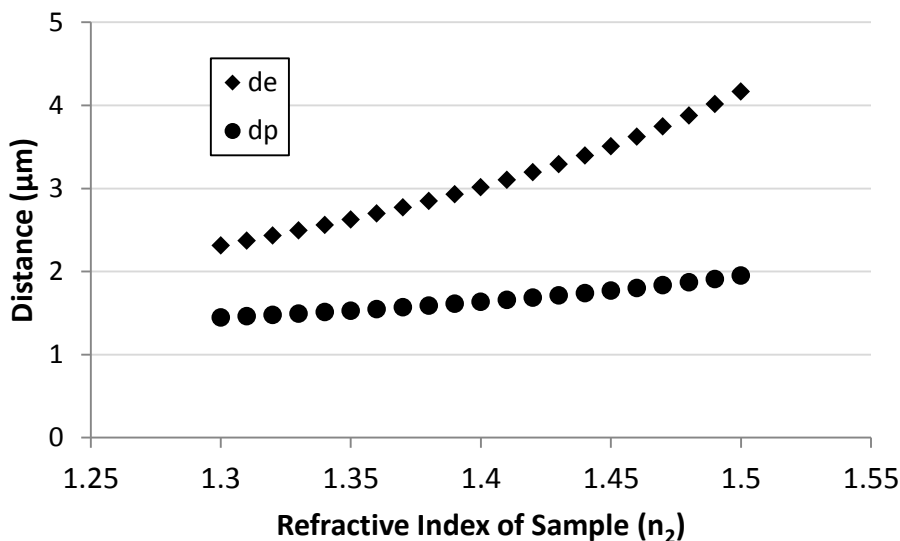
Figure A.4. The calculated affect of sample refractive index (n_2) on the penetration depth (d_p) and effective thickness (d_e). (λ_1 = 2400 cm^{-1}, θ = 45°, and n_1 = 2.4)

The points were calculated using λ_1 = 2400 cm^{-1}, θ = 45°, and n_1 = 2.4, representative of the system being examined in Chapter 2. Using the data from Figure A.4, the calculated error in approximation for using d_p over d_e will exceed 5% for Δn_2 > 0.03. Therefore, the use of d_p for calculating the pathlength used in the Beer-Lambert Law will fail as n_2 approaches n_1 and for cases where sample refractive indices fluctuate greatly.

Concentration (c)

Concentration is the solution sought after when researchers utilize quantitative ATR IR spectroscopy. Once all constraints have been met to achieve agreement with the Beer-Lambert Law and the ATR IR technique, knowledge of absorbance, extinction coefficient, and pathlength will yield the concentration of the desired species. Detailed information about how the sample is being affected by the experimental conditions can then be extracted from the absorbance data collected.

Conclusion

The use of quantitative reflectance infrared spectroscopy is a useful tool for the *in situ* examination of everything from thermodynamic to kinetic information for both reactive and non-reactive systems. Solution procedures can be greatly simplified by application of limiting assumptions, incurring only small errors. The proper use of such techniques can be complicated, and an intimate knowledge of the governing principles is required to maintain analytical integrity. Presented here is the fundamental information necessary for applying quantitative reflectance infrared spectroscopic techniques to a limitless number of systems relevant to chemical engineers and chemists alike.

References

(1)   Taylor, A. M.; Glover, A. M. *Journal of the Optical Society of America* **1933**, *23*, 206.

(2)   Spring, M.; Ricci, C.; Peggie, D. A.; Kazarian, S. G. *Analytical and Bioanalytical Chemistry* **2008**, *392*, 37.

(3)   Boncheva, M.; Tay, F. H.; Kazarian, S. G. *Journal of Biomedical Optics* **2008**, *13*.

(4)   Chan, K. L. A.; Kazarian, S. G. *Applied Spectroscopy* **2007**, *61*, 48.

(5)   Chan, K. L. A.; Kazarian, S. G. *Analyst* **2006**, *131*, 126.

(6)   Aylor, A. W.; Larsen, S. C.; Reimer, J. A.; Bell, A. T. *Journal of Catalysis* **1995**, *157*, 592.

(7)   Meredith, J. C.; Johnston, K. P.; Seminario, J. M.; Kazarian, S. G.; Eckert, C. A. *J. Phys. Chem.* **1996**, *100*, 10837.

(8)   Schultz, R. H.; Bengali, A. A.; Tauber, M. J.; Weiller, B. H.; Wasserman, E. P.; Kyle, K. R.; Moore, C. B.; Bergman, R. G. *Journal of the American Chemical Society* **1994**, *116*, 7369.

(9)   *Handbook of Instrumental Techniques for Analytical Chemistry*; Settle, F., Ed.; Prentive-Hall, Inc., 1997.

(10)   Socrates, G. *Infrared Characteristic Group Frequencies: Tables and Charts*; Second ed.; John Wiley & Sons, Inc., 1994.

(11)   Vollhardt, K. P. C.; Schore, N. E. *Organic Chemistry: Structure and Function*; Fourth ed.; W.H. Freeman and Company: New York, 2003.

(12)   Silverstein, R. M.; Webster, F. X.; Kiemle, D. J. *Spectrometric Identification of Organic Compounds*; Seventh ed.; John Wiley & Sons, Inc., 2005.

(13)   *Internal Reflection Spectroscopy: Theory and Applications*; Mirabella, F. M., Jr., Ed.; Marcel Dekker, Inc., 1993; Vol. 15.

(14)   Harrick, N. J.; Dupre, F. K. *Applied Optics* **1966**, *5*, 1739.

(15)   Pasquali, I.; Andanson, J. M.; Kazarian, S. G.; Bettini, R. *Journal of Supercritical Fluids* **2008**, *45*, 384.

(16)   Duarte, A. R. C.; Anderson, L. E.; Duarte, C. M. M.; Kazarian, S. G. *Journal of Supercritical Fluids* **2005**, *36*, 160.

(17)   Harrick, N. J.; Carlson, A. I. *Applied Optics* **1971**, *10,* 19.

(18)   Hu, C. G.; Sun, L. D.; Flores-Camacho, J. M.; Hohage, M.; Liu, C. Y.; Hu, X. T.; Zeppenfeld, P. *Rev. Sci. Instrum.* **2010**, *81*.

(19)   Harrick, N. J. *Internal Reflection Spectroscopy*; Inerscience-Wiley: New York, 1967.

(20)   Mirabella, F. M. *J. Polym. Sci. Pt. B-Polym. Phys.* **1983**, *21*, 2403.

The ε_{CO_2} values found via the technique described in Chapter 3 (using both absorbance maxima and area) are compared to the values reported in literature in Table B.1.

Table B.1. Comparison of ε_{CO_2} values reported in literature to the values obtained here.

ε_{CO_2}	Method and Reference
1×10^6 cm^2/mol	Maxima – Jones, 1958[1]
1.5×10^6 cm^2/mol	Maxima – Falk, 1992[2]
1.52×10^6 cm^2/mol	Maxima – Kieke, 1996[3]
0.89×10^6 cm^2/mol	Maxima – Maiella, 1999[4]
1.58×10^7 cm/mol	Area – Maiella, 1999[4]
0.37×10^6 cm^2/mol	Maxima – This work
1.19×10^7 cm/mol	Area – This work

Surprisingly, the extinction coefficient for physically absorbed CO_2 has been reported only 5 times, coming from 3 different research laboratories (Kieke and Maiella are from the same research group). Many studies have used quantitative infrared spectroscopy and did not report the ε_{CO_2} values. This is because the primary method for quantitative infrared spectroscopy is transmission, where the pathlength between

calibration samples and unknown samples is identical. Therefore, the ε_{CO_2}/b value is commonly determined from a plot of A versus concentration, and the result is unique to the experimental apparatus. This treatment is valid for the case of transmission spectroscopy, but not when reflectance spectroscopy is used and the refractive indices of the calibration and unknown samples are significantly different. Although the values reported here are on the same order-of-magnitude as previously reported values, the differences are significant. A look into the methods by which the values were determined offers an explanation.

First, all researchers used the water and CO_2 system with transmission infrared spectroscopy to determine the ε_{CO_2} values in the literature reports. Jones and coworkers obtained the value of 1×10^6 cm^2/mol by first preparing a CO_2 saturated water mixture by bubbling CO_2 through distilled water at room temperature. The exact concentration of CO_2 in the water was never measured, and assumed to be the value for 1 atm of CO_2 in equilibrium with water at 25°C. The authors acknowledge that "some time passed" between preparation of the sample and the infrared measurements, implying the concentration of CO_2 in the infrared sample is different than the value used in the calculation of ε_{CO_2} from analysis of the infrared spectrum.

Similarly, Falk and coworkers prepared CO_2 saturated water samples by bubbling CO_2 through distilled water. The CO_2 concentration in the water sample was determined by manual titration of the sample. The authors again acknowledge that the titration method involves diluting and stirring the sample over a period of minutes, ultimately lowering the measured value of CO_2 in the water used for the calculation of ε_{CO_2}. Because the concentration value used in calculation of ε_{CO_2} is lower than the actual concentration of CO_2 in the infrared sample, the resulting ε_{CO_2} value is larger than if the proper concentration had been used.

The experimental procedure used by Kieke and coworkers is convoluted as the full experimental details are dispersed throughout a series of publications.[3,5,6] The researchers used a custom built micro sized transmission infrared reactor. The pathlength used for the calculation of ε_{CO2} was not the value used from the design of the apparatus. Instead, the authors used an infringement pattern technique to approximate the pathlength. Upon further investigation, it was found that the infringement pattern technique used is not valid for the mid-IR range investigated.[7] The pathlength value used by the researchers was smaller than the value taken from the experimental design, which results in the calculation of a larger ε_{CO2} value.

Maiella and coworkers hail from the same laboratory as Kieke – Prof. Brill at the University of Delaware. Maiella presents a different, lower, value of ε_{CO2} in 1999 compared to the value reported by Kieke in 1996. Maiella attributes the lower value to an "incorrect data analysis method used previously," but no insight is provided that would allow readers to understand the differences. However, the group maintains the use of the infringement pattern technique for estimating the pathlength of the apparatus, ultimately giving rise to larger ε_{CO2} values than are reported here.

It is not the purpose of this discussion to discredit the valuable work done by other researchers. Instead, the intent is to shed light on the implications of assumptions made on the results obtained when utilizing quantitative infrared spectroscopy. In fact, the focus of the work by Kieke and Maiella was to determine the kinetics of hydrothermal degradation reactions in near-critical water. Because the treatment of pathlength was consistent within their laboratory for the calibration and unknown samples, accurate results from the hydrothermal reactions were obtained. Common to the majority of researchers using quantitative infrared spectroscopy, Maiella and Kieke could easily have lumped the pathlength term into the expression for ε_{CO2} by examining A versus CO_2

concentration. Again, this is valid for transmission spectroscopy. The attempt to determine and report ε_{CO2} is what makes discussions such as this possible. Their efforts should therefore be applauded.

To conclude the discussion of the ε_{CO2} reported here and elsewhere, it should be emphasized that researchers should take much care when using extinction coefficient values reported in literature for their own research. Within the same laboratory, the extinction coefficient for the asymmetric CO_2 stretch was found to differ by a factor of 2 depending on the analysis technique. The use of reflectance infrared spectroscopy introduces more complications than the transmission counterpart. Researchers must be diligent and take the care to understand all assumptions made, and the implications of said assumptions, on the research being conducted. Regarding quantitative infrared spectroscopy, especially reflectance, researchers should perform calibration and validation experiments for the unique apparatus and analysis scheme used. The reality is that quantitative reflectance infrared spectroscopy is a complicated technique, but when the proper care and understanding is taken, it can afford accurate results with many benefits listed previously.

References

(1)   Jones, L. H.; McLaren, E. *Journal of Chemical Physics* **1958**, *28*, 995.

(2)   Falk, M.; Miller, A. G. *Vibrational Spectroscopy* **1992**, *4*, 105.

(3)   Kieke, M. L.; Schoppelrei, J. W.; Brill, T. B. *J. Phys. Chem.* **1996**, *100*, 7455.

(4)   Maiella, P. G.; Schoppelrei, J. W.; Brill, T. B. *Applied Spectroscopy* **1999**, *53*, 351.

(5)   Schoppelrei, J. W.; Kieke, M. L.; Brill, T. B. *J. Phys. Chem.* **1996**, *100*, 7463.

(6)   Schoppelrei, J. W.; Kieke, M. L.; Wang, X.; Klein, M. T.; Brill, T. B. *J. Phys. Chem.* **1996**, *100*, 14343.

(7)   Thormahlen, I.; Straub, J.; Grigull, U. *Journal of Physical and Chemical Reference Data* **1985**, *14*, 933.

APPENDIX C HOT WATER FOR ENVIRONMENTALLY BENIGN DEPROTECTION REACTIONS

Introduction

Increasing public demand and stiffer governmental regulations have caused the chemical industry to pursue innovative, sustainable technology development. Although sustainability is a clear driver for the laboratory scale development of new processing technology, implementation on an industrial is always a function of process cost. The chemical industry can be divided into two main segments: (1) commodity chemical production and (2) pharmaceutical/fine chemical production. Commodity chemicals are produced in massive quantities using well established and efficient processes, where products are generated at a cost of pennies per kilogram. Pharmaceuticals and fine chemicals syntheses are complicated, by comparison, typically involving many separation and reaction steps to yield the final product. As a result, the products are highly valuable and can be sold for over hundreds of dollars per gram. Due to the large number of processing steps and valuable products, many opportunities exist for the development of revolutionary processing techniques with decreased environmental footprints in the pharmaceutical and fine chemical industries.

At the heart of the pharmaceutical industry are protecting reactions, used to isolate potentially reactive sites from unwanted chemical reaction. Following, the protecting groups must be removed – these deprotection reactions account for up to 15% of all reactions carried out in the industry.[1] Nearly all deprotection reactions, even those involving solid-supported acid catalysts, invariably require the use of organic solvents whose separation and disposal have an inherently negative environmental impact.[2]

Deprotection reactions can be catalyzed by acids[3-5] or bases,[6] although acids typically offer improved kinetic rates relative to base catalyzed deprotections.[7] Commonly, strong acids such as sulfuric acid, phosphoric acid, and hydrobromic acid are used for deprotections. The acid concentration is always in excess and must be neutralized and separated from the reaction mixture to avoid negative effects on subsequent processing steps. This results in increasing the overall number of steps for the synthetic procedure, as well as the production of copious amounts of salt-contaminated aqueous waste.

Hot water, or near- subcritical water, is defined as water above its normal boiling point – from 100°C to 200°C under elevated pressures. Under these conditions, water exhibits properties favorable for sustainable technology development, and the advantages for replacing potentially harmful organic compounds have been reported.[8,9] First, the dissociation constant of water increases drastically with temperature, as shown in Figure C.1, exhibiting a maximum at 275°C and resulting in high concentrations of hydroxide and hydronium ions.[10] The hydroxide and hydronium ions are capable of acting as catalysts, and the neutralization is as simple as cooling the system. In fact, hot water has been successfully applied to a broad range of synthetic reactions utilizing the *in situ* catalyst formation.[11-16]

In addition to the formation of an *in situ* catalyst, hot water exhibits solvent properties drastically different from water below its normal boiling point,[17,18] and has been shown to offer increased solubilities of nonpolar compounds.[19,20] The unique properties of hot water give way to opportunities for application to sustainable technology development in pharmaceutical and fine chemical industries. To investigate the application to deprotection reactions, *tert*-butylcarbamate (Boc) was chosen as the protecting group of interest due to its broad applicability to amine functionalities in

organic synthesis. The general acid catalyzed deprotection of Boc-protected amines is given in Figure C.2, showing the deprotected amine, carbon dioxide (CO_2), and *tert*-butanol as primary products. The *tert*-butanol can undergo further dehydration, giving the iso-butylene product.
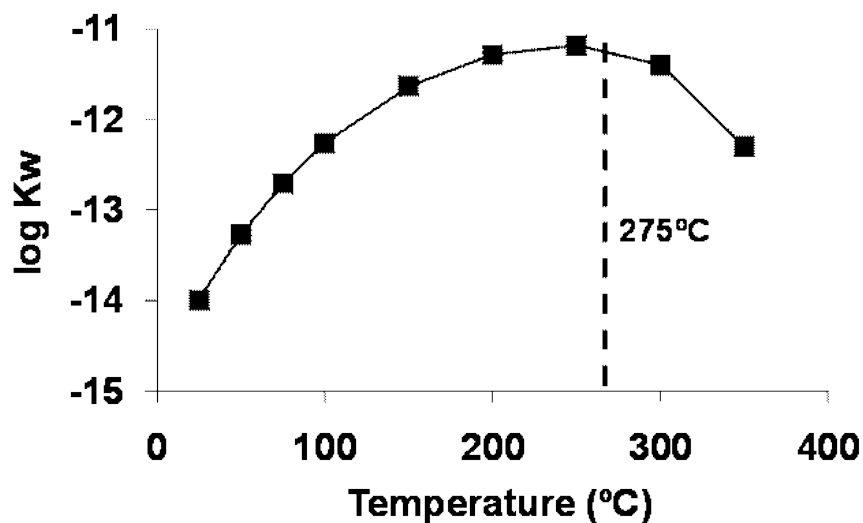

Figure C.1. The dissociation constant of water as a function of temperature.
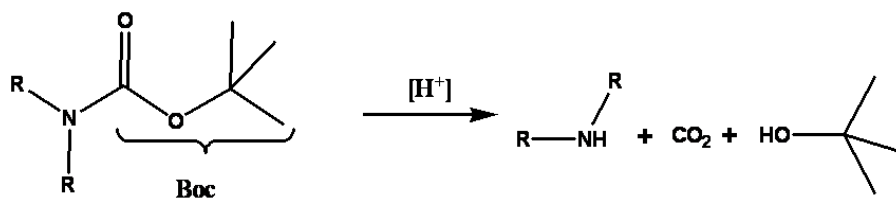

Figure C.2. The acid catalyzed deprotection of Boc-protected amines yielding the amine, CO_2, and *tert*-butanol.

The removal of Boc-protected amines using traditional acids has been extensively studied, and good yields have been reported.[21] However, the use of traditional acids for the deprotection suffers from many economic and environmental drawbacks due to cooling costs (the deprotection is highly exothermic), neutralization using caustic solutions, generation of significant amounts of salt waste, use of organic solvents such as toluene which must be separated and disposed of. The use of hot water as a replacement for traditional organic solvent/acid systems for Boc deprotection reactions is discussed here, focusing on the mechanism and kinetics of the reaction. The environmental benefits by replacing the conventional process include: replacing organic solvents with water, in situ acid generation, facile neutralization of the catalyst, and efficient separation of the products from the solvent. Additionally, the identification of a valuable urea reaction intermediate was observed, and a mechanism for formation of the intermediate is proposed.

Experimental Methods

Materials

High performance liquid chromatographic (HPLC) grade acetonitrile was used as received (Sigma-Aldrich, HPLC 99+%). The deionized water was obtained in-house using a Barnstead B-Pure dual filter water filtration system, with the product water having a resistivity >18 MΩ. The N-Boc-aniline (Sigma-Aldrich, 97%), aniline (Sigma-Aldrich, ACS reagent grade, ≥ 99.5%), acetonitrile (Sigma-Aldrich, HPLC 99+%), and 1,3-diphenylurea (Sigma-Aldrich, 98%) were used as received.

Analytical Procedure

The concentrations of all compounds were determined using high performance liquid chromatography (HPLC). A Phenomenex Luna 5μ C18(2) reverse phase column was used in conjunction with a guard column to prevent clogging. The solvent system consisted of HPLC grade acetonitrile and HPLC grade water with a 0.1% trifluoroacetic acid buffer. The flow rate and column temperature were set to 1.5 mL/min and 40°C, respectively. The method ran for fifteen minutes then had a post-run time of four minutes. The UV detector was set to 210 nm. Calibration curves were prepared for the pure components containing known concentrations, and the linear fit of HPLC response versus concentration was determined. The R^2 value for all calibrations was > 0.99.

Experimental Apparatus and Procedure

An insulated aluminum block with 1.5 mL titanium reactors was used for the kinetic experiments. A full description of the experimental apparatus is offered elsewhere.[16] A stock solution of N-Boc-aniline in acetonitrile with a concentration of 0.2 M, and 300 μL of the stock solution was added to each reactor. The acetonitrile was removed by placing the reactor in an 80°C water bath for one hour. Samples were run following the acetonitrile evaporation to confirm no degradation of the starting material had taken place. One mL of deionized was then placed in the reactors, and the titanium caps, with Teflon tape, were secured.

The titanium reactors were then placed in the heated aluminum block, and withdrawn at appropriate times and quenched in a room temperature water bath. The samples were then extracted from the reactors using acetonitrile, and diluted 10:1 in acetonitrile for HPLC analysis.

Results and Discussion

The model Boc protected amine compound studied was N-Boc-aniline (NBA). NBA is convenient for the analysis, but also industrially relevant as many pharmaceutical intermediates and products contain phenyl-amine segments. The general reaction mechanism for the hot water facilitated deprotection of NBA is given in Figure C.3.
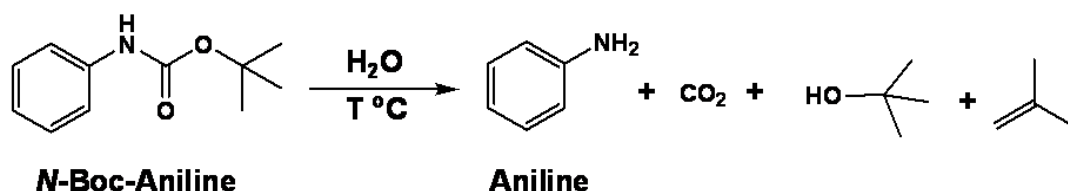
Figure C.3. The hot water facilitated deprotection of N-Boc-aniline (NBA).

With initial NBA concentrations of 0.2 M, the reaction was observed to go to completion within 10 minutes at 250°C. This is consistent with reports of near- subcritical water for the deprotection of NBA,[22,23] and fast reaction kinetics are ideal for industrial scale processing. To ascertain the kinetics and mechanism of the reaction, the temperature was lowered to give slower deprotection rates. The HPLC chromatogram for the deprotection of NBA in hot water, at an initial concentration of 0.2 M, at 10 minutes and 200°C is given in Figure C.4.

The aniline product, at a retention time of 0.972 minutes, and NBA starting material, at a retention time of 7.071 minutes, is clearly visible. However, an unknown peak was observed at a retention time of 3.919 minutes. The analysis of the product mixture at 200°C and 20 minutes indicated only the desired aniline product, with negligible degradation products. Thus, an intermediate of the reaction has been observed. Although the hot water facilitated deprotection of NBA has been reported in literature, no documentation of an intermediate has ever been reported. The molecular

weight of the intermediate was determined to be 212 g/mol using mass spectrometry, consistent with the structure of 1,3-diphenylurea (DPU). The proposed mechanism for the deprotection of NBA, going through the DPU intermediate, is given in Figure C.5.
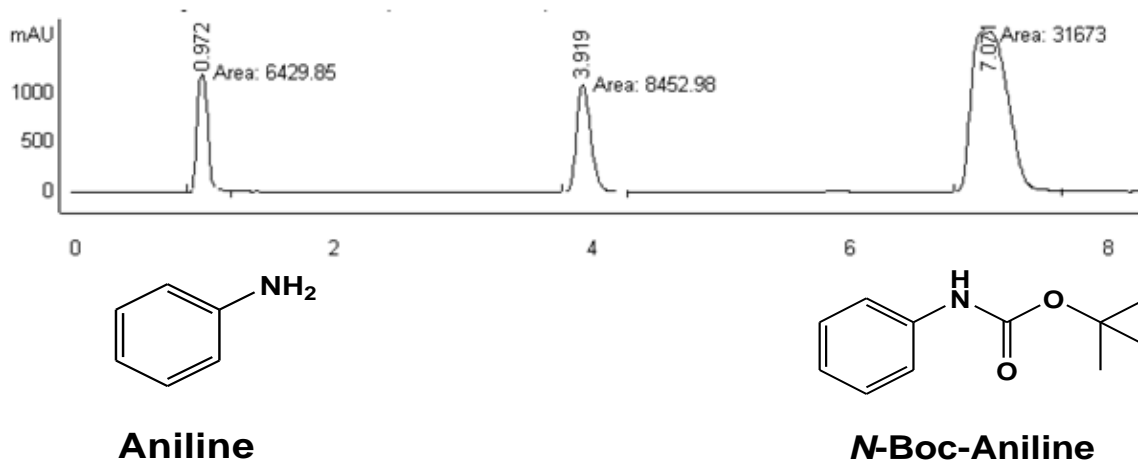
Figure C.4. The HPLC chromatogram of the product mixture from the hot water facilitated deprotection of NBA at 200°C and 10 minutes.
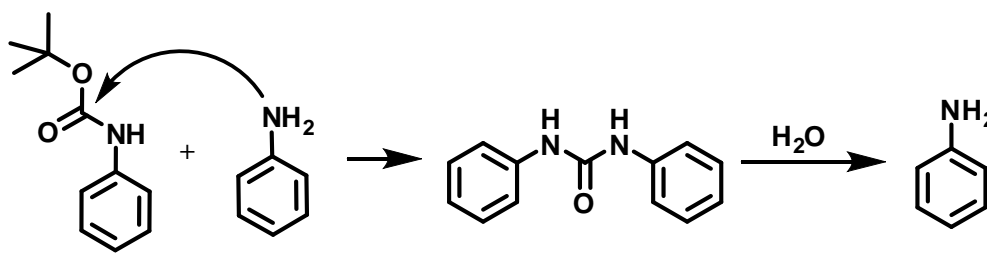
Figure C.5. The proposed mechanism for the hot water facilitated deprotection of NBA, going through the DPU intermediate.

As described by the proposed mechanism shown in Figure C.5, the product aniline acts as a nucleophile, attacking unreacted NBA starting material. The DPU intermediate then decomposes in the hot water medium to yield the desired aniline product. With the mechanism of the hot water facilitated deprotection of NBA

185

understood, the kinetics of the deprotection can now be addressed. Recall that at 200°C, the reaction goes to completion within 20 minutes. To slow the reaction further, the deprotection was examined at 150°C. A graph showing the conversion of NBA at 150°C versus time (minutes) is given in Figure C.6.
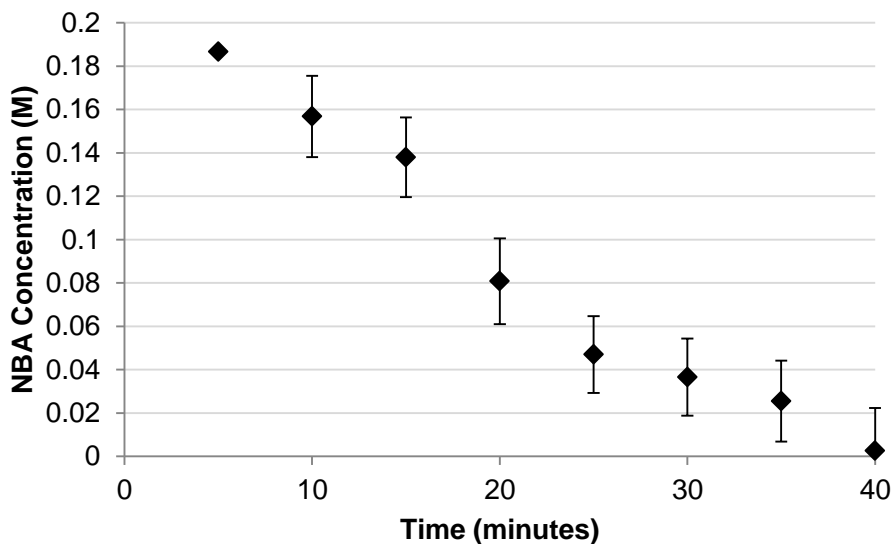
Figure C.6. The kinetics of the hot water facilitated deprotection of NBA at 150°C.

Each data point on the graph represents a separate reaction, with each point run in triplicate, for a total of 24 experiments. The error bars represent the standard deviation of the reaction. The "S-shape" of the curve is indicative of an auto-catalytic reaction, consistent with the proposed mechanism (Figure C.5) that involves the formation of the DPU intermediate by reaction of the product (aniline) with the starting material (NBA).

The reaction was determined to be first order in NBA concentration ([NBA], M), shown by the plot of ln[NBA] versus time (seconds), given in Figure C.7. The first-order rate constant is then determined to be 1.3×10^{-3} sec^{-1} at a temperature of 150°C.
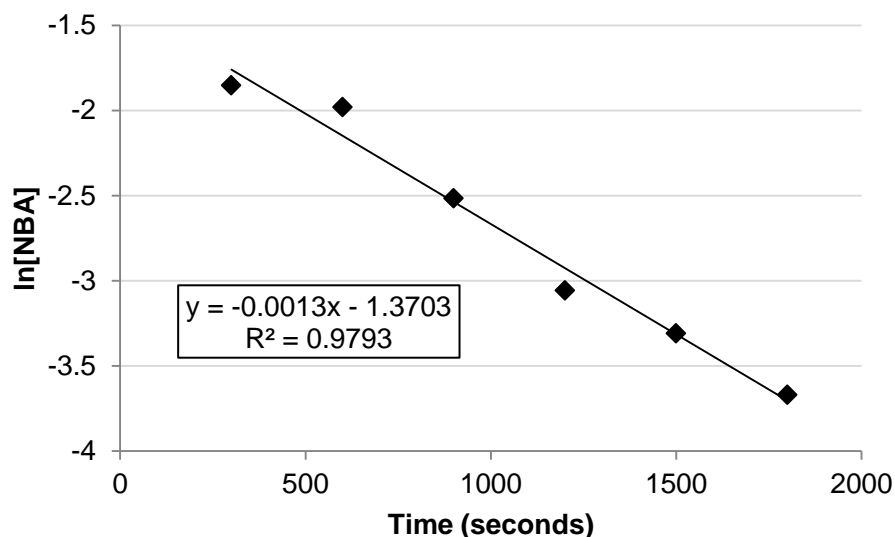
Figure C.7. The first-order plot of ln[NBA] versus time (seconds).

Conclusions and Path Forward

The results reported here are encouraging for the development of a benign solvent that utilizes a self-neutralizing *in situ* catalyst. Water as an alternative to organic solvents and traditional acid catalysts is attractive not only from a sustainability standpoint, but also an economic one. Water is the most abundant, cheapest, and benign solvent on the planet. By harnessing the dissociation of water at high temperatures, acid and base catalyzed reactions can be run effectively. Additionally, by eliminating the need for traditional acid catalysts, the processing is simplified and salt-contaminated aqueous wastes are avoided.

Hot water has been shown to be successful for the fast and efficient deprotection of NBA. For all the experiments, the degradation products, if any, were determined to be < 1%. The identification of a urea intermediate was confirmed, and the proposed auto-catalytic mechanism is consistent with the observed reaction kinetics. Although the experiments at 150°C are less than ideal for industrial processing, where faster rates are

187

desired, the information gathered gave a first-order rate constant for the reaction. Additionally, the experiments performed at higher temperatures indicated negligible degradation products present after reaction completion – promising for the implementation of this technology on an industrial scale.

At higher concentrations of NBA, one would expect mass transfer limitations to play a major role in the observed kinetics, as the solubility of Boc protected amines in water is low. Phase behavior studies would be of much interest, but due to the decomposition of NBA in hot water, knowledge of the kinetic rate constant (where mass transfer limitations are negligible) is crucial for understanding the phase behavior in these reactive systems. In addition to the removal of Boc protected amines, there are a plethora of other protecting groups relevant to the pharmaceutical and fine chemical industries. Such investigations, as well as competitive deprotections where more than one protecting group is present on a molecule, are paramount to the widespread application of hot water as a solvent and catalyst for industrially relevant deprotection reactions.

References

(1)   Carey, J. S.; Laffan, D.; Thomson, C.; Williams, M. T. *Organic & Biomolecular Chemistry* **2006**, *4*, 2337.

(2)   Hermkens, P. H. H.; Ottenheijm, H. C. J.; Rees, D. *Tetrahedron* **1996**, *52*, 4527.

(3)   Ross, S. A.; Pitie, M.; Meunier, B. *Journal of the Chemical Society-Perkin Transactions 1* **2000**, 571.

(4)   Li, B.; Bemish, R.; Buzon, R. A.; Chiu, C. K. F.; Colgan, S. T.; Kissel, W.; Le, T.; Leeman, K. R.; Newell, L.; Roth, J. *Tetrahedron Letters* **2003**, *44*, 8113.

(5)   Houghten, R. A.; Beckman, A.; Ostresh, J. M. *International Journal of Peptide and Protein Research* **1986**, *27*, 653.

(6)   Kim, J. D.; Han, G.; Zee, O. P.; Jung, Y. H. *Tetrahedron Letters* **2003**, *44*, 733.

(7)   Kavala, V.; Patel, B. K. *European Journal of Organic Chemistry* **2005**, 441.

(8)   Katritzky, A. R.; Allin, S. M.; Siskin, M. *Accounts of Chemical Research* **1996**, *29*, 399.

(9)   Katritzky, A. R.; Barcock, R. A.; Ignatchenko, E. S.; Allin, S. M.; Siskin, M.; Hudson, C. W. *Energy & Fuels* **1997**, *11*, 150.

(10)   Sweeton, F. H.; Mesmer, R. E.; Baes, C. F. *Journal of Solution Chemistry* **1974**, *3*, 191.

(11)   Hallett, J. P.; Pollet, P.; Liotta, C. L.; Eckert, C. A. *Accounts of Chemical Research* **2008**, *41*, 458.

(12)   Eckert, C. A.; Liotta, C. L.; Bush, D.; Brown, J. S.; Hallett, J. P. *Journal of Physical Chemistry B* **2004**, *108*, 18108.

(13)   Nolen, S. A.; Liotta, C. L.; Eckert, C. A.; Glaser, R. *Green Chemistry* **2003**, *5*, 663.

(14)   Patrick, H. R.; Griffith, K.; Liotta, C. L.; Eckert, C. A.; Glaser, R. *Industrial & Engineering Chemistry Research* **2001**, *40*, 6063.

(15)   Lesutis, H. P.; Glaser, R.; Liotta, C. L.; Eckert, C. A. *Chemical Communications* **1999**, 2063.

(16)   Chandler, K.; Deng, F. H.; Dillow, A. K.; Liotta, C. L.; Eckert, C. A. *Industrial & Engineering Chemistry Research* **1997**, *36*, 5175.

(17)   Lu, J.; Brown, J. S.; Boughner, E. C.; Liotta, C. L.; Eckert, C. A. *Industrial & Engineering Chemistry Research* **2002**, *41*, 2835.

(18)   Lu, J.; Brown, J. S.; Liotta, C. L.; Eckert, C. A. *Chemical Communications* **2001**, 665.

(19)   Chandler, K.; Eason, B.; Liotta, C. L.; Eckert, C. A. *Industrial & Engineering Chemistry Research* **1998**, *37*, 3515.

(20)   Brown, J. S.; Hallett, J. P.; Bush, D.; Eckert, C. A. *Journal of Chemical and Engineering Data* **2000**, *45*, 846.

(21)   Wuts, P. G. M. *Greene's protective groups in organic synthesis*; 4th ed. / ed.; Wiley-Interscience: Hoboken, N.J. :, 2007.

(22)   Wang, G.; Li, C. J.; Li, J.; Jia, X. S. *Tetrahedron Letters* **2009**, *50*, 1438.

(23)   Wang, J.; Liang, Y. L.; Qu, J. *Chemical Communications* **2009**, 5144.

APPENDIX D   ATR FT-IR ASSISTED DESIGN OF POLYMERS FOR CO$_2$ MEMBRANE SEPARATIONS

Introduction and Background

Energy-related scientific and engineering research is inherently linked to the future viability of the United States economy and national security as well as the overall health of the citizens and the environment.   Energy-efficient separations of carbon dioxide (CO$_2$) from valuable natural gas reserves (as those in Utah and elsewhere in the United States) can help gain energy independence on foreign oil and boost the national economy.   Cement kiln effluent gases contain high concentrations of CO$_2$ mixed with otherwise valuable gases such as H$_2$, N$_2$, and CH$_4$.   Energy-efficient separation of CO$_2$ from such streams could have a positive financial impact as well as reduce the national carbon footprint when paired with a suitable CO$_2$ sequestration technology.

Polymeric membrane based separations are promising energy-efficient solutions to these problems due to their low capital costs and simplicity of installation and operation.   Unfortunately, polymeric membranes typically undergo an unfavorable response (plasticization) to high partial pressures of CO$_2$ that are encountered in many natural gas reserves and cement kiln effluents.[1]   Plasticization is a phenomenon where polymer chain mobility is greatly enhanced by absorption of high concentrations of CO$_2$. The consequence is increased flux of all feed penetrants and a drastic downturn in CO$_2$ separation efficiency.   Furthermore, polymeric membranes have a trade-off between productivity and separation efficiency[2] which often results in properties that cannot compete with current, albeit expensive and environmentally harmful, technologies such as cryogenic distillation and amine scrubbing of acid gases.

Despite these pitfalls, polymeric gas separation membranes have grown in popularity in recent decades and are still seen as an attractive alternative to costly, wasteful, traditional separation technologies. Great strides have been made in suppressing CO_2 plasticization with the use of cross-linkable polymers and highly rigid polymers that are far less susceptible to gas separation efficiency downturns in the presence of high CO_2 concentrations.[3] Similarly, impressive progress has been made in pushing the productivity-efficiency trade-off into economically viable territory via advanced polymer design and polymeric-inorganic filler, such as zeolites or composites.[4] Unfortunately, a comprehensive and detailed understanding of molecular scale processes that dictate membrane performance in high CO_2 concentration feeds and lead to productivity/efficiency trade-offs is a daunting task and is currently unavailable.

Although the effect of CO_2 on polymeric membranes is generally negative, the goal of this project is to utilize favorable CO_2/polymer interactions to enhance the performance of polymeric membranes for CO_2 separations from high pressure and high concentration feed streams. Before an optimal material can be designed, one must identify the specific intermolecular interactions between CO_2 and common polymers. For this structure-property relationship, the common polymers would ideally exhibit differing interactions with CO_2. Once the specific interactions that lead to favorable separation performance have been identified, next generation materials can be synthesized, taking advantage of these favorable interactions. The ultimate goal would then be the creation of functional polymeric membranes leading to bench scales tests for the selective separation of CO_2 from aggressive natural gas and cement kiln effluent feeds to assess the industrially viability of the designer materials.

The initial goal of the project is to understand the molecular level interactions that give way to CO_2 induced plasticization of polymers. Although much is known and

theorized about CO_2 plasticization in polymers, only a thorough understanding of how absorbed CO_2 induces chain mobility can lead to designer polymer structures that will overcome this problem. The CO_2 interactions with commercially available polymers are probed using attenuated total reflection (ATR) Fourier Transform Infrared (FT-IR) spectroscopy. ATR FT-IR spectroscopy allows for molecular level insight into what interactions are taking place in CO_2/polymer systems, as well as *in-situ* measurement capability of CO_2 sorption and polymer swelling. The current apparatus we are using allows for the examination of CO_2/polymer systems at conditions up to 200°C and 2000 psi, which allows for the examination of samples exposed to supercritical CO_2 conditions and more than covers the operational constraints of most commercial CO_2 membrane separations. This apparatus also allows multi-component sorption testing which is typically quite troublesome with traditional sorption experiments. For a detailed explanation of the ATR FT-IR technique, please refer to Chapter 3.

From this experimentation the fundamental knowledge of how the molecular structure affects the plasticization will be examined, and an understanding of what makes polymers have good plasticization resistance will be developed. This information will lead to the design of novel compounds with enhanced properties for CO_2 capture from aggressive feed streams.

Experimental Methods

Materials

Polymeric materials are basically large organic molecules made up of the assembly of several repeating units, commonly two. To examine a broad range of CO_2 plasticization responses among commercially available polymeric materials, cellulose acetate (CA), Matrimid, and Torlon were chosen.

The polymer CA represents the benchmark material, due to its abundance and cheapness. The general structure of CA is given in Figure D.1.
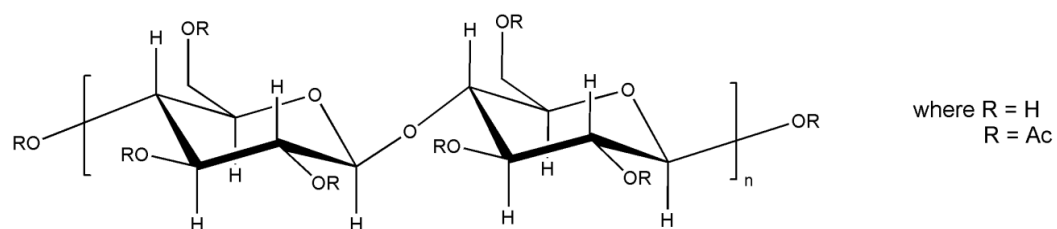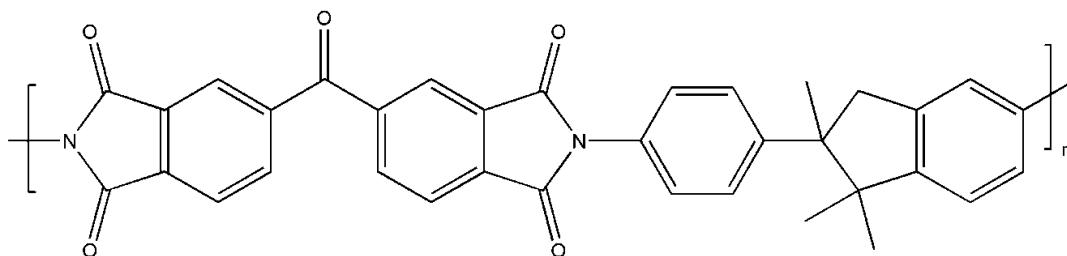

Figure D.1. The general structure of the cellulose acetate (CA) repeat unit.

Although less than ideal due to a low CO_2 plasticization pressure, CA has been examined for use as a CO_2 separation membrane.[5] CA is available in many versions, depending on the average molecular weight of the polymer chains and the degree of acetylation (or number of –OH groups replaced by –OCH$_3$). CA exhibits a relatively low glass transition temperature, implying a low rigidity of the polymeric chains (the chains are able to move about with some freedom). One would expect poor plasticization resistance due to the low rigidity. However, due to the abundance of hydrogen bonding sites, the intra- and inter-chain hydrogen bonding results in relatively good plasticization resistance.

Another commercially available polymer of interest is Matrimid, shown in Figure D.2. Polyimide membranes, such as Matrimid, have been applied to CO_2 separations and have shown to exhibit a high degree of plasticization resistance.[3,6] Matrimid has a high glass transition temperature due to the highly rigid repeat unit. Because the chains aren't able to move about as freely as other polymers (e.g. CA), Matrimid exhibits a relatively good plasticization resistance. Unlike CA, there is a limited potential for intra-

and inter-chain hydrogen bonding to aid in plasticization resistance. Therefore, the plasticization resistance is largely attributed to the rigid chain segments.

Figure D.2. The general structure of the Matrimid repeat unit.

The final commercially available polymeric material of interest is Torlon, shown in Figure D.3.
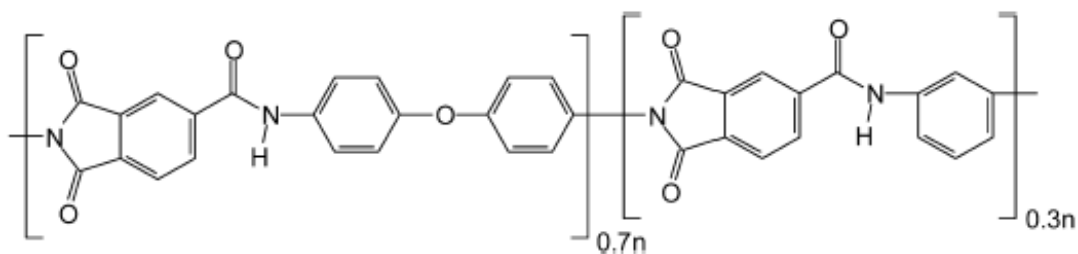
Figure D.3. The general structure of the Torlon repeat units.

Torlon is a polyamide-imide polymer, and it's use as a CO_2 separation membrane has been explored.[7] Polyamide-imides combine rigid backbones, similar to polyimides, with hydrogen bonding similar to CA. The result is a highly plasticization resistant polymeric membrane. To date, the plasticization pressure has not been reported for Torlon.

Apparatus

A Shimadzu IRPrestige-21 FT-IR spectrophotometer (with a DLaTGS detector) was used for collection of the IR spectroscopic data. For all measurements, a total of 32 scans with a resolution of 2.0 cm^{-1} were used. The ATR IR accessory used in this study was a Specac, Inc. Reaction Cell Golden Gate with ZnSe lenses. The cell utilizes a Peltier temperature controller capable of experimentation up to 200°C, and pressures up to 3000 psi.

Polymeric films were prepared *in situ* by preparing an NMP/polymer solution (30%) and depositing approximately 100 μL on the surface of the diamond. The reactor was assembled, heated to 50°C, and vacuum was applied to evaporate the solvent and cast the film directly on the surface of the diamond. NMP has a low boiling point, and was determined to be completely removed from the film when the FT-IR spectrum revealed no solvent present for a period of 24 hours. The time to completely evaporate the solvent (~70 μL) was found to be 3 days. Carbon dioxide (CO_2) was supercritical fluid chromatography (SFC) grade (Air Gas, 99.999%) and further purified via a Matheson gas purifier and filter cartridge (Model 450B, Type 451 filter) to remove water. Measurements were collected at 35°C and various CO_2 pressures up to 1800 psi.

The analysis follows that prescribed in Chapter 3 for the determination of physically absorbed CO_2. Integrated absorbance areas were used; covering the range of 2200-2500 cm^{-1} for the CO_2 asymmetric stretch vibration and 1180-1275 cm^{-1} for the determination of swelling.

Results and Discussion

The CO_2 solubility was examined at 35°C in a Torlon film, given in Figure D.4. The results indicate that at a CO_2 pressure of approximately 1000 psi, the Torlon film is

completely saturated with CO_2. The uptake up to 1000 psi appears to be linear. After 1000 psi, the solubility appears to start decreasing. Examination of the swelling of the polymer can shed some light as to why. The swelling of Torlon at 35°C and varying CO_2 pressures is given in Figure D.5.
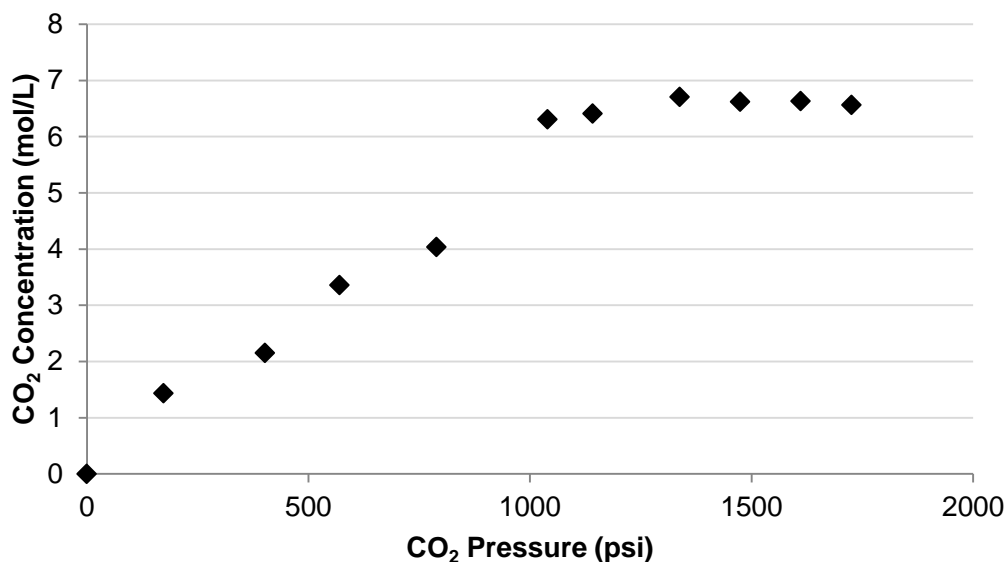
Figure D.4. The solubility of CO_2 in Torlon at 35°C and pressure up to 1800 psi.

The CO_2 induced swelling behavior of Torlon yields interesting information about the CO_2/polymer system. The swelling of Torlon at high CO_2 pressures is minimal, approaching only 6%. This is attributed to the rigidity and hydrogen bonding afforded by the molecular structure. Additionally, as the maximum solubility of CO_2 is reached at approximately 1000 psi, the swelling appears to decline. This is indicative of the film density increasing as high CO_2 pressures are applied, becoming denser than the initial film at pressures exceeding 1500 psi. As the density of film starts to decrease, CO_2 is "pushed" out of the polymeric matrix, resulting in a decrease in the CO_2 solubility.
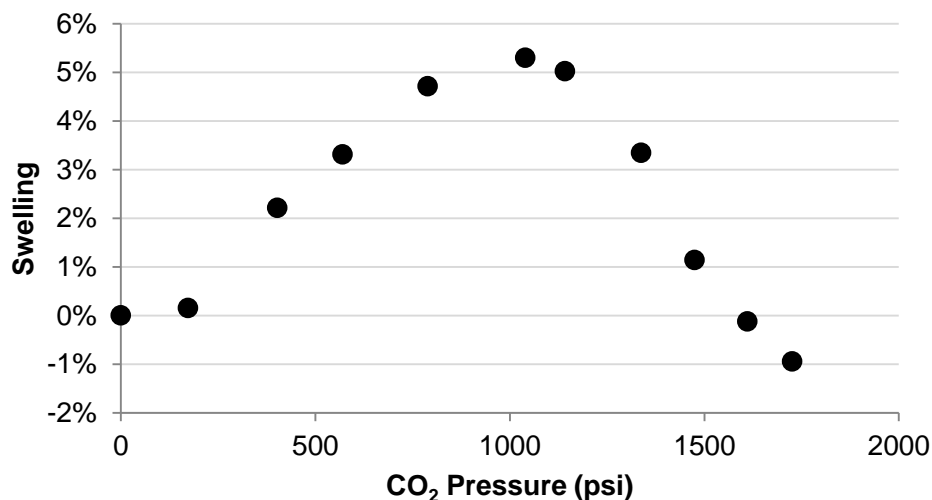
Figure D.5. The CO_2 induced swelling in Torlon at 35°C and pressure up to 1800 psi.

Conclusions

The ATR FT-IR assisted study of the CO_2/polymer system results in both the CO_2 solubility and swelling information. The relationship between solubility and swelling in Torlon reveals interesting behavior regarding the saturation and densification of the film, useful for the application of the material to industrial processes and the design of future materials. Not only does the unique structure of polyamide-imides result in high CO_2 loadings, but the rigidity and hydrogen bonding prevent swelling that is commonly associated with plasticization and reorganization of polymer chains exposed to high partial pressures of CO_2.

Path Forward

To overcome the plasticization that occurs with polymeric membranes under high CO_2 loadings, one can imagine a "smart" polymer that alters its structure to overcome the unfavorable effects of plasticization. This can be achieved by attaching

functionalities to the polymer backbone that will react with CO_2 and form cross-linking *in-situ*, not only preventing plasticization but using CO_2 to enhance the polymer's behavior. Ideally this behavior will be completely reversible, and the extent of *in-situ* cross-linking will be controlled by the concentration of absorbed CO_2. Similar behavior is recorded in membrane literature and is often called "anti-plasticization".[8,9] This is typically seen with trace amounts of heavier hydrocarbons and is a poorly understood phenomenon.

It is proposed to engineer novel molecular architectures which contain functional groups that can react with CO_2 to form reversible ionic cross-linkages. The basic structure would consist of basic nitrogen species alone and in combination with hydroxyl functionalities and weak Lewis acids to optimize ionic cross-linking capabilities of the polymers upon reaction with CO_2, shown in Figure D.6.
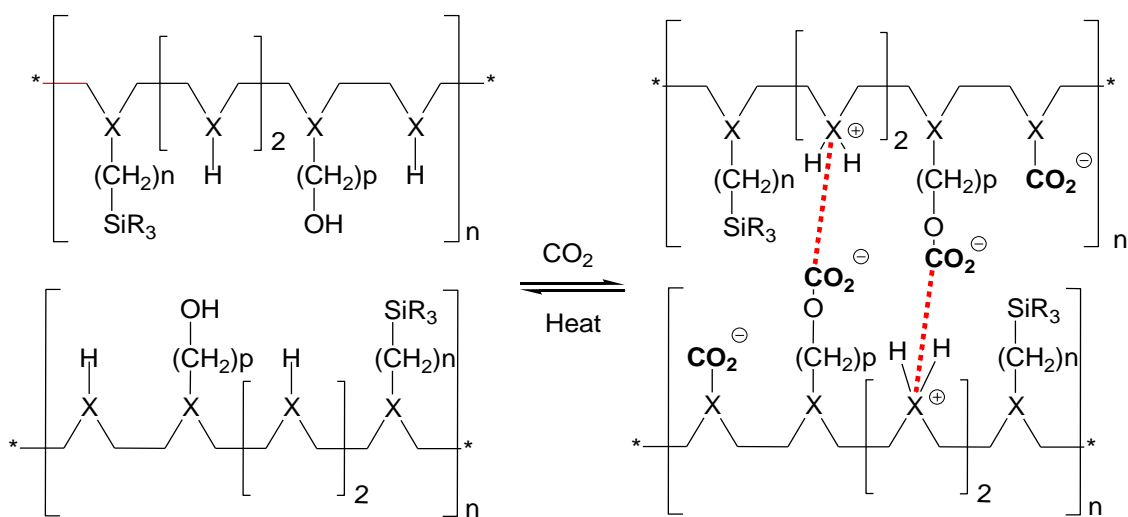
Figure D.6. Concept for molecular structure of reversible cross-linking polymeric membrane materials.

Where (1) X is the basic nitrogen species, (2) m, and p are the lengths of the tethers connecting the various functionalities, and (3) R is alkyl or alkoxy. By varying the proximities and concentrations of these functionalities, optimized structures can be

synthesized. Using ATR FT-IR as well as traditional gas permeation experiments, the effectiveness of the reversible cross-linking polymers can be assayed, and that information coupled with structure-property relationships can be used to design polymers with the physical and chemical properties desirable for application in industrial systems.

References

(1) Bos, A.; Punt, I. G. M.; Wessling, M.; Strathmann, H. *Journal of Membrane Science* **1999**, *155*, 67.

(2) Robeson, L. M. *Journal of Membrane Science* **1991**, *62*, 165.

(3) Bos, A.; Punt, I. G. M.; Wessling, M.; Strathmann, H. *Separation and Purification Technology* **1998**, *14*, 27.

(4) Zimmerman, C. M.; Singh, A.; Koros, W. J. *Journal of Membrane Science* **1997**, *137*, 145.

(5) Stern, S. A. *Journal of Membrane Science* **1994**, *94*, 1.

(6) Wind, J. D.; Paul, D. R.; Koros, W. J. *Journal of Membrane Science* **2004**, *228*, 227.

(7) Kosuri, M. R.; Koros, W. J. *Journal of Membrane Science* **2008**, *320*, 65.

(8) Shao, L.; Chung, T. S.; Goh, S. H.; Pramoda, K. P. *Journal of Membrane Science* **2005**, *256*, 46.

(9) Sundgren, N.; Bergman, G.; Shur, Y. J. *Journal of Applied Polymer Science* **1978**, *22*, 1255.

VITA

Ryan Joseph Hart was born in a little Wyoming town, Lander, on October 27th, 1983 to Tyke and Raylene Hart. He moved with his parents to Rock Springs, WY at the age of five. During his youth in Rock Springs, he played many sports, enjoyed the outdoors, and helped his neighbors and friends whenever possible. His secondary education culminated with his graduation from Rock Springs High School in 2002. He then traveled to Laramie, WY to pursue his Bachelor of Science degree in Chemical Engineering, with successful completion in Spring 2006. Vowing to never forget his friends that helped him along the way, he left his homeland after 22 years to pursue his PhD at Georgia Institute of Technology in Atlanta, GA. The departure from Wyoming opened him up to the concept of travel – international and national. Taking advantage of numerous opportunities, he traveled all over the US and Europe to participate in conferences, give lectures, and find the company of good friends. With this chapter of his life at a close, Ryan will be moving with his trusty dog Buster to Chicago, IL where he will be employed as a technology consultant for the failure-analysis firm Exponent, Inc.